Distribution Agreement

In presenting this thesis or dissertation as a partial fulfillment of the requirements for an advanced degree from Emory University, I hereby grant to Emory University and its agents the non-exclusive license to archive, make accessible, and display my thesis or dissertation in whole or in part in all forms of media, now or hereafter known, including display on the world wide web. I understand that I may select some access restrictions as part of the online submission of this thesis or dissertation. I retain all ownership rights to the copyright of the thesis or dissertation. I also retain the right to use in future works (such as articles or books) all or part of this thesis or dissertation.

Signature:

_____ _____

Liz Dreggors-Walker Date

Box C/D snoRNP assembly factors regulate translation and contribute to disease

By

Liz Dreggors-Walker
Doctor of Philosophy
Graduate Division of Biological and Biomedical Sciences Biochemistry, Cell, and Developmental Biology

_____
Homa Ghalei, Ph.D.
Advisor

_____
Anita Corbett, Ph.D.
Committee Member

_____
Lawrence Boise, Ph.D.
Committee Member

_____
Daniel Reines, Ph.D.
Committee Member

_____
Bing Yao, Ph.D.
Committee Member
Accepted:

_____
Kimberly J. Arriola, Ph.D.
Dean of the James T. Laney School of Graduate Studies

_____
Date

Box C/D snoRNP assembly factors regulate translation and contribute to disease

By

Liz Dreggors-Walker
B.S., Mercer University, 2018

Advisor: Homa Ghalei, Ph.D.

An abstract of
a dissertation submitted to the Faculty of the
James T. Laney School of Graduate Studies of Emory University
in partial fulfillment of the requirements for the degree of
Doctor of Philosophy
in Biochemistry, Cell and Developmental Biology
2022

Abstract

Regulation of protein synthesis is critical for the control of gene expression in all cells. Ribosomes are RNA-protein machines responsible for translating all proteins, and defects in ribosome production, function, or regulation result in disease. Ribosomal RNA (rRNA) is highly modified, and these modifications are critical for proper ribosome biogenesis and translation. One abundant class of rRNA modifications is 2'-O-methylation. 2'-O-methylations are guided by box C/D small nucleolar RNAs (snoRNAs), which assemble with evolutionarily conserved proteins to form active RNA-protein complexes (snoRNPs) to deposit rRNA modifications. The assembly of snoRNPs relies on several transient assembly factors through a poorly understood mechanism. In this dissertation, I use budding yeast as a model system to uncover a novel mechanism in snoRNP assembly, novel aspects of snoRNA-mediated regulation of translation, and how dysregulation of snoRNP assembly can lead to disease. The first part of this dissertation characterizes the box C/D snoRNP assembly factor Bcd1. We show that interactions between Bcd1 and Snu13 as well as interactions between Bcd1 and snoRNAs are critical for snoRNP assembly, unveiling a novel step in the hierarchal assembly of snoRNPs. Next, we use a mutant with impaired Bcd1 function and decreased rRNA 2'-O-methylation to determine how rRNA 2'-O-methylations impact translation. We reveal that hypo 2'-O-methylation impacts ribosome efficiency and fidelity by altering ribosome dynamics and the rotational status of ribosomes. The bulk of my dissertation work has focused on characterizing the box C/D snoRNP assembly factor Hit1. Mutations in the human homolog of Hit1 (*ZNHIT3*) result in the devastating neurodevelopmental disease PEHO syndrome. I generated budding yeast models of these PEHO-linked variants. My studies revealed that the PEHO-linked mutants in yeast result in loss of box C/D snoRNAs, impaired rRNA processing, decreased levels of rRNA 2'-O-methylations, impaired translation fidelity, and impaired ribosomal ligand binding. These data provide the first insights into the molecular basis of PEHO syndrome and suggest that PEHO syndrome is a ribosomopathy that is likely caused by impaired translation. Taken together, the studies presented in this dissertation reveal novel aspects of box C/D snoRNP biogenesis that are essential for proper translation and suggest that dysregulation of snoRNP assembly can result in human disease.

Box C/D snoRNP assembly factors regulate translation and contribute to disease

By

Liz Dreggors-Walker
B.S., Mercer University, 2018

Advisor: Homa Ghalei, Ph.D.

A dissertation submitted to the Faculty of the
James T. Laney School of Graduate Studies of Emory University
in partial fulfillment of the requirements for the degree of
Doctor of Philosophy
in Biochemistry, Cell and Developmental Biology
2022

Acknowledgements

Thank you to my undergraduate mentors, Drs. Amy Wiles and Garland Crawford, for helping me get started on this journey. I'm so grateful to have had your help and influence.

To my dissertation committee, Drs. Anita Corbett, Bing Yao, Danny Reines, and Larry Boise, thank you for supporting and uplifting me at every meeting. Graduate school has been a difficult journey at times, but I've always left our meetings feeling so encouraged. Thank you for the great discussions, for caring about both me and my science, and for always being willing to help.

Thank you to my family- to my dad for always listening and providing wisdom, to Jenny for always caring, to Bella for keeping me young, to Mac for providing comfort, and to my mom for believing in me. Thank you to my best friends that are also my family- Julie, Alex, and Victoria for supporting me and bringing joy to my life, even from afar. Thank you most of all to my biggest supporter Brandon for all the sacrifices you have made to help me get here and for always uplifting and encouraging me when I need it.

Thank you to my friends, lab mates, and everyone in the BCDB program who openly discussed the importance of mental health and who gave me the courage to take care of my own. I am especially grateful for Saman, Kate, and Lauren for empowering me to get through the final stretch of my graduate career.

Last, thank you to Drs. Homa Ghalei and Sohail Khoshnevis for teaching me and pushing me. Your insights have greatly influenced my science and my life trajectory.

Table of Contents

Abbreviations

eEF2 eukaryotic elongation factor 2

eIF1 eukaryotic initiation factor 1

HPG L-Homopropargylglycine

IDR intrinsically disordered region

IRES internal ribosome entry site

LSU large subunit

mRNA messenger RNA

Ni-NTA nickel-nitrilotriacetic acid

PEHO progressive encephalopathy with edema hypsarrhythmia and optic atrophy

RNA ribonucleic acid

rRNA ribosomal RNA

RNP ribonucleoprotein

RT-qPCR quantitative reverse transcription PCR

r-protein ribosomal protein

PAGE polyacrylamide gel electrophoresis

PGO phenylglyoxal

PTC peptidyl-transferase center

snoRNA small nucleolar RNA

snoRNP small nucleolar ribonucleoprotein

SSU small subunit

Ti inflection temperature

tRNA transfer RNA

Zf-HIT zinc finger HIT

ZNHIT3 Zinc Finger HIT-Type Containing 3

ZNHIT6 Zinc Finger HIT-Type Containing 6

Chapter 1: Insights into the regulation of ribosome biogenesis by ribosomal RNA modification

Small nucleolar RNAs and their cellular functions

Protein synthesis is a critical process in every cell of all living organisms. The macromolecular machinery that catalyzes the synthesis of proteins is the ribosome. In the model organism budding yeast, the ribosome is a ribonucleoprotein complex composed of 4 ribosomal RNAs (rRNA) and 78 ribosomal proteins (r-proteins). Biogenesis of ribosomes is an intricate process which relies on the actions of over 200 assembly factors (1,2). A critical step in ribosome biogenesis is the chemical modification of rRNAs. Approximately 90% of all known rRNA modifications in budding yeast and 95% in humans fall within one of two classes: 2'-O-methylations or pseudouridylations (3,4). Both of these modifications are guided by a critical and evolutionarily conserved class of small non-coding RNAs found in the nucleolus, termed small nucleolar RNAs (snoRNAs) (5).

snoRNAs are divided into two classes based on their conserved sequence features. The first class, box C/D snoRNAs contain the well-conserved box C (RUGAUGA) and box D (CUGA) motifs along with the less-conserved box C' and box D' motifs (6,7) (**Figure 1A**). These conserved motifs allow the RNA to adopt a specific structure necessary for protein recognition. Boxes C and D come together at the base of a stem to form a kink-turn structure necessary for recognition of snoRNAs by their protein binding partners, as do boxes C' and D', forming a pseudo-symmetric structure with two kink-turns (6,7). In between the two kink-turns lie one to two antisense sequences which base-pair with a substrate RNA, bringing the snoRNA along with its associated proteins to its target for modification (6,7). In yeast, the proteins Snu13, Nop56, Nop58, and Nop1 associate with the box C/D snoRNA to form the mature, functional small nucleolar

ribonucleoprotein (snoRNP) complex which deposits 2'-O-methylation on the rRNA (8) (**Figure 1B**).

Another class of snoRNAs are box H/ACA snoRNAs, which contain a box H (ANANNA) and box ACA motif (**Figure 1A**). Box H/ACA snoRNAs contain two hairpins, one upstream of the box H and another in between the H and ACA boxes. Each hairpin contains an internal loop with sequences complementary to the target RNA (6,7). These H/ACA sequence elements are critical for the binding of the core proteins, Nhp2, Nop10, Gar1, and Dyskerin, to the snoRNA for the formation of an H/ACA snoRNP complex that can guide the conversion of uridines to pseudouridines. (8) (**Figure 1B**).

snoRNPs are best known for their conserved role in ribosome biogenesis by facilitating proper rRNA processing, folding, and modification. The majority of box C/D snoRNAs guide 2'-O-methylation, a modification in which a methyl group is added to the 2'-hydroxyl of the ribose moiety of the RNA (9). Ribose 2'-O-methylation stabilizes certain RNA structures and facilitates proper rRNA folding (10-13). Ribosomes lacking 2'-O-methylations are impaired in translation efficiency and fidelity (12-18). Most box H/ACA snoRNAs guide pseudouridylation, an isomerization of the uridine residue. Pseudouridylations also impact RNA structure and pre-rRNA folding and are critical for proper translation (12,18). However, some snoRNAs do not direct modification. Two box C/D snoRNAs (U14 and U3) and two H/ACA snoRNAs (snR10 and snR30) participate in pre-rRNA processing by base-pairing with the pre-rRNA to coordinate long-range folding (19-25). In addition, a few snoRNAs have roles beyond 2'-O-methylation or pseudouridylation of rRNAs, including two yeast box C/D snoRNAs (snR4 and snR45) which guide two sites of rRNA acetylation and many human snoRNAs which guide modification of additional targets (26,27). Recent data also suggest that yeast snoRNAs could have roles in

scaffolding or modification of other RNAs (28), however this remains to be experimentally determined.

For many decades, budding yeast has served as an important model organism for the study of snoRNAs. Both box C/D and H/ACA snoRNAs are well conserved between budding yeast and human, with approximately 80% of yeast snoRNAs and their functions in ribosome biogenesis conserved in humans (29). The yeast genome encodes only 76 snoRNAs, however, mammalian genomes code for many additional snoRNAs. The human genome encodes 760 snoRNAs with known or predicted targets and over 1300 additional snoRNA genes whose targets are unknown, which are collectively termed orphan snoRNAs (30). On the human rRNA, snoRNAs guide 112 2'-O-methylations and 105 pseudouridylations (4), compared to 55 rRNA 2'-O-methylations and 45 rRNA pseudouridylations on the budding yeast rRNA (3,31,32). Because humans are a more complex multicellular organism with greater need for translational control, the greater number of rRNA modifications is proposed to provide greater ability to fine-tune the rRNA modification pattern for control of translation (9,33). In humans, snoRNAs also guide the modification of many additional targets, including snRNAs, tRNAs, mRNAs, and snoRNAs (26,34) and are implicated in regulating other cellular processes such as alternative splicing and cholesterol trafficking (35-37). While mammalian snoRNAs are encoded primarily in introns, the majority of yeast snoRNAs are transcribed independently under the control of their own promoter (38). The fewer number of snoRNA genes, their simpler genomic organization, and the ease of genetic manipulations in budding yeast have made yeast an excellent organism for studies of snoRNA function and for studies of the rRNA modifications which they guide.

Small nucleolar RNAs and human disease

Proper ribosome biogenesis is critical for maintaining the cellular proteome, and dysregulation

of ribosome biogenesis leads to a number of genetic diseases and cancers (39,40). Ribosomopathies are a diverse class of genetic diseases caused by defects in ribosome production, function, or regulation (41,42). For the majority of ribosomopathies, treatments are symptomatic only and do not address the underlying causes. Although ribosomes are important for protein synthesis in all cells, ribosomopathies manifest in tissue-specific defects (41,43). For example, many ribosomopathies affect craniofacial development (such as Treacher Collins Syndrome, Diamond-Blackfan Anemia, and Schwachman-Diamond syndrome), while only a subset of ribosomopathies (i.e. Diamond-Blackfan Anemia and Shwachman-Diamond syndrome) result in bone marrow failure (43-45). Why disruptions in ribosome biogenesis result in different tissue-specific phenotypes is still unclear and requires further investigation. Specifically, mutations in snoRNAs, snoRNP assembly factors, or core snoRNP proteins can contribute to ribosomopathies and cancers, including dyskeratosis congenita and head and neck squamous cell carcinoma (46,47). However, in many cases, how they contribute to disease progression or cause disease is still unclear.

Processing of snoRNAs and snoRNP assembly in yeast

The yeast genome contains 76 snoRNA genes (47 box C/D and 29 box H/ACA), which guide 55 rRNA 2'-O-methylations and 45 rRNA pseudouridylations (3,31,32). The majority of yeast snoRNAs are transcribed from individual genes by RNA polymerase II (38). For these snoRNAs, processing and snoRNP assembly begins co-transcriptionally and occurs in the nucleus (8,38). At the 5' end of the precursor snoRNA, the m^7G cap is either modified or removed and the snoRNA is processed both endonucleolytically and exonucleolytically, until the exonuclease reaches a protein-protected region (38). snoRNAs are also trimmed at their 3' end by the RNA exosome, again until the exonuclease reaches a portion of the RNA protected by proteins. Thus, proper

protein binding is essential to the maintenance of snoRNA levels (8,38).

In yeast, eight snoRNA genes are found within introns (U18, U24, snR38, snR39, snR54, snR59, snR44, and snR191). These snoRNAs are processed similarly to individually encoded snoRNAs, with the addition of a splicing step prior to 3' end trimming. Approximately 20% of snoRNAs in yeast are encoded by polycistronic genes, where multiple snoRNAs are produced from one transcript. These snoRNAs are processed first by exonucleolytic cleavage between the mature snoRNA sequences, followed by the same 3' and 5' end exonuclease trimming as individual snoRNAs (38). Only one snoRNA (snR52) in yeast is transcribed by RNA polymerase III (48). Unlike other RNAs transcribed by pol III, this snoRNA undergoes both 3' and 5' end processing in a manner similar to snoRNAs transcribed by pol II (7,49).

The proper binding of core proteins during snoRNP assembly is essential for maintaining steady-state snoRNA levels and is therefore also critical for ribosome biogenesis (8,38). Assembly of box C/D snoRNPs in yeast occurs hierarchically and relies on the actions of several conserved and transient assembly factors, including Hit1, Bcd1, Rsa1, and Rvb1/2 (8). Early in assembly, the Hit1/Rsa1 complex is responsible for loading Snu13 onto the snoRNA (50,51), and Bcd1 is responsible for facilitating the co-transcriptional binding of Nop58 to the snoRNA (52). A conserved region within Bcd1 is also essential for coordinating the interaction of the protein with snoRNAs and Snu13 (53). The AAA+ ATPases Rvb1 and Rvb2 form a heterohexamer and stabilize the interaction between Nop58 and Snu13 (54,55). While the basic functions of each assembly factor are known, the precise timing and order of eukaryotic box C/D snoRNP assembly and the cellular impact of dysregulated snoRNP assembly is still not fully characterized (34). Box H/ACA snoRNP assembly also requires the actions of conserved and transient assembly factors. Naf1 is involved in the co-transcriptional recruitment of core H/ACA snoRNP proteins (56), and

the assembly factor Shq1 chaperones and recruits the pseudouridine synthase Dyskerin to the pre-snoRNP (57). The snoRNP assembly factor Rvb1/2 is also involved in H/ACA snoRNP assembly (58).

The impact of snoRNAs on ribosome biogenesis in yeast

snoRNPs influence rRNA structure and protein recruitment to the ribosome by both base pairing and depositing modifications which modulate the interaction capabilities of nucleotides (3,5,7). In this section, I review how snoRNAs influence ribosome biogenesis.

snoRNA-rRNA base pairing

Most snoRNAs direct between one to three site-specific rRNA modifications via guide sequences that base pair with the rRNA, forming a helix and allowing the snoRNP to deposit a modification. The guide sequences within box C/D snoRNAs lie in the spacer regions between the boxes D and C' or C and D' elements. On average, the guide region of box C/D snoRNAs shares 12 nucleotide complementarity with the substrate, with 7 nucleotides being the shortest guide region, found within snR70, and 19-nucleotides the longest guide, found in snR60 (59). Structural and biochemical studies of archaeal sRNPs suggest that a maximum of 10 nucleotides of complementarity can be accommodated in the active box C/D snoRNP complex (60,61). The guide sequences in box H/ACA snoRNAs lie within the pseudouridylation pocket and on average contain 14 nucleotides of complementary to their targets, with 10 nuclotides being the shortest guide region found in many H/ACA snoRNAs and 18 nucleotides the longest, found in snR82 (59,62). Biochemical studies have shown that yeast H/ACA snoRNAs require a minimum of 8 nucleotides of complementarity to their target RNA to guide pseudouridylation (63). Some yeast snoRNAs contain additional rRNA complementarity at regions other than their guide sequence, facilitating snoRNA recruitment to the rRNA (64). However, why eukaryotic snoRNA guide sequences

contain additional complementarity to their target rRNA is still not known.

snoRNA-guided rRNA modifications

In yeast, there are 32 snoRNA-guided modifications on the 18S rRNA, which are guided by 27 different snoRNAs, and 67 modifications on the 25S rRNA deposited by 52 different snoRNAs. One 25S site, U2347, can be both 2'-O-methylated and pseudouridylated by snR65 and snR9, respectively. Methylations at two other 25S sites are guided by snoRNAs with overlapping functions. Modification of 25S-A807 is guided by both snR39 and snR59, while 2'-O-methylation of 25S-U2921 is guided by both snR52 and the methyltransferase Sbp1. Throughout the 25S, 7 snoRNAs (U18, snR13, U24, snR48, snR3, snR82, snR9) guide modifications at adjacent sites, allowing one guide sequence to direct more than one modification (65). Four yeast snoRNAs (snR8, U24, snR3, snR191) guide nearby modifications using two different guide sequences. Two of these snoRNAs (U24 and snR3) deposit modifications using both mechanisms, allowing just one snoRNA to guide three modifications to the same region. snoRNA-guided modifications are not evenly dispersed across ribosome structure and are instead clustered in hotspots of the ribosome, particularly around the peptidyl transferase center and tRNA binding regions (3).

snoRNAs and ribosomal protein contacts

The majority of snoRNA-guided modifications are deposited co-transcriptionally (66,67). Similarly, ribosomal protein binding and assembly factor recruitment start co-transcriptionally as the nascent ribosomal RNA emerges. Thus, the base pairing between snoRNAs and pre-rRNA could affect many of the early steps of ribosome assembly. Besides snoRNAs that are involved in rRNA processing, the contributions of snoRNA-rRNA base pairings to ribosome assembly remain largely unknown.

RNA modifications play an important role in maintaining local and long-range structures by

impacting base stacking, helix stability, hydrogen bonding potential, and base pairing (68-70). rRNA modifications can, therefore, influence ribosome assembly by modulating r-protein interactions with the rRNA. Mapping of rRNA modifications and r-protein contacts shows that 49% of pseudouridylated sites (22/45) and 45% of 2'-O-methylated sites (25/55) are 4Å or less away from the binding site of a ribosomal protein and thus directly interact with at least one r-protein (**Figure 2** and **Figure 3**). Furthermore, 87% (48/55) of rRNA 2'-O-methylations and 78% (35/45) of rRNA pseudouridylations are within 3 nucleotides of an r-protein contact (71) (**Figure 2** and **Figure 3**). Attesting to the importance of rRNA modifications for protein binding, eL41, a critical protein for formation of the eB14 intersubunit bridge at the center of the ribosomal subunit interface, contacts the 18S rRNA at four chemically modified nucleotides including the 2'-O-methylated nucleotide G1126 (3). Supporting the hypothesis that rRNA modifications are critical for ribosome interactions and function, yeast ribosomes with globally decreased 2'-O-methylation levels have impaired binding to eIF1 and altered dynamics (13). Furthermore, the Sbp1-guided 2'-O-methylation at G2922 on the 25S rRNA is necessary for proper ribosome assembly factor binding and pre-60S maturation (72).

Nearly all snoRNA binding regions (95/100) on the rRNA directly overlap with sites of r-protein contacts. Therefore, it is also possible that snoRNP binding itself could influence protein binding early in ribosome biogenesis. In humans, SNORD27 binds pre-mRNAs and competes for binding with other interactors to regulate gene expression (37,73). How snoRNA binding may influence ribosome biogenesis is still largely unclear. snoRNP binding may facilitate ribosome assembly by blocking access and preventing premature binding of ribosomal ligands such as tRNAs, r-proteins, assembly factors, and translation factors. For example, snR35 binds the helical loop l31 on the small subunit to prevent premature folding, thereby chaperoning the folding of a

critical P-site helix junction (74). Some snoRNAs interact with r-proteins, such as the interaction between the box A region of the box C/D snoRNA U3 with Rps23 (75). Ribosome assembly factors are also known to act in a blocking mechanism during ribosome biogenesis. For example, the rRNA modifying enzyme Dim1 serves as a steric block for the binding of eIF1 and the initiator tRNA to prevent subunit binding during small subunit maturation (76,77). Similarly, other late-acting assembly factors can prevent premature 40S particles from participating in translation (77). It is tempting to speculate that snoRNPs may also function as steric blocks during ribosome biogenesis given the overlap between snoRNA and r-protein binding regions on the rRNA.

snoRNA binding and ribosomal protein recruitment

Ribosome biogenesis requires hierarchical and coordinated binding of 79 r-proteins in budding yeast (2,78). Ribosome assembly begins in the nucleolus, where rRNAs are processed and r-protein binding begins co-transcriptionally (1,78). Nearly a third of the proteins in each of the ribosomal subunits (10/32 in the small subunit and 14/47 in the large subunit) bind early and co-transcriptionally in the nucleolus. Another 6 proteins from the small subunit and 11 from the large subunit bind intermediately during co-transcriptional ribosome assembly. Finally, 12 proteins from the small subunit and 16 from the large subunit bind later, only interacting with more mature pre-ribosomes either in the nucleus or cytoplasm. For a number of r-proteins, when they bind during ribosome assembly is still unknown (78).

In total, there are over 600 sites of RNA-protein contact on the 25S rRNA (**Figure 3**) and over 300 sites on the 18S rRNA (71) (**Figure 2**). Like snoRNA binding, the binding of r-proteins is not evenly dispersed across the length of the rRNA. Instead, r-protein binding generally occurs in a gradient, where early-binding r-proteins more frequently bind towards the 5' of the rRNA, and late-binding r-proteins more frequently bind towards the 3' of the rRNA. This distribution is most

pronounced on the 18S rRNA where 78% of early-binding r-protein contacts occur on the 5' half of the rRNA, while the majority (83%) of late-binding r-protein contacts occur on the 3' half of the rRNA. On the 25S rRNA, most early-binding r-protein contacts are also on the 5' half (~70%), although late-binding protein contacts are evenly distributed between 5' and 3' half.

At the intersubunit interface of the ribosome, six r-proteins from the 60S make contacts with18S rRNA (eL19, eL24, eL41, eL43, uL14, and uL2), and three 40S r-proteins make contacts with the 25S rRNA (eS1, eS8, and uS19). There are four snoRNA-guided rRNA modifications at the 18S rRNA subunit interface (at sites U999, C1007, U1181, and G1126) and eight at the 25S rRNA interface (at sites A2256, U2258, U2260, U2264, U2266, A2280, A2281, and G2288). While these modifications are critical for ribosome biogenesis and fidelity (12), the precise role they play and how they affect ribosomal subunit joining is not yet understood.

Timing of snoRNA-guided rRNA modifications

In yeast, most snoRNA-guided rRNA modifications are deposited early in ribosome biogenesis, primarily co-transcriptionally (66). Eight snoRNA-guided modifications are deposited later during nuclear ribosome biogenesis (18S- Am100, 25S- Am817, Gm867, Am876, Um898, Am2256, Um2421, and Am2640) (3,67). Why these snoRNAs act later on pre-ribosomes is not yet known. One hypothesis is that these snoRNAs are dependent on helicases (3). Some rRNA modifications are dependent on helicases for structural remodeling of pre-ribosomes, allowing snoRNAs to access their target site (79). Another hypothesis is that late-acting snoRNAs compete with other snoRNAs for rRNA binding. Supporting the model that snoRNAs compete for rRNA binding, introduction of an artificial snoRNA impacts levels of modification at adjacent sites (67). The binding regions of seven of the eight late-acting snoRNAs overlap with other snoRNA binding regions. This supports a hierarchal model of rRNA modification, where late-binding snoRNAs can

compete for binding with early-acting snoRNAs.

Methods for the study of snoRNAs in yeast

The model eukaryotic organism budding yeast is a powerful tool for the study of snoRNAs and the rRNA modifications which they guide (3). The sequence and structural homology of the snoRNAs between yeast and human has suggested that most snoRNA functions are conserved in all eukaryotes. For example, over 80% of yeast snoRNAs and their corresponding functions in ribosome biogenesis are conserved in humans (29). However, yeast and humans also have differences with regards to the total number of expressed snoRNAs, the diversity of snoRNA sizes, the genome organization and expression of snoRNAs, and the non-ribosomal functions of snoRNAs (7,26,49). Thus, even though a yeast model is insufficient for understanding all aspects of snoRNA biogenesis and function that are relevant for human health, yeast provide a robust model system for studying the conserved and fundamental roles of snoRNAs, in particular snoRNA functions in ribosome biogenesis and translation regulation. The genetic malleability of yeast has allowed for rapid characterization of conserved snoRNA features, roles, and interactions (3,5,7,8,34). In this section, I review the tools that researchers have used for studies of snoRNAs in yeast cells (**Table 1**).

Knocking out snoRNAs in yeast

Because most snoRNAs in yeast are not essential for cell survival, both classical and recent studies of snoRNAs and rRNA modifications have employed deletion of either a single snoRNA gene or a cluster of multiple snoRNA genes (12,14-18,23,28,80-88). Early studies to uncover the functions of snoRNAs revealed that loss of most individual snoRNAs has no impact on the cell growth, and even combinatorial deletions of the snoRNA genes known at the time did not cause any apparent cellular defects (80,89). As a more complete rRNA epitranscriptome emerged, a

number of studies on the functions of rRNA modifications employed systematic deletion of multiple snoRNAs which guide modifications in the same critical region of the ribosome. For example, yeast strains with multiple snoRNA deletions that result in loss of modifications in helix 69, the decoding center, the peptidyl transferase center, and the A-site finger revealed the importance of rRNA modifications in maintaining ribosome structure, translation efficiency, and fidelity (12,14-18).

Eight yeast snoRNAs are encoded within introns, complicating simple snoRNA deletion for studying their function. To knockout intronic snoRNAs without disrupting the function of its host gene, most studies have employed knockout of the snoRNA and the host gene, transforming in either the snoRNA gene (often in the intron of another gene) or the host gene without its snoRNA intron on a plasmid (12,81,88,90,91). Overall, the ease of snoRNA gene deletion by homologous recombination in yeast continues to be a valuable tool for fundamental studies of snoRNAs and the snoRNA-guided rRNA modifications. A careful assessment of snoRNA gene location and proximity to other coding or noncoding genomic elements should be a critical consideration for studies involving snoRNA knockouts.

Ectopic expression of snoRNAs in yeast

Three yeast snoRNAs (U3, U14, and snR30), which are involved in rRNA processing, are essential for cell survival in yeast and thus cannot be studied by knockout experiments. The expression of essential snoRNAs can be regulated using a tunable promoter. Most commonly, the endogenous promoter of a snoRNA is replaced with the galactose-inducible promoter (e.g. *GAL1*) within the genomic locus, allowing for expression of the snoRNA in galactose media and repression of its expression in glucose media (22,24,92-97). Similarly, the expression of essential snoRNA genes can be regulated by deleting the snoRNA gene in a strain carrying a plasmid copy

of the snoRNA gene under the control of the *GAL1* promoter (19). The *GAL* promoter has also been used to control the expression of many other non-essential snoRNAs and snoRNA mutants (12,84,97-102). Constitutive promoters such as *ADH* and *GPD* have also been used for overexpression of snoRNAs (2,33,36). It is important to note that, under these conditions, the expression levels of the snoRNAs are not comparable to their physiological levels, which may be intentional for specific studies but may also cause unexpected outcomes. For example, overexpression of snoRNAs can saturate their transacting factors and result in blocking a step in their localization pathway which leads to snoRNA accumulation in the nucleolar body (103).

Expression of the wild-type or mutant snoRNAs from plasmids with their endogenous promoter and terminator is also commonly used (22,23,82,84,95,96,104). Alternatively, snoRNAs can be cloned downstream of the promoters of other snoRNAs (12,24,84,105). Similar systems have also been developed to express polycistronic snoRNAs. For example, the U14 and snR190 snoRNAs have been expressed from plasmids using their own promoter and terminator (22,92,94,96). A polycistronic system which expresses 4 snoRNAs downstream of the snR84 promoter has also been used (12). Intronic snoRNAs, however, can require a splicing step as part of their maturation, complicating simpler snoRNA expression systems. Several expression systems have been used for the ectopic expression of intronic snoRNAs. In one expression system, intronic snoRNAs were cloned into the intron of the actin host gene downstream of a constitutive promoter (81,90,91,103). Other studies have utilized plasmids containing both the snoRNA and its own host gene under control of the *GAL1* promoter (98-101), which results in overexpression of both the snoRNA and the host gene.

Engineering artificial snoRNAs

Box C/D and box H/ACA snoRNAs are defined by conserved sequence features which are

necessary for proper protein binding and snoRNP formation. Box C/D snoRNAs contain the well-conserved box C and box D motifs along with the less-conserved box C' and box D' motifs, while box H/ACA snoRNAs contain the conserved box H and box ACA motifs. Extensive research in yeast has revealed the importance of these conserved sequence elements for protein binding, snoRNA processing, and rRNA modification by mutating residues within these conserved sequences (82,84,92,93,96,99,104). Outside the box motifs, mutations within guide regions of snoRNAs have also unveiled the importance of yeast snoRNAs U3, U14, snR10 and snR30 for coordinating pre-rRNA folding and processing (18,22,24,92,93,104). Non-conserved and nonfunctional sequences of yeast snoRNAs have also been manipulated to characterize their importance in snoRNA processing and structure, including the 5' UTR, the length of the sequence between boxes C and D, the length between the ACA box and target, and the intron sequence flanking the snoRNA (81,82,94,97).

Some snoRNAs serve multiple roles in ribosome biogenesis, such as guiding the modification of more than one rRNA site or playing roles in both rRNA modification and pre-rRNA processing. Thus, simple snoRNA deletion is not ideal to study the function of individual modifications guided by these snoRNAs. To explore the functions of individual rRNA modifications, mutations have been made in the snoRNA guide sequences which either disrupt base pairing between the guide and the target sequence or guide the snoRNP to modify an adjacent rRNA position (12,18,23), allowing independent characterization of functional snoRNA domains.

Several snoRNA expression systems have been engineered to allow manipulation of the guide sequence for the modification of alternative targets. Expression systems using U24 and the intronic snoRNA snR38 have been engineered to guide the 2'-O-methylation of alternative targets (72,101,106,107), and an H/ACA hybrid containing guide sequences from two different snoRNAs

has also been created (23). Yeast-optimized expression systems have also been created for both Xenopus and human snoRNAs, revealing that paradigms in snoRNA processing and snoRNA-guided modifications are conserved between lower and higher eukaryotes (105,108,109). Yeast snoRNA guide sequences have also been engineered to target non-ribosomal RNA target sites. For example, mutations in the guide sequence of snR50 that target 2'-O-methylations to *ACT1*, *RPL17A*, *COF1*, *PRE3*, *RPS13*, and *URP1* pre-mRNAs, prevent the splicing of these mRNAs, which decreases their expression (102). Guide sequence mutations in snR52 that target 2'-O-methylation of the telomerase RNA modulate telomerase activity (110). An engineered version of the H/ACA snoRNA snR81 targeting pseudouridylation to mRNAs suppresses nonsense codons (111). Overall, the proof of principle studies of engineered yeast and human snoRNAs that target precursor mRNAs, mature mRNAs, or the telomerase RNA suggest that snoRNA-targeted modification of specific RNAs could be considered as a potential therapeutic tool for treatment of cancer, aging, and other diseases (112). This emerging area appears as a promising aspect of snoRNA research that may inform the path to rational RNA drug design.

CRISPR-Cas mediated snoRNA gene manipulations

The majority of snoRNA manipulation studies in yeast have relied on either snoRNA deletion paired with expression of a mutant snoRNA on a plasmid or on homologous recombination to express the mutant snoRNA from the endogenous locus. Recent advances in CRISPR-Cas mediated genome editing have made snoRNA editing faster and more efficient. CRISPR-Cas genome editing has proved especially useful for studies of snoRNAs in mammalian cell lines (113-115). In yeast, CRISPR-Cas9 genome editing was recently employed to mutate the C-box of snR191 (116). With the emergence of new and efficient genome engineering tools, snoRNA gene editing is likely to be more widely employed for studies in yeast. Using CRISPR/Cas snoRNA

gene editing will allow for precise deletions or mutations without the need for complicated expression plasmids and without disrupting the nearby host genes, neighboring snoRNA genes, or endogenous expression and processing mechanisms.

Tagging, labelling and visualization of snoRNAs

Similar to other RNAs, tagging, labeling and probing are convenient methods to explore snoRNA processing and localization. For example, processing of snoRNAs can be monitored by pulse-labeling with 4-thiouracil (117) or northern blotting (97,118,119). Sequence tags which bind to fluorophores can also be inserted within the snoRNA gene and enable the determination of snoRNA localization (25,103,120). Sequence tags are also critically useful tools for discrimination between an exogenous snoRNA that is expressed in the presence of the endogenous snoRNA, for studies of snoRNA processing or localization. Fluorescence *in situ* hybridization (FISH) allows to track tagged or untagged snoRNA localization (94,97,121,122). Tags have been added to the 3'-end of snoRNAs (99,100), upstream of the box D (84), or into a hairpin in a snoRNA (104). Tagging has also been used for purification of snoRNAs in yeast and human cells (95). Major considerations in tagging snoRNAs include the complex structure of the snoRNAs and their processing and trafficking that can be disturbed by insertion of tags at inappropriate locations.

Summary of introduction

In this introduction, I have detailed what is known about snoRNAs, their assembly into active snoRNPs, their role in ribosome biogenesis, and the methods used to study snoRNAs in yeast. Despite our knowledge of snoRNA structures, interactomes, and functions, the precise steps and mechanisms of snoRNP assembly and how mutations in snoRNP assembly factors can cause disease were unknown. My dissertation work fills a gap in our knowledge of snoRNP assembly by characterizing novel aspects of the function of the snoRNP assembly factors Bcd1 and Hit1. In

this dissertation I discuss yeast models in which snoRNP assembly is globally dysregulated, allowing us to study the specific impacts of rRNA 2'-O-methylations on ribosome biogenesis and translation. This system provides an advance over the traditional cumbersome snoRNA deletion strategies discussed in this introduction. Finally, my dissertation work describes an example of how dysregulation of snoRNP assembly can impair translation in a disease model, illustrating the importance of studying snoRNAs and their functions.

References

1. Woolford, J. L., and Baserga, S. J. (2013) Ribosome biogenesis in the yeast Saccharomyces cerevisiae. *Genetics* **195**, 643-681
2. Klinge, S., and Woolford, J. L. (2019) Ribosome assembly coming into focus. *Nat Rev Mol Cell Biol* **20**, 116-131
3. Sloan, K. E., Warda, A. S., Sharma, S., Entian, K. D., Lafontaine, D. L. J., and Bohnsack, M. T. (2017) Tuning the ribosome: The influence of rRNA modification on eukaryotic ribosome biogenesis and function. *RNA Biol* **14**, 1138-1152
4. Taoka, M., Nobe, Y., Yamaki, Y., Sato, K., Ishikawa, H., Izumikawa, K., Yamauchi, Y., Hirota, K., Nakayama, H., Takahashi, N., and Isobe, T. (2018) Landscape of the complete RNA chemical modifications in the human 80S ribosome. *Nucleic Acids Res* **46**, 9289-9298
5. Decatur, W. A., and Fournier, M. J. (2003) RNA-guided nucleotide modification of ribosomal and other RNAs. *J Biol Chem* **278**, 695-698
6. Tollervey, D., and Kiss, T. (1997) Function and synthesis of small nucleolar RNAs. *Curr Opin Cell Biol* **9**, 337-342
7. Watkins, N. J., and Bohnsack, M. T. (2012) The box C/D and H/ACA snoRNPs: key players in the modification, processing and the dynamic folding of ribosomal RNA. *Wiley Interdiscip Rev RNA* **3**, 397-414
8. Massenet, S., Bertrand, E., and Verheggen, C. (2017) Assembly and trafficking of box C/D and H/ACA snoRNPs. *RNA Biol* **14**, 680-692
9. Monaco, P. L., Marcel, V., Diaz, J. J., and Catez, F. (2018) 2'-O-Methylation of Ribosomal RNA: Towards an Epitranscriptomic Control of Translation? *Biomolecules* **8**

10. Prusiner, P., Yathindra, N., and Sundaralingam, M. (1974) Effect of ribose O(2')-methylation on the conformation of nucleosides and nucleotides. *Biochim Biophys Acta* **366**, 115-123

11. Adamiak, D. A., Milecki, J., Popenda, M., Adamiak, R. W., Dauter, Z., and Rypniewski, W. R. (1997) Crystal structure of 2'-O-Me(CGCGCG)2, an RNA duplex at 1.30 A resolution. Hydration pattern of 2'-O-methylated RNA. *Nucleic Acids Res* **25**, 4599-4607

12. Liang, X. H., Liu, Q., and Fournier, M. J. (2007) rRNA modifications in an intersubunit bridge of the ribosome strongly affect both ribosome biogenesis and activity. *Mol Cell* **28**, 965-977

13. Khoshnevis, S., Dreggors-Walker, R. E., Marchand, V., Motorin, Y., and Ghalei, H. (2022) Ribosomal RNA 2'-. *Proc Natl Acad Sci U S A* **119**, e2117334119

14. Baudin-Baillieu, A., Fabret, C., Liang, X. H., Piekna-Przybylska, D., Fournier, M. J., and Rousset, J. P. (2009) Nucleotide modifications in three functionally important regions of the Saccharomyces cerevisiae ribosome affect translation accuracy. *Nucleic Acids Res* **37**, 7665-7677

15. Liang, X. H., Liu, Q., and Fournier, M. J. (2009) Loss of rRNA modifications in the decoding center of the ribosome impairs translation and strongly delays pre-rRNA processing. *RNA* **15**, 1716-1728

16. Baxter-Roshek, J. L., Petrov, A. N., and Dinman, J. D. (2007) Optimization of ribosome structure and function by rRNA base modification. *PLoS One* **2**, e174

17. Piekna-Przybylska, D., Przybylski, P., Baudin-Baillieu, A., Rousset, J. P., and Fournier, M. J. (2008) Ribosome performance is enhanced by a rich cluster of pseudouridines in the A-site finger region of the large subunit. *J Biol Chem* **283**, 26026-26036

18. King, T. H., Liu, B., McCully, R. R., and Fournier, M. J. (2003) Ribosome structure and activity are altered in cells lacking snoRNPs that form pseudouridines in the peptidyl transferase center. *Mol Cell* **11**, 425-435

19. Li, H. D., Zagorski, J., and Fournier, M. J. (1990) Depletion of U14 small nuclear RNA (snR128) disrupts production of 18S rRNA in Saccharomyces cerevisiae. *Mol Cell Biol* **10**, 1145-1152

20. Hughes, J. M., and Ares, M. (1991) Depletion of U3 small nucleolar RNA inhibits cleavage in the 5' external transcribed spacer of yeast pre-ribosomal RNA and impairs formation of 18S ribosomal RNA. *EMBO J* **10**, 4231-4239

21. Beltrame, M., and Tollervey, D. (1995) Base pairing between U3 and the pre-ribosomal RNA is required for 18S rRNA synthesis. *EMBO J* **14**, 4350-4356

22. Liang, W. Q., and Fournier, M. J. (1995) U14 base-pairs with 18S rRNA: a novel snoRNA interaction required for rRNA processing. *Genes Dev* **9**, 2433-2443

23. Liang, X. H., Liu, Q., King, T. H., and Fournier, M. J. (2010) Strong dependence between functional domains in a dual-function snoRNA infers coupling of rRNA processing and modification events. *Nucleic Acids Res* **38**, 3376-3387

24. Atzorn, V., Fragapane, P., and Kiss, T. (2004) U17/snR30 is a ubiquitous snoRNA with two conserved sequence motifs essential for 18S rRNA production. *Mol Cell Biol* **24**, 1769-1778

25. Fayet-Lebaron, E., Atzorn, V., Henry, Y., and Kiss, T. (2009) 18S rRNA processing requires base pairings of snR30 H/ACA snoRNA to eukaryote-specific 18S sequences. *EMBO J* **28**, 1260-1270

26. Bratkovič, T., Božič, J., and Rogelj, B. (2020) Functional diversity of small nucleolar RNAs. *Nucleic Acids Res* **48**, 1627-1651

27. Sharma, S., Yang, J., van Nues, R., Watzinger, P., Kötter, P., Lafontaine, D. L. J., Granneman, S., and Entian, K. D. (2017) Specialized box C/D snoRNPs act as antisense guides to target RNA base acetylation. *PLoS Genet* **13**, e1006804

28. Dudnakova, T., Dunn-Davies, H., Peters, R., and Tollervey, D. (2018) Mapping targets for small nucleolar RNAs in yeast. *Wellcome Open Res* **3**, 120

29. Lestrade, L., and Weber, M. J. (2006) snoRNA-LBME-db, a comprehensive database of human H/ACA and C/D box snoRNAs. *Nucleic Acids Res* **34**, D158-162

30. Bouchard-Bourelle, P., Desjardins-Henri, C., Mathurin-St-Pierre, D., Deschamps-Francoeur, G., Fafard-Couture, É., Garant, J. M., Elela, S. A., and Scott, M. S. (2020) snoDB: an interactive database of human snoRNA sequences, abundance and interactions. *Nucleic Acids Res* **48**, D220-D225

31. Marchand, V., Blanloeil-Oillo, F., Helm, M., and Motorin, Y. (2016) Illumina-based RiboMethSeq approach for mapping of 2'-O-Me residues in RNA. *Nucleic Acids Res* **44**, e135

32. Marchand, V., Pichot, F., Neybecker, P., Ayadi, L., Bourguignon-Igel, V., Wacheul, L., Lafontaine, D. L. J., Pinzano, A., Helm, M., and Motorin, Y. (2020) HydraPsiSeq: a method for systematic and quantitative mapping of pseudouridines in RNA. *Nucleic Acids Res* **48**, e110

33. Ferretti, M. B., and Karbstein, K. (2019) Does functional specialization of ribosomes really exist? *RNA* **25**, 521-538

34. Baldini, L., Charpentier, B., and Labialle, S. (2021) Emerging Data on the Diversity of Molecular Mechanisms Involving C/D snoRNAs. *Noncoding RNA* **7**

35. Brandis, K. A., Gale, S., Jinn, S., Langmade, S. J., Dudley-Rucker, N., Jiang, H., Sidhu, R., Ren, A., Goldberg, A., Schaffer, J. E., and Ory, D. S. (2013) Box C/D small nucleolar RNA (snoRNA) U60 regulates intracellular cholesterol trafficking. *J Biol Chem* **288**, 35703-35713

36. Jinn, S., Brandis, K. A., Ren, A., Chacko, A., Dudley-Rucker, N., Gale, S. E., Sidhu, R., Fujiwara, H., Jiang, H., Olsen, B. N., Schaffer, J. E., and Ory, D. S. (2015) snoRNA U17 regulates cellular cholesterol trafficking. *Cell Metab* **21**, 855-867

37. Falaleeva, M., Pages, A., Matuszek, Z., Hidmi, S., Agranat-Tamir, L., Korotkov, K., Nevo, Y., Eyras, E., Sperling, R., and Stamm, S. (2016) Dual function of C/D box small nucleolar RNAs in rRNA modification and alternative pre-mRNA splicing. *Proc Natl Acad Sci U S A* **113**, E1625-1634

38. Kufel, J., and Grzechnik, P. (2019) Small Nucleolar RNAs Tell a Different Tale. *Trends Genet* **35**, 104-117

39. Mills, E. W., and Green, R. (2017) Ribosomopathies: There's strength in numbers. *Science* **358**

40. Sulima, S. O., Kampen, K. R., and De Keersmaecker, K. (2019) Cancer Biogenesis in Ribosomopathies. *Cells* **8**

41. Farley-Barnes, K. I., Ogawa, L. M., and Baserga, S. J. (2019) Ribosomopathies: Old Concepts, New Controversies. *Trends Genet* **35**, 754-767

42. Narla, A., and Ebert, B. L. (2010) Ribosomopathies: human disorders of ribosome dysfunction. *Blood* **115**, 3196-3205

43. Yelick, P. C., and Trainor, P. A. (2015) Ribosomopathies: Global process, tissue specific defects. *Rare Dis* **3**, e1025185

44. Danilova, N., and Gazda, H. T. (2015) Ribosomopathies: how a common root can cause a tree of pathologies. *Dis Model Mech* **8**, 1013-1026

45. Kampen, K. R., Sulima, S. O., Vereecke, S., and De Keersmaecker, K. (2019) Hallmarks of ribosomopathies. *Nucleic Acids Res*

46. Deogharia, M., and Majumder, M. (2018) Guide snoRNAs: Drivers or Passengers in Human Disease? *Biology (Basel)* **8**

47. McMahon, M., Contreras, A., and Ruggero, D. (2015) Small RNAs with big implications: new insights into H/ACA snoRNA function and their role in human disease. *Wiley Interdiscip Rev RNA* **6**, 173-189

48. Harismendy, O., Gendrel, C. G., Soularue, P., Gidrol, X., Sentenac, A., Werner, M., and Lefebvre, O. (2003) Genome-wide location of yeast RNA polymerase III transcription machinery. *EMBO J* **22**, 4738-4747

49. Dieci, G., Preti, M., and Montanini, B. (2009) Eukaryotic snoRNAs: a paradigm for gene expression flexibility. *Genomics* **94**, 83-88

50. Rothe, B., Saliou, J. M., Quinternet, M., Back, R., Tiotiu, D., Jacquemin, C., Loegler, C., Schlotter, F., Pena, V., Eckert, K., Morera, S., Dorsselaer, A. V., Branlant, C., Massenet, S., Sanglier-Cianferani, S., Manival, X., and Charpentier, B. (2014) Protein Hit1, a novel box C/D snoRNP assembly factor, controls cellular concentration of the scaffolding protein Rsa1 by direct interaction. *Nucleic Acids Res* **42**, 10731-10747

51. Bizarro, J., Charron, C., Boulon, S., Westman, B., Pradet-Balade, B., Vandermoere, F., Chagot, M. E., Hallais, M., Ahmad, Y., Leonhardt, H., Lamond, A., Manival, X.,

Branlant, C., Charpentier, B., Verheggen, C., and Bertrand, E. (2014) Proteomic and 3D structure analyses highlight the C/D box snoRNP assembly mechanism and its control. *J Cell Biol* **207**, 463-480

52. Paul, A., Tiotiu, D., Bragantini, B., Marty, H., Charpentier, B., Massenet, S., and Labialle, S. (2019) Bcd1p controls RNA loading of the core protein Nop58 during C/D box snoRNP biogenesis. *RNA* **25**, 496-506

53. Khoshnevis, S., Dreggors, R. E., Hoffmann, T. F. R., and Ghalei, H. (2019) A conserved Bcd1 interaction essential for box C/D snoRNP biogenesis. *J Biol Chem*

54. McKeegan, K. S., Debieux, C. M., and Watkins, N. J. (2009) Evidence that the AAA+ proteins TIP48 and TIP49 bridge interactions between 15.5K and the related NOP56 and NOP58 proteins during box C/D snoRNP biogenesis. *Mol Cell Biol* **29**, 4971-4981

55. Kakihara, Y., Makhnevych, T., Zhao, L., Tang, W., and Houry, W. A. (2014) Nutritional status modulates box C/D snoRNP biogenesis by regulated subcellular relocalization of the R2TP complex. *Genome Biol* **15**, 404

56. Fatica, A., Dlakić, M., and Tollervey, D. (2002) Naf1 p is a box H/ACA snoRNP assembly factor. *RNA* **8**, 1502-1514

57. Grozdanov, P. N., Roy, S., Kittur, N., and Meier, U. T. (2009) SHQ1 is required prior to NAF1 for assembly of H/ACA small nucleolar and telomerase RNPs. *RNA* **15**, 1188-1197

58. Machado-Pinilla, R., Liger, D., Leulliot, N., and Meier, U. T. (2012) Mechanism of the AAA+ ATPases pontin and reptin in the biogenesis of H/ACA RNPs. *RNA* **18**, 1833-1845

59. Piekna-Przybylska, D., Decatur, W. A., and Fournier, M. J. (2007) New bioinformatic tools for analysis of nucleotide modifications in eukaryotic rRNA. *RNA* **13**, 305-312

60. Lin, J., Lai, S., Jia, R., Xu, A., Zhang, L., Lu, J., and Ye, K. (2011) Structural basis for site-specific ribose methylation by box C/D RNA protein complexes. *Nature* **469**, 559-563

61. Yang, Z., Lin, J., and Ye, K. (2016) Box C/D guide RNAs recognize a maximum of 10 nt of substrates. *Proc Natl Acad Sci U S A* **113**, 10878-10883

62. Kiss, A. M., Jády, B. E., Bertrand, E., and Kiss, T. (2004) Human box H/ACA pseudouridylation guide RNA machinery. *Mol Cell Biol* **24**, 5797-5807

63. De Zoysa, M. D., Wu, G., Katz, R., and Yu, Y. T. (2018) Guide-substrate base-pairing requirement for box H/ACA RNA-guided RNA pseudouridylation. *RNA* **24**, 1106-1117

64. van Nues, R. W., Granneman, S., Kudla, G., Sloan, K. E., Chicken, M., Tollervey, D., and Watkins, N. J. (2011) Box C/D snoRNP catalysed methylation is aided by additional pre-rRNA base-pairing. *EMBO J* **30**, 2420-2430

65. van Nues, R. W., and Watkins, N. J. (2017) Unusual C′/D′ motifs enable box C/D snoRNPs to modify multiple sites in the same rRNA target region. *Nucleic Acids Research* **45**, 2016-2028

66. Kos, M., and Tollervey, D. (2010) Yeast pre-rRNA processing and modification occur cotranscriptionally. *Mol Cell* **37**, 809-820

67. Birkedal, U., Christensen-Dalsgaard, M., Krogh, N., Sabarinathan, R., Gorodkin, J., and Nielsen, H. (2015) Profiling of ribose methylations in RNA by high-throughput sequencing. *Angew Chem Int Ed Engl* **54**, 451-455

68. Decatur, W. A., and Fournier, M. J. (2002) rRNA modifications and ribosome function. *Trends Biochem Sci* **27**, 344-351

69. Helm, M. (2006) Post-transcriptional nucleotide modification and alternative folding of RNA. *Nucleic Acids Res* **34**, 721-733

70. Abou Assi, H., Rangadurai, A. K., Shi, H., Liu, B., Clay, M. C., Erharter, K., Kreutz, C., Holley, C. L., and Al-Hashimi, H. M. (2020) 2'-O-Methylation can increase the abundance and lifetime of alternative RNA conformational states. *Nucleic Acids Res* **48**, 12365-12379

71. Ben-Shem, A., Garreau de Loubresse, N., Melnikov, S., Jenner, L., Yusupova, G., and Yusupov, M. (2011) The structure of the eukaryotic ribosome at 3.0 Å resolution. *Science* **334**, 1524-1529

72. Yelland, J. N., Bravo, J. P. K., Black, J. J., Taylor, D. W., and Johnson, A. W. (2022) A single 2'-O-methylation of ribosomal RNA gates assembly of a functional ribosome. *bioRxiv*, 2022.2002.2016.480697

73. Bergeron, D., Fafard-Couture, É., and Scott, M. S. (2020) Small nucleolar RNAs: continuing identification of novel members and increasing diversity of their molecular mechanisms of action. *Biochem Soc Trans* **48**, 645-656

74. Huang, H., and Karbstein, K. (2021) Assembly factors chaperone ribosomal RNA folding by isolating helical junctions that are prone to misfolding. *Proc Natl Acad Sci U S A* **118**

75. Barandun, J., Chaker-Margot, M., Hunziker, M., Molloy, K. R., Chait, B. T., and Klinge, S. (2017) The complete structure of the small-subunit processome. *Nat Struct Mol Biol* **24**, 944-953

76. Granneman, S., Petfalski, E., Swiatkowska, A., and Tollervey, D. (2010) Cracking pre-40S ribosomal subunit structure by systematic analyses of RNA-protein cross-linking. *EMBO J* **29**, 2026-2036

77. Strunk, B. S., Loucks, C. R., Su, M., Vashisth, H., Cheng, S., Schilling, J., Brooks, C. L., Karbstein, K., and Skiniotis, G. (2011) Ribosome assembly factors prevent premature translation initiation by 40S assembly intermediates. *Science* **333**, 1449-1453

78. de la Cruz, J., Karbstein, K., and Woolford, J. L. (2015) Functions of ribosomal proteins in assembly of eukaryotic ribosomes in vivo. *Annu Rev Biochem* **84**, 93-129

79. Leeds, N. B., Small, E. C., Hiley, S. L., Hughes, T. R., and Staley, J. P. (2006) The splicing factor Prp43p, a DEAH box ATPase, functions in ribosome biogenesis. *Mol Cell Biol* **26**, 513-522

80. Samarsky, D. A., Balakin, A. G., and Fournier, M. J. (1995) Characterization of three new snRNAs from Saccharomyces cerevisiae: snR34, snR35 and snR36. *Nucleic Acids Res* **23**, 2548-2554

81. Kiss-Laszlo, Z., Henry, Y., Bachellerie, J. P., Caizergues-Ferrer, M., and Kiss, T. (1996) Site-specific ribose methylation of preribosomal RNA: a novel function for small nucleolar RNAs. *Cell* **85**, 1077-1088

82. Ni, J., Tien, A. L., and Fournier, M. J. (1997) Small nucleolar RNAs direct site-specific synthesis of pseudouridine in ribosomal RNA. *Cell* **89**, 565-573

83. Lowe, T. M., and Eddy, S. R. (1999) A computational screen for methylation guide snoRNAs in yeast. *Science* **283**, 1168-1171

84. Morlando, M., Ballarino, M., Greco, P., Caffarelli, E., Dichtl, B., and Bozzoni, I. (2004) Coupling between snoRNP assembly and 3' processing controls box C/D snoRNA biosynthesis in yeast. *EMBO J* **23**, 2392-2401

85. Torchet, C., Badis, G., Devaux, F., Costanzo, G., Werner, M., and Jacquier, A. (2005) The complete set of H/ACA snoRNAs that guide rRNA pseudouridylations in Saccharomyces cerevisiae. *RNA* **11**, 928-938

86. Esguerra, J., Warringer, J., and Blomberg, A. (2008) Functional importance of individual rRNA 2'-O-ribose methylations revealed by high-resolution phenotyping. *RNA* **14**, 649-656

87. Begik, O., Lucas, M. C., Pryszcz, L. P., Ramirez, J. M., Medina, R., Milenkovic, I., Cruciani, S., Liu, H., Vieira, H. G. S., Sas-Chen, A., Mattick, J. S., Schwartz, S., and Novoa, E. M. (2021) Quantitative profiling of pseudouridylation dynamics in native RNAs with nanopore sequencing. *Nat Biotechnol* **39**, 1278-1291

88. Badis, G., Fromont-Racine, M., and Jacquier, A. (2003) A snoRNA that guides the two most conserved pseudouridine modifications within rRNA confers a growth advantage in yeast. *RNA* **9**, 771-779

89. Parker, R., Simmons, T., Shuster, E. O., Siliciano, P. G., and Guthrie, C. (1988) Genetic analysis of small nuclear RNAs in Saccharomyces cerevisiae: viable sextuple mutant. *Mol Cell Biol* **8**, 3150-3159

90. Li, Z., Lee, I., Moradi, E., Hung, N. J., Johnson, A. W., and Marcotte, E. M. (2009) Rational extension of the ribosome biogenesis pathway using network-guided genetics. *PLoS Biol* **7**, e1000213

91. Kouba, T., Rutkai, E., Karásková, M., and Valášek, L. (2012) The eIF3c/NIP1 PCI domain interacts with RNA and RACK1/ASC1 and promotes assembly of translation preinitiation complexes. *Nucleic Acids Res* **40**, 2683-2699

92. Jarmolowski, A., Zagorski, J., Li, H. V., and Fournier, M. J. (1990) Identification of essential elements in U14 RNA of Saccharomyces cerevisiae. *EMBO J* **9**, 4503-4509

93. Samarsky, D. A., and Fournier, M. J. (1998) Functional mapping of the U3 small nucleolar RNA from the yeast Saccharomyces cerevisiae. *Mol Cell Biol* **18**, 3431-3444

94. Samarsky, D. A., Fournier, M. J., Singer, R. H., and Bertrand, E. (1998) The snoRNA box C/D motif directs nucleolar targeting and also couples snoRNA synthesis and localization. *EMBO J* **17**, 3747-3757

95. Lemay, V., Hossain, A., Osheim, Y. N., Beyer, A. L., and Dragon, F. (2011) Identification of novel proteins associated with yeast snR30 small nucleolar RNA. *Nucleic Acids Res* **39**, 9659-9670

96. Huang, G. M., Jarmolowski, A., Struck, J. C., and Fournier, M. J. (1992) Accumulation of U14 small nuclear RNA in Saccharomyces cerevisiae requires box C, box D, and a 5', 3' terminal stem. *Mol Cell Biol* **12**, 4456-4463

97. Grzechnik, P., Szczepaniak, S. A., Dhir, S., Pastucha, A., Parslow, H., Matuszek, Z., Mischo, H. E., Kufel, J., and Proudfoot, N. J. (2018) Nuclear fate of yeast snoRNA is determined by co-transcriptional Rnt1 cleavage. *Nat Commun* **9**, 1783

98. Ooi, S. L., Samarsky, D. A., Fournier, M. J., and Boeke, J. D. (1998) Intronic snoRNA biosynthesis in Saccharomyces cerevisiae depends on the lariat-debranching enzyme: intron length effects and activity of a precursor snoRNA. *RNA* **4**, 1096-1110

99. Vincenti, S., De Chiara, V., Bozzoni, I., and Presutti, C. (2007) The position of yeast snoRNA-coding regions within host introns is essential for their biosynthesis and for efficient splicing of the host pre-mRNA. *RNA* **13**, 138-150

100. Villa, T., Ceradini, F., Presutti, C., and Bozzoni, I. (1998) Processing of the intron-encoded U18 small nucleolar RNA in the yeast Saccharomyces cerevisiae relies on both exo- and endonucleolytic activities. *Mol Cell Biol* **18**, 3376-3383

101. Liu, B., Liang, X. H., Piekna-Przybylska, D., Liu, Q., and Fournier, M. J. (2008) Mis-targeted methylation in rRNA can severely impair ribosome synthesis and activity. *RNA Biol* **5**, 249-254

102. Zhao, X., and Yu, Y. T. (2008) Targeted pre-mRNA modification for gene silencing and regulation. *Nat Methods* **5**, 95-100

103. Verheggen, C., Mouaikel, J., Thiry, M., Blanchard, J. M., Tollervey, D., Bordonné, R., Lafontaine, D. L., and Bertrand, E. (2001) Box C/D small nucleolar RNA trafficking involves small nucleolar RNP proteins, nucleolar factors and a novel nuclear domain. *EMBO J* **20**, 5480-5490

104. Wormsley, S., Samarsky, D. A., Fournier, M. J., and Baserga, S. J. (2001) An unexpected, conserved element of the U3 snoRNA is required for Mpp10p association. *RNA* **7**, 904-919

105. Kiss-László, Z., Henry, Y., and Kiss, T. (1998) Sequence and structural elements of methylation guide snoRNAs essential for site-specific ribose methylation of pre-rRNA. *EMBO J* **17**, 797-807

106. Liu, B., and Fournier, M. J. (2004) Interference probing of rRNA with snoRNPs: a novel approach for functional mapping of RNA in vivo. *RNA* **10**, 1130-1141

107. Liu, B., Ni, J., and Fournier, M. J. (2001) Probing RNA in vivo with methylation guide small nucleolar RNAs. *Methods* **23**, 276-286

108. Deryusheva, S., Talross, G. J. S., and Gall, J. G. (2021) SnoRNA guide activities: real and ambiguous. *RNA* **27**, 1363-1373

109. Talross, G. J. S., Deryusheva, S., and Gall, J. G. (2021) Stable lariats bearing a snoRNA (slb-snoRNA) in eukaryotic cells: A level of regulation for guide RNAs. *Proc Natl Acad Sci U S A* **118**

110. Huang, C., and Yu, Y. T. (2010) Targeted 2'-O methylation at a nucleotide within the pseudoknot of telomerase RNA reduces telomerase activity in vivo. *Mol Cell Biol* **30**, 4368-4378

111. Karijolich, J., and Yu, Y. T. (2011) Converting nonsense codons into sense codons by targeted pseudouridylation. *Nature* **474**, 395-398

112. Adachi, H., Hengesbach, M., Yu, Y. T., and Morais, P. (2021) From Antisense RNA to RNA Modification: Therapeutic Potential of RNA-Based Technologies. *Biomedicines* **9**

113. Bochukova, E. G., Lawler, K., Croizier, S., Keogh, J. M., Patel, N., Strohbehn, G., Lo, K. K., Humphrey, J., Hokken-Koelega, A., Damen, L., Donze, S., Bouret, S. G., Plagnol, V., and Farooqi, I. S. (2018) A Transcriptomic Signature of the Hypothalamic Response to Fasting and BDNF Deficiency in Prader-Willi Syndrome. *Cell Rep* **22**, 3401-3408

114. Filippova, J. A., Matveeva, A. M., Zhuravlev, E. S., Balakhonova, E. A., Prokhorova, D. V., Malanin, S. J., Shah Mahmud, R., Grigoryeva, T. V., Anufrieva, K. S., Semenov, D. V., Vlassov, V. V., and Stepanov, G. A. (2019) Are Small Nucleolar RNAs "CRISPRable"? A Report on Box C/D Small Nucleolar RNA Editing in Human Cells. *Front Pharmacol* **10**, 1246

115. Vitali, P., and Kiss, T. (2019) Cooperative 2'-O-methylation of the wobble cytidine of human elongator tRNA. *Genes Dev* **33**, 741-746

116. Jaafar, M., Contreras, J., Dominique, C., Martín-Villanueva, S., Capeyrou, R., Vitali, P., Rodríguez-Galán, O., Velasco, C., Humbert, O., Watkins, N. J., Villalobo, E., Bohnsack, K. E., Bohnsack, M. T., Henry, Y., Merhi, R. A., de la Cruz, J., and Henras, A. K. (2021) Association of snR190 snoRNA chaperone with early pre-60S particles is regulated by the RNA helicase Dbp7 in yeast. *Nat Commun* **12**, 6153

117. Barrass, J. D., Reid, J. E., Huang, Y., Hector, R. D., Sanguinetti, G., Beggs, J. D., and Granneman, S. (2015) Transcriptome-wide RNA processing kinetics revealed using extremely short 4tU labeling. *Genome Biol* **16**, 282

118. Fatica, A., Morlando, M., and Bozzoni, I. (2000) Yeast snoRNA accumulation relies on a cleavage-dependent/polyadenylation-independent 3'-processing apparatus. *EMBO J* **19**, 6218-6229

119. Peng, W.-T., Robinson, M. D., Mnaimneh, S., Krogan, N. J., Cagney, G., Morris, Q., Davierwala, A. P., Grigull, J., Yang, X., Zhang, W., Mitsakakis, N., Ryan, O. W., Datta, N., Jojic, V., Pal, C., Canadien, V., Richards, D., Beattie, B., Wu, L. F., Altschuler, S. J., Roweis, S., Frey, B. J., Emili, A., Greenblatt, J. F., and Hughes, T. R. (2003) A Panoramic View of Yeast Noncoding RNA Processing. *Cell* **113**, 919-933

120. Zinskie, J. A., Roig, M., Janetopoulos, C., Myers, K. A., and Bruist, M. F. (2018) Live-cell imaging of small nucleolar RNA tagged with the broccoli aptamer in yeast. *FEMS Yeast Res* **18**

121. Narayanan, A., Eifert, J., Marfatia, K. A., Macara, I. G., Corbett, A. H., Terns, R. M., and Terns, M. P. (2003) Nuclear RanGTP is not required for targeting small nucleolar RNAs to the nucleolus. *J Cell Sci* **116**, 177-186

122. Qiu, H., Eifert, J., Wacheul, L., Thiry, M., Berger, A. C., Jakovljevic, J., Woolford, J. L., Corbett, A. H., Lafontaine, D. L., Terns, R. M., and Terns, M. P. (2008) Identification of genes that function in the biogenesis and localization of small nucleolar RNAs in Saccharomyces cerevisiae. *Mol Cell Biol* **28**, 3686-3699

Figures

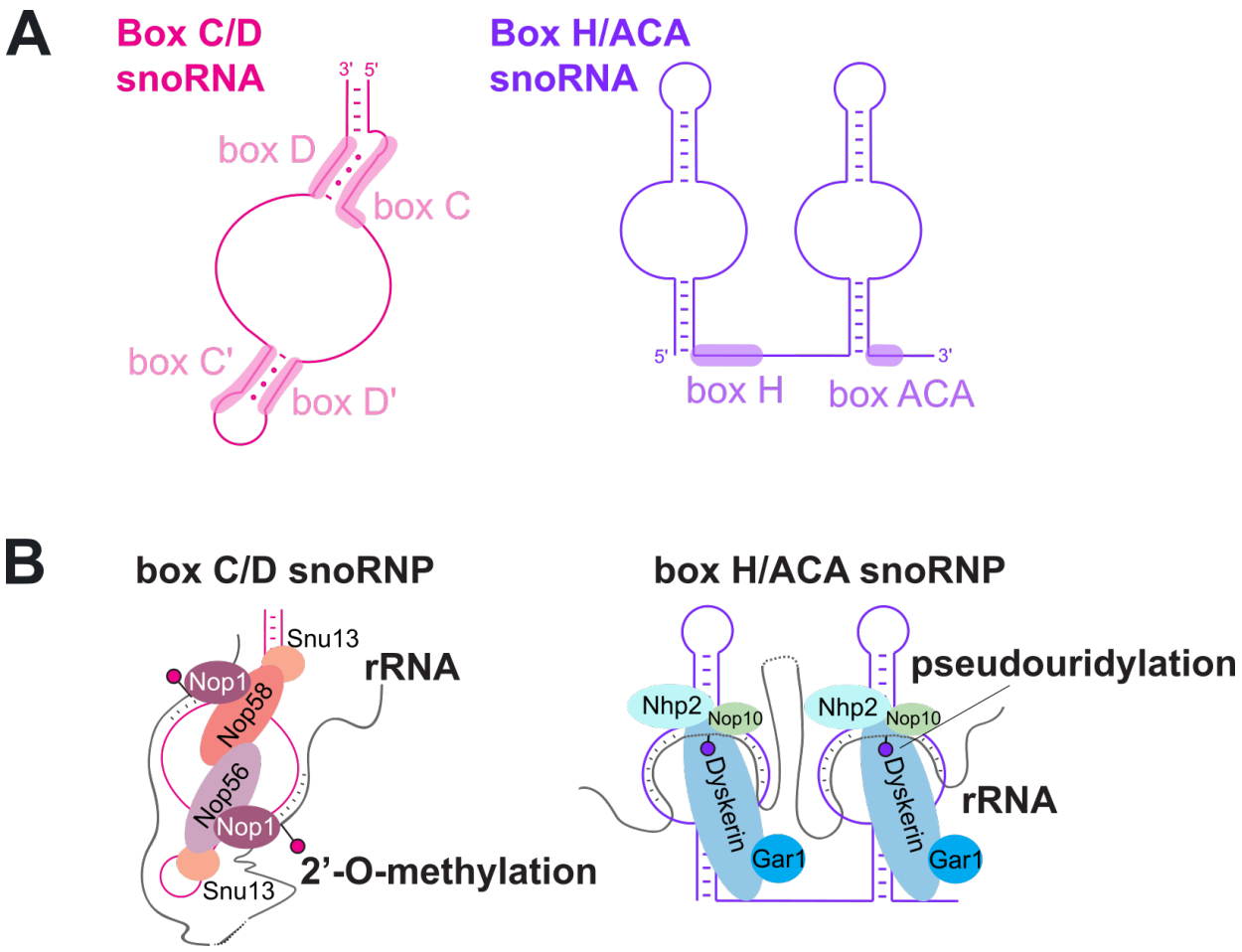

Figure 1. A) Box C/D and box H/ACA typical secondary structure. Conserved sequence regions are highlighted in pink for box C/D and purple for H/ACA. **B)** Schematic of the mature box C/D and box H/ACA snoRNPs.

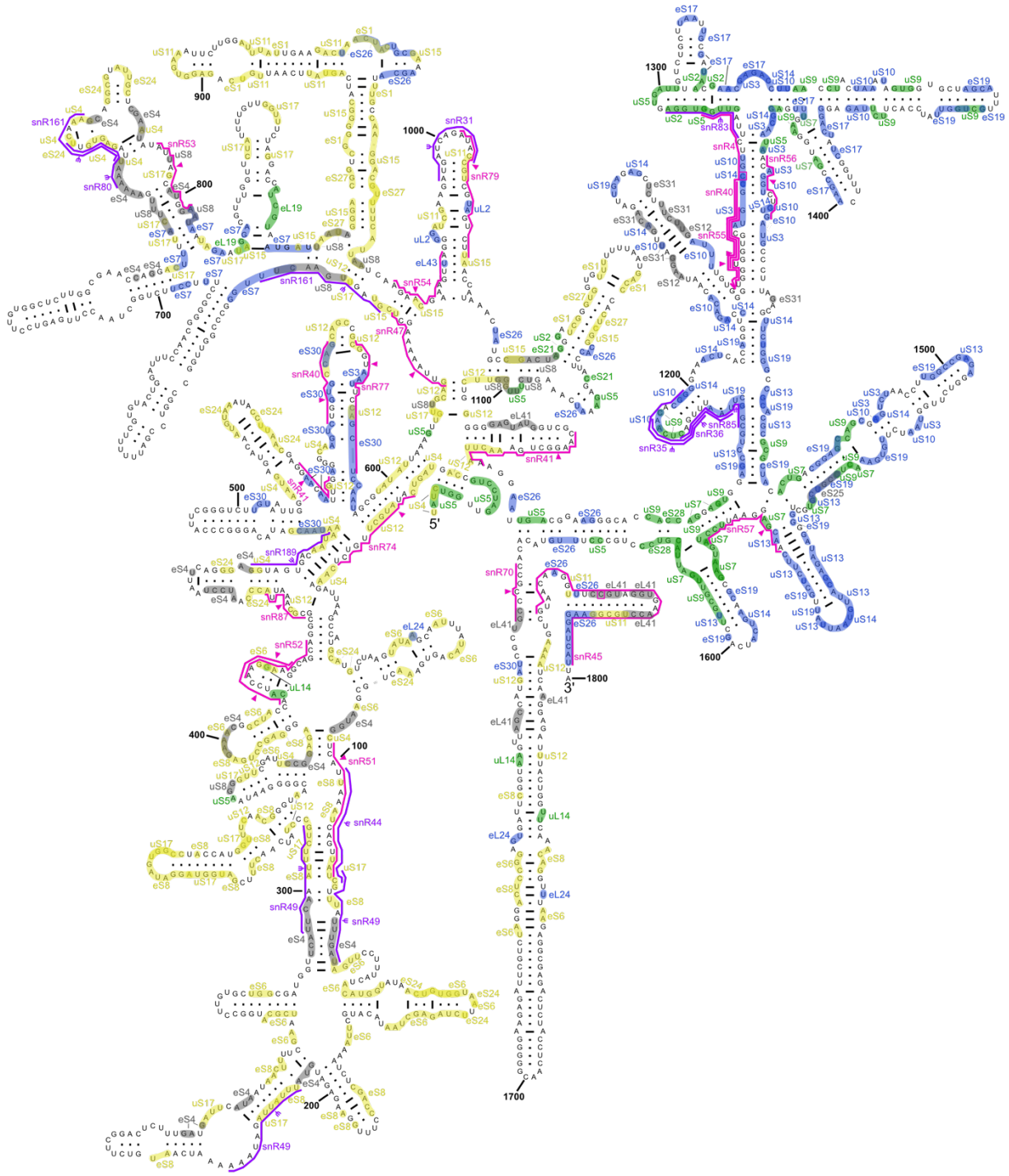

Figure 2. Secondary structure of the yeast 18S rRNA highlighting snoRNA and protein-binding regions. Structure downloaded from the Comparative RNA Web Site and Project at https://crw-site.chemistry.gatech.edu/DAT/. Protein binding sites mapped using PDB id: 4v88. Yellow

indicates early-binding r-protein contacts, green intermediate, blue late-binding, and grey unknown. Box C/D snoRNAs are indicated in magenta, with a magenta triangle indicating the 2'-O-methylation site. Box H/ACA snoRNAs are indicated in purple, and pseudouridylated sites are indicated with a Ψ.

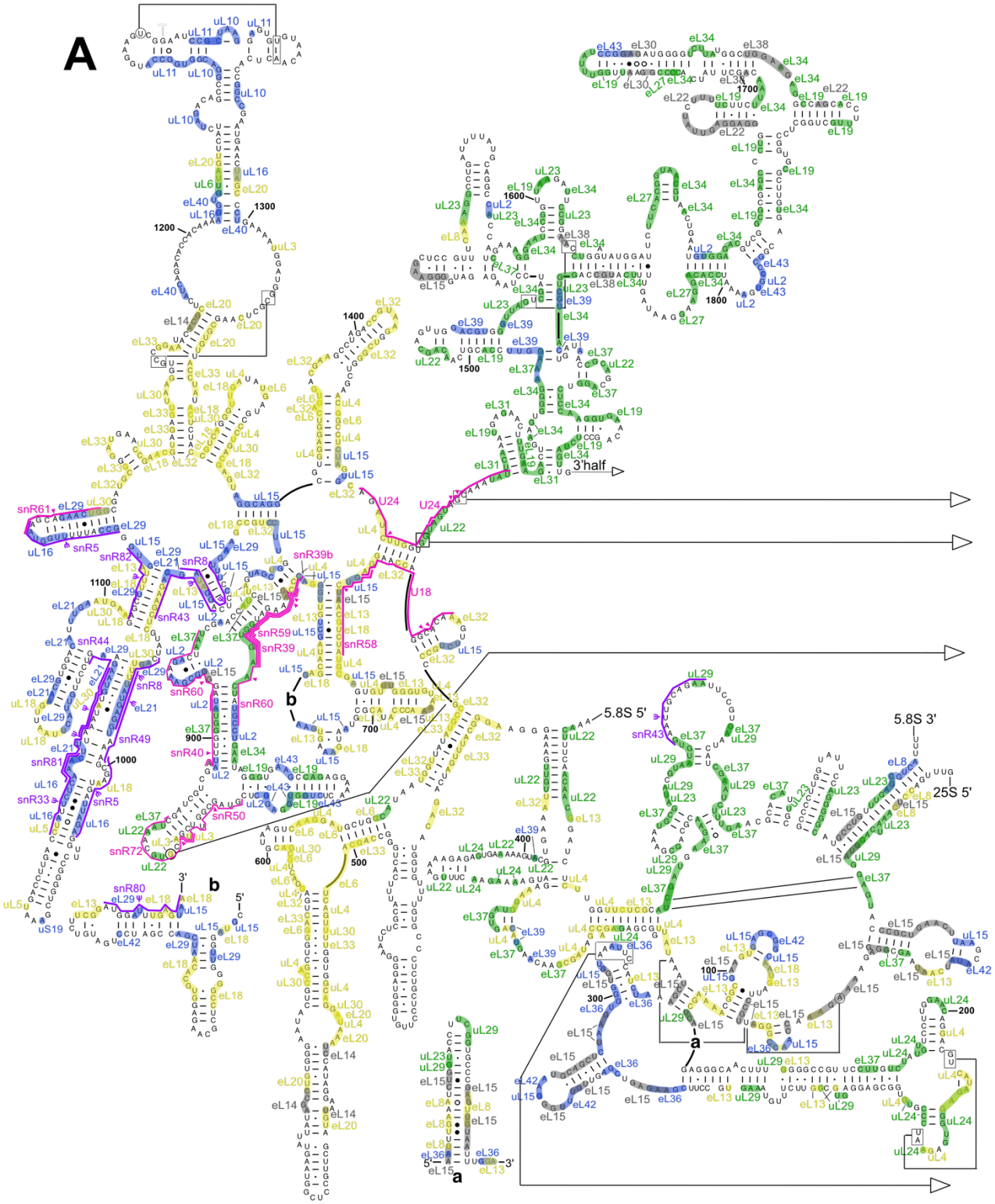
A
3'half
5.8S 5'
5.8S 3'
25S 5'
a
b

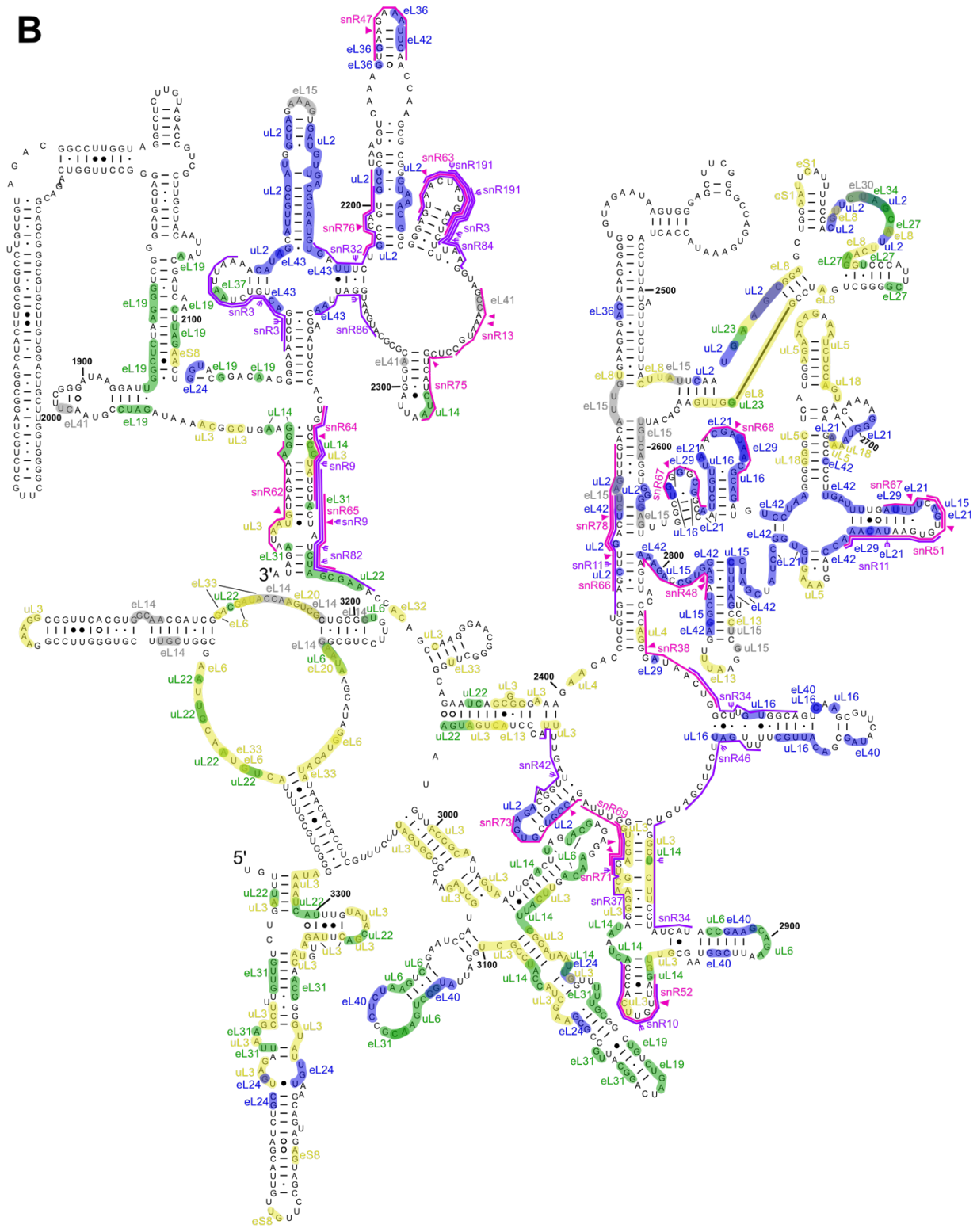

Figure 3. Secondary structure of the yeast 25S rRNA highlighting snoRNA and protein-binding regions. Structures downloaded from the Comparative RNA Web Site and Project at https://crw-

site.chemistry.gatech.edu/DAT/. Protein binding sites mapped using PDB id: 4v88. Yellow indicates early-binding r-protein contacts, green intermediate, blue late-binding, and grey unknown. Box C/D snoRNAs are indicated in magenta, with a magenta triangle indicating the 2'-O-methylation site. Box H/ACA snoRNAs are indicated in purple, and pseudouridylated sites are indicated with a Ψ. **A)** 5' half of the 25S rRNA, **B)** 3' half of the 25S rRNA.

Tables

Category	Tool/Method	Ref
snoRNA knockout	Deletion of single snoRNA genes	(80), (82), (83), (18), (84), (85), (12), (86), (23), (28), (87)
	Deletion of multiple snoRNA genes	(80), (18), (12), (17), (15), (16), (14), (89)
	Deletion of intronic snoRNA and host gene	(81), (12), (88), (90), (91)
snoRNA expression systems	snoRNA expression controlled by GAL1 promoter	(12), (22), (92), (93), (94), (95), (96), (97), (24), (19), (98), (99), (100), (101), (102)
	Exogenous snoRNA expression with own promoter and terminator	(82), (84), (23), (22), (95), (96), (104)
	Exogenous snoRNA expression with other snoRNA promoter	(84), (12), (24), (107)
	Intronic expression	(81), (90), (91), (98), (99), (100), (101), (103)
	Polycistronic expression	(12), (22), (92), (94), (96)
snoRNA engineering/ manipulation	Mutations of conserved elements	(82), (84), (22), (92), (93), (96), (99), (104)
	Mutations in guide sequence	(18), (12), (23)
	Modified snoRNA length	(81), (94), (97)
	Artificial yeast snoRNA	(23), (101), (102), (110), (106), (107), (72), (111)
	Yeast-optimized artificial snoRNAs from other species	(105), (108), (109)
	CRISPR-Cas9 mediated genome editing	(116)
snoRNA labelling	FISH	(94), (97), (121), (122)
	Spinach and broccoli RNA aptamers	(120)
	MS2 tag	(103), (25)
	Sequence tag on snoRNA for differentiation from endogenous snoRNA	(84), (99), (100), (104),
	S1 aptamer	(95)
	Pulse-labeling with 4-thiouracil (4tU)	(117)

Table 1. Tools and Methods to explore snoRNA function

Chapter 2. Studies of mutations of snoRNP assembly factor Hit1 in budding yeast suggest translation defects as the molecular basis for human PEHO syndrome

Summary

Using budding yeast models of the genetic disease PEHO syndrome, we show that PEHO-linked mutations result in loss of box C/D snoRNAs, impaired rRNA processing, decreased levels of rRNA 2'-O-methylations, impaired translation fidelity, and impaired ribosomal ligand binding. This provides the first insights into the molecular basis of PEHO syndrome and strongly suggest that PEHO syndrome is a ribosomopathy caused by impaired translation. I assisted in conceptualizing and performed almost all experiments, with the exception of RiboMeth-seq and the dual luciferase assay, and I performed all data analysis.

These findings were accepted for publication in *Journal of Biological Chemistry* in July, 2022. Supplemental tables can be found online.

Abstract

Regulation of protein synthesis is critical for control of gene expression in all cells. Ribosomes are ribonucleoprotein machines responsible for translating cellular proteins. Defects in ribosome production, function, or regulation are detrimental to the cell and cause human disease, such as progressive encephalopathy with edema, hypsarrhythmia, and optic atrophy (PEHO) syndrome. PEHO syndrome is a devastating neurodevelopmental disorder caused by mutations in the ZNHIT3 gene, which encodes an evolutionarily conserved nuclear protein. The precise mechanisms by which ZNHIT3 mutations lead to PEHO syndrome are currently unclear. Previous studies of the ZNHIT3 homolog in budding yeast (Hit1) revealed that this protein is critical for formation of small nucleolar ribonucleoprotein complexes (snoRNPs) that are required for rRNA processing and 2'-O-methylation. Here, we use budding yeast as a model system to reveal the basis for the molecular pathogenesis of PEHO syndrome. We show that missense mutations modelling those found in PEHO syndrome patients cause a decrease in steady-state Hit1 protein levels, a significant reduction of box C/D snoRNA levels, and subsequent defects in rRNA processing and altered cellular translation. Using RiboMethSeq analysis of rRNAs isolated from actively translating ribosomes, we reveal site-specific changes in the rRNA modification pattern of PEHO syndrome mutant yeast cells. Our data suggest that PEHO syndrome is a result of ribosomopathy and reveal potential new aspects of the molecular basis of this translation dysregulation disease.

Introduction

Ribosome biogenesis is an essential process that is tightly regulated by the action of over 200 assembly factors including proteins and non-coding RNAs (1,2). Mutations in ribosome components or ribosome assembly factors are deleterious to the cell and can result in human

diseases that are collectively termed ribosomopathies (3,4). Among the critical ribosome biogenesis factors are small nucleolar RNAs (snoRNAs) that participate in the processing, folding, and modification of rRNAs (5,6). snoRNAs are an abundant class of small non-coding RNAs that fall into two major classes based on their conserved elements: box H/ACA snoRNAs guide the isomerization of uridines into pseudouridines, and box C/D snoRNAs are responsible for the 2'-O-methylation of rRNAs (7,8). snoRNA-guided rRNA modifications are critical to the structure and function of the ribosome (9), and their dysregulation is linked to human diseases including cancer and devastating disorders such as dyskeratosis congenita and Treacher Collins syndrome (10-22).

Four evolutionarily conserved proteins, including a methyltransferase, interact with box C/D snoRNAs to form functional ribonucleoprotein complexes (snoRNPs) for 2'-O-methylation of over 50 nucleotides in yeast rRNAs (over 100 in humans) (6,7). Formation of box C/D snoRNP complexes is regulated by several transiently-acting assembly factors that are mostly evolutionarily conserved from yeast to humans (23). Hit1 (human zinc finger HIT-type containing protein 3, ZNHIT3), an evolutionarily conserved nuclear protein, is an assembly factor required for the biogenesis of box C/D snoRNPs (24). Both ZNHIT3 and Hit1 are members of the family of zinc finger HIT (Zf-HIT) domain-containing proteins (25,26) and are involved in ribosome biogenesis through a critical network of protein-protein interactions required for the production of box C/D snoRNPs (24,27). Specifically, Hit1 cooperates with another assembly factor, Rsa1 (human nuclear fragile X mental retardation protein-interacting protein 1- NUFIP1), to recruit the core box C/D snoRNP protein, Snu13 (24,27). This is an essential early step in the biogenesis of snoRNPs which initiates the hierarchical assembly of snoRNPs (28) and prevents the catalytic activity of pre-mature snoRNPs (27). Consistent with the critical role of Hit1, deletion of the *HIT1* gene in yeast results in low steady-state levels of box C/D snoRNAs and impairs both box C/D

snoRNP assembly and ribosome biogenesis (24). Furthermore, mutations in the *ZNHIT3* gene, which encodes the human homolog of Hit1, cause a severe neurodevelopmental disorder termed PEHO syndrome (Progressive Encephalopathy with edema, Hypsarrhythmia, and Optic atrophy) (29,30).

PEHO syndrome is a rare and fatal autosomal recessive disease characterized by progressive cerebellar atrophy, infantile spasms, arrest of psychomotor development, and a poor prognosis (31-33). ZNHIT3-associated amino acid variations that cause PEHO syndrome are found within the Zf-HIT domain of the protein (29,34). These include the missense variation Ser31Leu (S31L) (29), and the compound heterozygous ZNHIT3 variants S31L and Cys14Phe (C14F) (34). The ZNHIT3 missense variant S31L is also found in a class of diseases with similar phenotypes to PEHO syndrome, called PEHO-like syndrome (33). Mechanistically, how amino acid variations in the ZNHIT3 protein contribute to pathogenesis in PEHO syndrome remains largely unknown to date.

ZNHIT3 is required for granule neuron survival and migration in cultured mouse cells and zebrafish (29). Studies in human cell culture have shown that the ZNHIT3-S31L variation destabilizes the protein, resulting in decreased steady-state protein levels (29). Thus, loss-of-function of ZNHIT3 is suggested to cause the molecular defects observed in ZNHIT3-associated PEHO syndrome. Interestingly, however, co-immunoprecipitation assays show that the ZNHIT3-S31L variation does not compromise the interaction of the protein with its significant binding partner, NUFIP1 (29), leaving the question of how loss-of-function of ZNHIT3 causes molecular defects in PEHO syndrome.

Here, we investigate the two PEHO-causing *ZNHIT3* mutations in the model organism budding yeast, to reveal the molecular basis by which they cause cellular defects and contribute to

pathogenesis in PEHO syndrome. Consistent with the findings from human cell culture models, we show that introduction of the PEHO-causing mutations into yeast *HIT1* causes growth defects and leads to a decrease in steady-state levels of the Hit1 protein at higher temperatures. Using these yeast models, we reveal that as a result of Hit1 deficiency due to PEHO-linked amino acid variations, cells demonstrate a significant defect in rRNA biogenesis and a decrease in steady-state box C/D snoRNA levels. Using RiboMethSeq, we further demonstrate a site-specific reduction in the rRNA 2'-O-methylation pattern of actively translating ribosomes, and a change in translation accompanied by ribosome fidelity defects. Our data offer new insights into the specific translational defects caused by loss of Hit1 and suggest that the molecular basis of PEHO syndrome pathogenesis likely lies within translation defects, adding PEHO syndrome to the list of ribosomopathies.

Materials and methods

Yeast strains and CRISPR-Cas9 genome editing of Hit1. All yeast strains used in this study are listed in **Table S1**, oligonucleotides are in **Table S2,** and plasmids are in **Table S3**. Genome editing was carried out as described previously (35). In brief, a primer was designed for mutagenesis of the guide recognition sequence and used to amplify the pCAS9 vector (Addgene 60847) (35). A double-stranded 160-mer repair DNA was generated and the BY4741 yeast cells were transformed with pCAS9-Hit1 and the PCR product. Transformants were plated onto YPD plates supplemented with G418 and allowed to grow for 72 h at 37°C. Individual colonies were selected and mutations in each colony were confirmed by sequencing and further validated in growth assays after transforming each strain with a plasmid expressing the wild-type control *HIT1* gene.

Yeast growth assays. For growth curves, BY7471, *hit1-C11F*, *hit1-S29L*, or *hit1*Δ cells were grown in YPD to mid-log phase (OD600 ~0.6) and diluted into fresh media. The OD600 was

recorded every 20 min in an Epoch2 microplate reader (BioTek) to determine the doubling times. For growth assays in the presence of translation inhibitors, the following concentrations were used: 500 µg/mL paromomycin, 15 µg/mL hygromycin B, 10 µg/mL anisomycin and 500 µg/mL homoharringtonine. For spot growth assays, cells were grown to saturation and serially diluted in sterile water, spotted on plates, and grown at 30°C or 37°C.

Western blot analysis. *hit1*Δ cells transformed with HA-Hit1 expression plasmids (see **Table S3**) were grown to mid-log phase in minimal media lacking histidine. An equivalent of 10 mL cells at OD600 0.6 was harvested, washed and lysed in 1 mL SUMEB buffer (1% SDS, 8 M urea, 10 mM MOPS pH 6.8, 10 mM EDTA, 0.01% bromophenol blue) with glass beads. Lysates were analyzed by SDS-PAGE on a Mini-PROTEAN TGX Stain-Free precast gel (Biorad), followed by western blotting. A high-affinity anti-HA antibody (Roche) was used for the detection of HA-tagged Hit1 and an anti-PGK1 antibody (ThermoFisher) was used to detect the control protein. Bands were quantified using Image Lab (BioRad).

Northern blot analysis. Total cell RNA was isolated from cells grown to OD600 ~0.6, in biological triplicates, using the hot phenol method. For analysis of rRNA processing defects, RNAs were separated on a 1% agarose/formaldehyde gel and passively transferred to a Hi-bond nylon membrane. Membranes were probed using oligos listed in **Table S2** and bands were quantified in Image Lab (BioRad).

RT-qPCR. Reverse transcription was performed with 1 µg of total cell RNA extracted using the hot phenol method. RNA was treated with DNase I (NEB) according to the manufacturer's instructions, and reverse transcribed with 50 ng random hexamers using 200 U SuperScript III reverse transcriptase (Invitrogen) in a 20 uL reaction for 10 minutes at 25°C followed by 50 minutes at 50°C. qPCR was performed using the oligos described in **Table S2** with the Maxima

SYBR Green qPCR master mix (Thermo Scientific) on a BioRad CFX96 instrument. RNA levels were calculated using the $2^{-\Delta\Delta Ct}$ method and were normalized to Alg9 and plotted relative to wild-type By4741.

Sucrose density gradient isolation of polysomal RNA. Cells were grown to mid-log phase in YPD and harvested after addition of 0.1 mg/ml cycloheximide. Harvested cells were washed and lysed in ice-cold gradient buffer (200 mM Hepes-KOH pH 7.4, 1 M KOAc pH 7.6, 25 mM $Mg(OAc)_2$), supplemented with 0.1 mg/ml cycloheximide, PMSF, pepstatin, E64, and Complete protease inhibitor cocktail (Roche). Cleared lysate was applied to 10–50% sucrose gradients in gradient buffer and centrifuged for 2 h at 40,000 RPM in an SW41Ti rotor (Beckman Coulter). Gradients were fractionated and scanned by UV 260 nm absorbance. Fractions corresponding to polysomes were pooled together for analysis of their rRNA 2'-O-methylation pattern by RTL-qP and RiboMethSeq.

Analysis of global 2'-O-methylation levels by reverse transcription. The 2'-O-methylation level of 25S rRNA was assayed at three sites as previously described (36). Briefly, 1 µg total cell RNA extracted using the hot phenol method was treated with DNase I (NEB) according to the manufacturer's instructions, then reverse transcribed with 50 ng random hexamers in a high dNTP concentration (20 mM) or low dNTP concentration (0.1 mM) using 200 U SuperScript III reverse transcriptase (Invitrogen) in a 20 uL reaction for 50 minutes at 50°C. Samples were treated with RNase H and cDNAs were analyzed by qPCR using the Quantitect Sybr Green enzyme and dye mixture (Qiagen) with the oligos listed in **Table S2**. The following thermocycler setup was used in a StepOnePlus instrument (Applied Biosystems): 15m at 95°C followed by 40 cycles of 15s at 94°C, 30s at 55°C and 30s at 72°C. The quantification cycle delay for each region was calculated as follows: ΔC_q = low dNTP C_q – high dNTP C_q. For each region, this value was normalized to the

threshold cycle delay of the unmethylated 25S region (Region 1). For analysis of rRNA 2'-O-methylation levels of polyribosomes, the protocol above was used with 700 ng RNA extracted from polysome fractions. Experiments were performed for samples from three biological replicates.

RiboMethSeq analysis of rRNA 2'-O-methylation pattern. For RiboMethSeq, 150 ng polysomal RNA was fragmented under denaturing conditions using an alkaline buffer (pH 9.4) to obtain an average size of 20-40 nt. Fragments were end-repaired and ligated to adapters using NEBNext Small RNA kit for Illumina. Sequencing was performed on Illumina HiSeq1000. Reads were mapped to the yeast rDNA sequences, and the RMS score (fraction methylated) was calculated as MethScore (for ±2 nt) (88), equivalent to "ScoreC" (30).

Analysis of global translation by HPG incorporation. Translation of newly synthesized peptides was measured with the Click-iT™ HPG Alexa Fluor™ 488 Protein Synthesis Assay Kit (ThermoFisher Scientific) according to the manufacturer's instructions. BY7471, *hit1-C11F*, or *hit1-S29L* cells transformed with pRS411 plasmid were grown in minimal media lacking methionine to late log phase. L-Homopropargylglycine (HPG) was added to 10 mL cultures to a final concentration of 50 μM, and cells were incubated for 30 minutes at 37°C. Negative controls received cycloheximide at a final concentration of 0.1 mg/mL before the addition of HPG. Flow Cytometry measurements were done at the Emory Flow Cytometry Core (EFCC). Cells were fixed, permeabilized, and subjected to click chemistry following the manufacturer's instructions. Cells were passed through a 0.37 μm Nitex mesh before flow cytometry analysis of fluorescence using the BD FACSymphony™ A3 Cell Analyzer. The fluorescence intensity of 50,000-100,000 cells was determined.

Dual-luciferase assays for translation fidelity. Cells were grown to OD600 ~0.6 in Ura$^-$ or Leu$^-$ synthetic glucose liquid media. 1 mL of cells were pelleted, washed and stored at -80˚C. Luciferase activities were measured using the Dual-Luciferase Reporter Assay kit (Promega). Cell pellets were resuspended in 100 µL 1 X Passive Lysis Buffer and incubated for 10 minutes. 30 µL of LARII was mixed with 10 µL of lysate in clear bottom 96W Microplates (Costar) and Firefly luciferase activity was measured. 30 µL of Stop and Glo solution was added and Renilla luciferase activity was measured. Measurements were performed using a Synergy Microplate reader (BioTek). For each replicate, the Firefly luciferase signal was normalized to the Renilla luciferase signal. For each strain, Firefly/Renilla ratio was normalized to the average Firefly/Renilla ratio of replicates containing a control plasmid.

Results

PEHO syndrome mutations cause a temperature-sensitive growth defect in yeast.

The ZNHIT3 protein contains two domains that are evolutionarily conserved from yeast to humman in sequence, structure, and function (24,27,37,38) (**Figure 1A**). The PEHO syndrome-causing missense mutations, which result in the ZNHIT3 variants C14F and S31L, lie within the highly conserved Zf-HIT domain of ZNHIT3 (29,34,37), which shares 33% sequence identity and 45% sequence similarity between human and yeast (**Figure 1B**). Mapping the position of C14 and S31 amino acids and their yeast homologs, C11 and S29, on the available structures of the Zf-HIT domains of ZNHIT3 and Hit1 (PDB IDs 2YQQ and 2N95 (26), respectively) shows that these amino acids play identical roles in the structure of the human and yeast proteins (**Figure 1C**). In both structures, the PEHO-linked amino acids are involved in stabilizing the protein fold by their direct (C14/C11, human/yeast) or indirect (S31/S29, human/yeast) engagement in the coordination of one of the Zn^{2+} ions within the Zf-HIT domain.

Previous work has established the functional conservation of Hit1 between eukaryotes, particularly between yeast and humman (24,38,39). To gain insight into the molecular basis of defects caused by PEHO-associated Hit1 mutations, we used CRISPR-Cas9 genome editing to generate budding yeast models that encode the C11F or S29L variants of the *HIT1* gene. Using growth assays on solid medium, we first assessed the growth of *hit1-C11F* and *hit1-S29L* yeast strains relative to wild-type control cells. Our results show that while neither mutant strain has a growth defect at 30°C, yeast expressing C11F grows significantly slower than wild-type control cells at 37°C (**Figure 2A**). Furthermore, the yeast strain expressing the Hit1-S29L variant has smaller colony size compared to the wild-type. To quantify and confirm our findings, we next measured the growth of cells expressing Hit1 variants in liquid medium at 30°C and 37°C. Similar to growth on plates, both *hit1-C11F* and *hit1-S29L* cells show a growth defect at 37°C in liquid medium, with that of C11F being more severe than S29L. Notably, the growth defect for both mutants is less severe than the defect observed upon deletion of *HIT1* (**Figure 2B**). These results indicate that PEHO-linked Hit1 variants cause cellular defects in yeast models, providing a convenient model system to further explore the molecular defects caused by these mutations.

PEHO syndrome mutations in yeast result in decreased steady-state Hit1 protein levels.

Because both C11F and S29L mutants show a slow-growth phenotype at 37°C, similar to the temperature-sensitive phenotype reported for *hit1Δ* cells, we next analyzed the steady-state Hit1 protein levels in wild-type control and *hit1* mutant cells at 30°C and 37°C. For this analysis, we transformed *hit1Δ* cells with plasmids that constitutively express the triple-HA (3xHA)-tagged or untagged wild-type or variant Hit1 (C11F or S29L). To test the effect from addition of the HA tag, we first compared the growth of HA-tagged and untagged *hit1* mutants relative to the wild-type control. This analysis confirmed that cells expressing HA-tagged wild-type Hit1 grow similar to

those expressing untagged wild-type Hit1, and the untagged *hit1* mutant strains have the same slow-growth phenotype as the HA-tagged *hit1* mutants (**Figure S1**). We then analyzed the steady-state levels of the 3xHA-tagged Hit1 protein by western blotting of total cell protein lysates. Both *hit1-C11F* and *hit1-S29L* mutants show significantly reduced steady-state Hit1 protein levels at 30°C (**Figure 2C-2D**) and 37°C (**Figure 2E-2F**). These data show a significant reduction of steady-state Hit1 PEHO variant levels and are in line with previous observations regarding a decrease in ZNHIT3 protein levels for the S31L PEHO variant in HeLa cells (29).

PEHO syndrome mutations in budding yeast lead to rRNA processing defects and decreased steady-state box C/D snoRNA levels.

Loss of Hit1 protein results in ribosome biogenesis defects (24). We therefore tested whether impaired ribosome biogenesis contributes to the growth defect of the PEHO syndrome Hit1 mutants, which have decreased steady-state Hit1 protein levels. To this end, we extracted total cell RNA from wild-type control and mutant C11F or S29L yeast cells grown at 37°C and analyzed rRNA processing by northern blotting (**Figure 3A**). In budding yeast, mature rRNAs are processed from a long polycistronic 35S precursor rRNA (**Figure 3B**) (2,40). rRNA processing in wild-type yeast typically occurs co-transcriptionally such that 35S levels are not detectable (2,41,42). We observe a striking increase in the levels of 35S precursor rRNA in the *hit1-C11F* cells (**Figure 3A, 3C**). Similarly, the 35S levels slightly increase in the *hit1-S29L* mutant (**Figure 3A, 3C**). These data suggest an early impairment of the co-transcriptional step of rRNA processing in PEHO mutant yeast strains, indicating a potential impact from the Hit1 variants on the quantity of mature ribosomes and cellular translation.

Hit1 is a box C/D snoRNP assembly factor necessary for the maintenance of box C/D snoRNA levels that are required for proper rRNA processing (24). We therefore tested the extent to which

the loss of Hit1 protein in PEHO mutant yeast cells would decrease box C/D snoRNA levels. We used RT-qPCR to quantify the snoRNA levels of both *hit1* variants compared to wild-type control and *hit1Δ* cells at 37°C (**Figure 3D**). Box C/D snoRNA levels were compared to the Alg9 mRNA and box H/ACA snoRNAs as controls, as these RNAs are not regulated by Hit1. Both PEHO-linked Hit1 mutants show an intermediate, but significant, loss of box C/D snoRNAs relative to wild-type control and *hit1Δ* cells. This loss is specific to box C/D snoRNAs, since box H/ACA snoRNA levels are not significantly changed relative to wild-type. Of the two PEHO syndrome mutants, *hit1-C11F* shows the more severe loss of box C/D snoRNAs (**Figure 3D**). These data are consistent with the observation that *hit1-C11F* cells have more severe growth and rRNA processing defects and show a greater loss of Hit1 protein levels.

PEHO syndrome mutations cause translation defects, impact the fidelity of protein synthesis and result in changes in sensitivity of cells to translation inhibitors.

Ribosome biogenesis defects can lower cellular ribosome concentration and cause defects in translation (43,44). Similarly, loss of snoRNAs and/or rRNA modifications can cause translation fidelity defects and impact the ability of ribosomes to initiate mRNA translation from internal ribosome entry sites (IRES) (6,9,45-49). To test whether translation is impacted by PEHO syndrome mutations in yeast, we first investigated the steady-state levels of the mature 18S and 25S rRNAs in the PEHO syndrome mutants by RT-qPCR. At 37°C, both *hit1Δ* and *hit1-C11F* cells have reduced 18S and 25S rRNA levels relative to wild-type. Cells expressing h*it1-S29L* exhibit the same trend, although the reduction is not significant compared to wild-type (**Figure 4A**).

To measure how translational output is affected in PEHO syndrome *hit1* mutant strains, we next performed an L-homopropargylglycine (HPG) incorporation assay to quantify global

translation in bulk at a given time point. HPG is a methionine analog with an alkyne moiety, which can be incorporated into newly synthesized proteins, allowing their detection by a click reaction with Alexa Fluor azide. We compared the incorporation of HPG into the newly synthesized proteins 30 minutes after the addition of HPG to the media. These results show that in both *hit1-C11F* and *hit1-S29L* cells, the translational output of proteins of all sizes is significantly decreased relative to wild-type control cells (**Figure 4B**). We further examined changes in bulk translation of PEHO mutant yeast by examining the effects on total polysome profiles. Cells were grown to mid-log phase and treated with cycloheximide before harvesting to stall polysomes. Free RNA-containing complexes were then resolved from small (40S) and large (60S) ribosomal subunits, monosomes, and polysomes by sedimentation through sucrose density gradients. Both the *hit1-C11F* and *hit1-S29L* mutations reduce the ratio of polysomes to monosomes, indicating a reduction in bulk translation compared to wild-type control cells (**Figure 4C-D**).

To reveal the nature of translational defects in *hit1-C11F* mutant cells, we used a series of previously established reporter plasmids to check the fidelity of protein synthesis (50-53). In these reporter plasmids, the translation of Firefly luciferase depends on alternate start codon selection, stop codon readthrough, miscoding of the CGC (Arg) codon by $tRNA^{His}GUG$, or initiation from an IRES element, while the translation of Renilla luciferase is constitutive and is used as an internal control. Relative to wild-type control cells, both PEHO syndrome mutants show a significant reduction in stop codon readthrough, a significant increase in initiation from a near-cognate UUG start codon, but no significant change in miscoding (**Figure 4E**). We also detect a significant decrease in IRES recognition in *hit1-C11F* cells relative to wild-type control, which is not observed for the *hit1-S29L* cells (**Figure 4E**). Together, these data establish that PEHO syndrome-associated Hit1 variants cause translation defects and impair the fidelity of protein synthesis in

yeast models. Given the evolutionarily conserved function of Hit1 and ZNHIT3 and the conservation of the ribosome biogenesis and translation pathways between yeast and human, these data strongly suggest that translation can be both globally and/or specifically affected in PEHO syndrome.

To gain further insight into the cause of translation defects observed in *hit1* mutant yeast cells, we tested whether these defects could be a result of ribosome structural changes. For this purpose, we used translation inhibitors that specifically bind to the small or large ribosomal subunits as tools for assessing changes in ribosome structure. Paromomycin and hygromycin B were used to probe defects near the decoding center, whereas anisomycin and homoharringtonine were chosen to probe changes near the peptidyl transferase center (54). Compared to wild-type cells, both *hit1Δ* and *hit1-C11F* cells are slightly more sensitive to the addition of paromomycin and hygromycin B, aminoglycosides that specifically bind to the small ribosomal subunit at the decoding center. In the presence of these drugs, the fold change in doubling time between wild-type and *hit1-C11F* strains is approximately 1.7 fold, compared to that with no drug at 1.4 fold (**Figure 4F**). Similarly, in the presence of these drugs, the fold change between *hit1Δ* and wild-type increases from 2.1 fold to 2.3-2.8 fold. Cells expressing Hit1-S29L exhibit minimal changes in sensitivity to paromomycin and hygromycin B. Interestingly, *hit1Δ*, *hit1-C11F* and *hit1-S29L* cells are less sensitive to anisomycin and homoharringtonine, inhibitors that bind in the large ribosomal subunit tRNA A-site (**Figure 4F**). In the presence of anisomycin and homoharringtonine, the fold change in doubling time between wild-type and both PEHO syndrome mutants, drops to 0.8-0.9 fold, while the fold change between wild-type and *hit1Δ* drops to 1.7-1.8 fold. These data suggest that there may be changes in both the small and large ribosomal subunits that can affect the binding between the ribosome and ligands such as translation inhibitors or tRNAs or IRES elements.

The rRNA 2'-O-methylation pattern of the *hit1-C11F* mutant is altered.

Because box C/D snoRNA levels are decreased in both PEHO syndrome mutants and we observed global and distinct translational defects, we hypothesized that PEHO syndrome mutations may alter the rRNA 2'-O-methylation pattern. To assess the level of rRNA 2'-O-methylation in PEHO mutant yeast cells, we first employed a reverse transcription-based assay to globally analyze the 2'-O-methylation of the 25S rRNA in total RNA that was isolated from wild-type control, *hit1-C11F* or *hit1-S29L* cells. We performed this analysis on three regions of the 25S rRNA which have 11, 10, or 12 2'-O-methylations, respectively, and used a region without any rRNA 2'-O-methylations as an internal control for normalization (**Figure 5A**). The results from this assay show a significant hypo 2'-O-methylation in all three regions of rRNA isolated from the *hit1-C11F* mutant yeast (**Figure 5B**). However, we only observe a slight hypo 2'-O-methylation in one region of 25S rRNA for the *hit1-S29L* mutant cells. Specifically, in region 2 of the 25S rRNA, the *hit1-C11F* cells show ~70% reduction in the level of rRNA 2'-O-methylation, compared to a modest 20% reduction in the *hit1-S29L* mutant cells (**Figure 5B**). These data are in line with the less severe growth phenotype and translational defects we observe in cells expressing Hit1-S29L compared to those expressing Hit1-C11F (**Figures 2A**, **4A-E**). The data also provide an explanation for the observed decrease in the ability of ribosomes from *hit1-C11F* cells to initiate translation from an IRES, as observed for other cells that have rRNA hypo 2'-O-methylation (9,15,45).

To reveal how the rRNA 2'-O-methylation pattern is affected in yeast expressing Hit1-C11F on both the small and large ribosomal subunits, we subjected the polysomal RNA isolated from actively growing wild-type control and *hit1-C11F* mutant cells to RiboMethSeq analysis (55). Our results show that most rRNA sites in polysomal RNA of wild-type control cells are fully methylated when cells are grown at 37°C (**Figure 5C-D**) (55). However, rRNAs isolated from

polysomes of *hit1-C11F* cells show significant global hypo 2'-O-methylation, with different rRNA locations being affected to different extents. Specifically, in *hit1-C11F* cells, ~44% (8/18) of 2'-O-methylation sites on the 18S rRNA are variable (MethScore 0.4-0.8) and ~17% (3/18) are hypo 2'-O-methylated (MethScore < 0.4) (**Figure 5C**). On the 25S rRNA, ~53% of 2'-O-methylation sites are variable (19/36) and ~17% of sites (6/36) are hypo 2'-O-methylated (**Figure 5D**). These data indicate that actively translating ribosomes from *hit1-C11F* cells are hypo 2'-O-methylated and have a distinct pattern of rRNA modification compared to those in wild-type control cells. The three most hypo 2'-O-methylated sites on the 18S rRNA are located in the head and body of the small ribosomal subunit (**Figure 6A**). The hypo 2'-O-methylated position 18S-A436 is located near the binding site of eIF5B and eEF2 and in vicinity of uS12 (**Figure S3A-B**). Similarly, the hypo 2'-O-methylated nucleotide 18S-G1572 is located near functional ribosomal sites close to the eIF2A binding site and in vicinity of the P-tRNA binding site on the small ribosomal subunit (**Figure 6C, S3C**). On the large ribosomal subunit, the hypo 2'-O-methylated sites are largely clustered around the peptidyl transferase center and the peptide exit tunnel (**Figure 6B** and **Figure 6D-E**). In summary, the RiboMethSeq analysis reveals that the PEHO-associated Hit1-C11F variant affects the rRNA 2'-O-methylation of actively translating ribosomes in a site-specific manner including at functionally important sites on both ribosomal subunits.

Discussion

In this study, using budding yeast as a model organism, we reveal the molecular defects caused by the ZNHIT3 pathogenic missense mutations which cause PEHO syndrome. We analyze both reported PEHO syndrome-causing ZNHIT3 variants by introducing them into the *HIT1* gene in yeast (*hit1-C11F* and -*S29L*), and assess their impact on yeast cell growth, ribosome biogenesis, and cellular translation. While both amino acid variants destabilize the steady-state Hit1 protein

levels, the Hit1-C11F variant causes more severe growth defects, lower box C/D snoRNA levels and more prominent defects in rRNA processing compared to Hit1-S29L (**Figures 2, 3**). The majority of the studied ZNHIT3- associated PEHO syndrome cases to date are caused by homozygous expression of the ZNHIT3-S31L variant (yeast Hit1-S29L) (33). PEHO syndrome can also be caused by the compound heterozygous variants C14F and S31L (30). Because the phenotype of yeast cells expressing the Hit1-C11F variant is more severe than that of the Hit1-S29L variant, we anticipate that homozygous ZNHIT3-C14F variants may be incompatible with survival and thus underrepresented in patients.

Our data show that low steady-state Hit1 protein levels cause significant rRNA processing impairments and result in lower steady-state levels of both the modifying and the processing box C/D snoRNAs (**Figure 3**). The observed rRNA processing defects in *hit1* mutant cells are reminiscent of defects observed for other early ribosome biogenesis factors as expected for a snoRNP assembly factor (56-58). Given the conserved role of Hit1 and ZNHIT3 between yeast and human (24,27), it is likely that the ZNHIT3 variants also cause ribosome biogenesis defects in human cells. Future studies are required to reveal the effect of low steady-state levels of PEHO-causing ZNHIT3 protein variants (29) on rRNA processing in human cells.

Deletion of Hit1 leads to decreased box C/D snoRNA levels and impaired rRNA processing (24). However, the specific outcomes of these changes for cellular translation were unexplored to date. The finding that Hit1-C11F expression results in heterogeneous modification of rRNA in polysomal fractions, representing actively translating ribosomes, strongly suggests the existence of distinct pools of translating ribosomes in the mutant cells (**Figure 4**). Strikingly, even though the levels of box C/D snoRNAs and their corresponding 2'-O-methylations are generally decreased, Hit1 loss preferentially affects 2'-O-methylation of certain rRNA positions more than

others. The pattern of hypo 2'-O-methylation observed in Hit1 mutant cells resembles changes recently identified for a mutant of another box C/D snoRNP assembly factor, Bcd1 (9). This similarity suggests that certain rRNA 2'-O-methylation sites are more vulnerable than others when snoRNP assembly is impaired. Interestingly, many of the vulnerable sites are conserved between yeast and humans. These include one of the three hypo 2'-O-methylated positions in the 18S (A436), and four of the hypo 2'-O-methylated sites in the 25S rRNA (A649, C663, U1888, U2421). Future studies are required to address whether PEHO-causing mutations in ZNHIT3 affect the 2'-O-methylation pattern of human ribosomes similarly.

Loss of box C/D snoRNAs in *hit1-C11F* cells does not correlate well with the decrease in their corresponding 2'-O-methylations. For example, in the *hit1-C11F* mutant yeast, the steady-state levels of snR52 are decreased to 20% compared to the wild-type control (**Figure 3D**), while the 2'-O-methylation levels at sites guided by snR52 (18S-A420 and 25S-U2921) are stable relative to wild-type (relative MethScores around 0.9, **Figure 5**). These data are in line with previous studies that yeast and human rRNA 2'-O-methylation levels do not correlate well with the level of their corresponding box C/D snoRNAs (9,59). Our data also strongly suggest that while a threshold level of each snoRNA is sufficient to guide 2'-O-methylation of the majority of rRNAs (9), differential stability and/or efficiency of snoRNP assembly of each snoRNA impacts the active pool of available snoRNAs, the pattern of rRNA modification, ribosome biogenesis, and translation when snoRNP biogenesis is defective (**Figure 7**).

Several studies have reported heterogeneity in the rRNA 2'-O-methylation pattern in both yeast and human cells (15,21,45,55,59-63). However, it was unclear whether globally hypo 2'-O-methylated rRNAs assembled into functional ribosomes, or if a population of hypo 2'-O-methylated rRNAs comprised immature or inactive ribosomes, while a more methylated

population of rRNAs comprised translationally active ribosomes. Here, we provide a global quantification of polysomal rRNA 2'-O-methylations using RiboMethSeq. Our results show that significantly hypo 2'-O-methylated rRNAs are part of translating ribosomes. Furthermore, similar to the previous report on the 2'-O-methylated 18S rRNA site A100 (61), our data indicate that rRNA 2'-O-methylation levels quantified in the total RNA pool are not significantly different than that of actively translating ribosomes (**Figure S2**). This suggests that quantification of rRNA 2'-O-methylation from the total RNA pool is an appropriate proxy for assessing the methylation status of actively translating ribosomes.

Several important conclusions can be drawn from this study that likely have significant implications for understanding the molecular basis of diseases that arise from defects in snoRNP biogenesis. Our data reveal that defects in snoRNP assembly can cause distinct translational defects. In both PEHO syndrome mutant yeast strains, we observe a decrease in global translation, an increase in initiation from a near-cognate start codon, and hyperaccuracy in stop codon readthrough. Both lower translation fidelity and higher accuracy in translation can negatively affect cellular homeostasis and growth and cause detrimental cellular defects (64). The trend of decreased translation paired with decreased stop codon readthrough is also observed in other yeast mutants lacking rRNA modifications (47). For example, the lack of 2'-O-methylation at the 25S-A2256 site in h69 leads to decreased stop codon readthrough (47). In *hit1-C11F* cells, A2256 is variably methylated (MethScore 0.7), however loss of multiple adjacent modifications can also have a combinatorial effect on translation fidelity (47). Loss of rRNA modifications in the decoding center of bacterial ribosome leads to both increased alternate start site usage and decreased stop codon readthrough (65), the same combination of fidelity defects we observe in the PEHO syndrome yeast mutant cells. While we do not observe a significant change in the

modification of sites at the decoding center, PEHO syndrome mutant yeast cells are sensitive to translation inhibitors which bind at the decoding center (**Figure 4F**). It is possible that hypo 2'-O-methylations in *hit1-C11F* ribosomes at sites neighboring the decoding center impact the events at the decoding center via long-range effects (9). For example, the hypo 2'-O-methylated site 18S-G1572 is a few nucleotides away from residues that provide a steric block for the P-site tRNA (**Figure 6C**). Impairments in start codon selection and stop codon readthrough are also observed in other ribosomopathy models. For example, ribosomopathy-causing mutations in uS12, positioned near the hypo 2'-O-methylated nucleotide 18S-A436 (**Figure S6A**), result in increased non-AUG translation initiation in bacteria (66). Additionally, a yeast variant of Dkc1 that is linked to the dyskeratosis congenita and causes a global decrease in rRNA pseudouridylation levels leads to lower rates of stop codon readthrough (67). On the 25S rRNA, many of the vulnerable sites are located around the peptidyl transferase center (**Figure 6E**), where we observe a loss of sensitivity to translational inhibitors in both mutants. The translation defects observed in PEHO syndrome mutant yeast cells could arise from changes in ribosome concentration or assembly defects that are caused by insufficient amounts of box C/D snoRNAs or lack of their corresponding modifications. Future studies are required to address the contribution of each of these factors to the observed defects and determine the effect from the local or long-range impact of rRNA modification changes on ribosomal protein, translation factor, or ligand binding.

PEHO syndrome is a neurodevelopmental disease characterized by the loss of cerebellar granule neurons. The tissue-specific defects of PEHO syndrome may arise from translation changes that impact cellular differentiation and neurodevelopment. Ribosome profiling performed in a human cell line reveals changes throughout neuronal differentiation in upstream ORF translation associated with near-cognate start codon usage which could impact neuronal

differentiation (68). Furthermore, 2'-O-methylation has been implicated in differentiation and development in human cell lines and zebrafish models (21,69). We, therefore, propose that changes in the 2'-O-methylation pattern, ribosome number, or the fidelity of translation in PEHO syndrome may alter the translation of specific mRNAs involved in neuronal differentiation to cause tissue-specific defects. Together, our results offer novel insights into molecular mechanisms of cellular defects caused by snoRNP assembly impairment and suggest that PEHO syndrome is likely a ribosomopathy arising from defective ribosome biogenesis due to loss of box C/D snoRNAs and change of the rRNA 2'-O-methylation pattern.

Acknowledgements

We thank Drs. David Bedwell, John Dinman, Alan Hinnebusch, and Sunnie Thompson for the gift of plasmids. We also thank members of the Ghalei lab and Dr. Anita Corbett for discussions and comments on the manuscript.

References

1. Klinge, S., and Woolford, J. L., Jr. (2019) Ribosome assembly coming into focus. *Nat Rev Mol Cell Biol* **20**, 116-131
2. Woolford, J. L., Jr., and Baserga, S. J. (2013) Ribosome biogenesis in the yeast Saccharomyces cerevisiae. *Genetics* **195**, 643-681
3. Farley-Barnes, K. I., Ogawa, L. M., and Baserga, S. J. (2019) Ribosomopathies: Old Concepts, New Controversies. *Trends in genetics : TIG* **35**, 754-767
4. Narla, A., and Ebert, B. L. (2010) Ribosomopathies: human disorders of ribosome dysfunction. *Blood* **115**, 3196-3205
5. Decatur, W. A., and Fournier, M. J. (2003) RNA-guided nucleotide modification of ribosomal and other RNAs. *J Biol Chem* **278**, 695-698
6. Sloan, K. E., Warda, A. S., Sharma, S., Entian, K. D., Lafontaine, D. L. J., and Bohnsack, M. T. (2017) Tuning the ribosome: The influence of rRNA modification on eukaryotic ribosome biogenesis and function. *RNA Biol* **14**, 1138-1152
7. Watkins, N. J., and Bohnsack, M. T. (2012) The box C/D and H/ACA snoRNPs: key players in the modification, processing and the dynamic folding of ribosomal RNA. *Wiley Interdiscip Rev RNA* **3**, 397-414
8. Maxwell, E., and Fournier, M. (1995) THE SMALL NUCLEOLAR RNAs. *Annual Review of Biochemistry* **64**, 897-934
9. Khoshnevis, S., Dreggors-Walker, R. E., Marchand, V., Motorin, Y., and Ghalei, H. (2022) Ribosomal RNA 2'-. *Proc Natl Acad Sci U S A* **119**, e2117334119
10. Marcel, V., Ghayad, S. E., Belin, S., Therizols, G., Morel, A. P., Solano-Gonzàlez, E., Vendrell, J. A., Hacot, S., Mertani, H. C., Albaret, M. A., Bourdon, J. C., Jordan, L.,

Thompson, A., Tafer, Y., Cong, R., Bouvet, P., Saurin, J. C., Catez, F., Prats, A. C., Puisieux, A., and Diaz, J. J. (2013) p53 acts as a safeguard of translational control by regulating fibrillarin and rRNA methylation in cancer. *Cancer Cell* **24**, 318-330

11. Marcel, V., Kielbassa, J., Marchand, V., Natchiar, K. S., Paraqindes, H., Nguyen Van Long, F., Ayadi, L., Bourguignon-Igel, V., Lo Monaco, P., Monchiet, D., Scott, V., Tonon, L., Bray, S. E., Diot, A., Jordan, L. B., Thompson, A. M., Bourdon, J. C., Dubois, T., André, F., Catez, F., Puisieux, A., Motorin, Y., Klaholz, B. P., Viari, A., and Diaz, J. J. (2020) Ribosomal RNA 2'O-methylation as a novel layer of inter-tumour heterogeneity in breast cancer. *NAR Cancer* **2**, zcaa036

12. Zhou, F., Liu, Y., Rohde, C., Pauli, C., Gerloff, D., Köhn, M., Misiak, D., Bäumer, N., Cui, C., Göllner, S., Oellerich, T., Serve, H., Garcia-Cuellar, M. P., Slany, R., Maciejewski, J. P., Przychodzen, B., Seliger, B., Klein, H. U., Bartenhagen, C., Berdel, W. E., Dugas, M., Taketo, M. M., Farouq, D., Schwartz, S., Regev, A., Hébert, J., Sauvageau, G., Pabst, C., Hüttelmaier, S., and Müller-Tidow, C. (2017) AML1-ETO requires enhanced C/D box snoRNA/RNP formation to induce self-renewal and leukaemia. *Nat Cell Biol* **19**, 844-855

13. Mei, Y. P., Liao, J. P., Shen, J., Yu, L., Liu, B. L., Liu, L., Li, R. Y., Ji, L., Dorsey, S. G., Jiang, Z. R., Katz, R. L., Wang, J. Y., and Jiang, F. (2012) Small nucleolar RNA 42 acts as an oncogene in lung tumorigenesis. *Oncogene* **31**, 2794-2804

14. Romano, G., Veneziano, D., Acunzo, M., and Croce, C. M. (2017) Small non-coding RNA and cancer. *Carcinogenesis* **38**, 485-491

15. Yi, Y., Li, Y., Meng, Q., Li, Q., Li, F., Lu, B., Shen, J., Fazli, L., Zhao, D., Li, C., Jiang, W., Wang, R., Liu, Q., Szczepanski, A., Qin, W., Weiner, A. B., Lotan, T. L., Ji, Z.,

Kalantry, S., Wang, L., Schaeffer, E. M., Niu, H., Dong, X., Zhao, W., Chen, K., and Cao, Q. (2021) A PRC2-independent function for EZH2 in regulating rRNA 2'-O methylation and IRES-dependent translation. *Nat Cell Biol* **23**, 341-354

16. Monaco, P. L., Marcel, V., Diaz, J. J., and Catez, F. (2018) 2'-O-Methylation of Ribosomal RNA: Towards an Epitranscriptomic Control of Translation? *Biomolecules* **8**

17. Gong, J., Li, Y., Liu, C. J., Xiang, Y., Li, C., Ye, Y., Zhang, Z., Hawke, D. H., Park, P. K., Diao, L., Putkey, J. A., Yang, L., Guo, A. Y., Lin, C., and Han, L. (2017) A Pan-cancer Analysis of the Expression and Clinical Relevance of Small Nucleolar RNAs in Human Cancer. *Cell Rep* **21**, 1968-1981

18. Bellodi, C., McMahon, M., Contreras, A., Juliano, D., Kopmar, N., Nakamura, T., Maltby, D., Burlingame, A., Savage, S. A., Shimamura, A., and Ruggero, D. (2013) H/ACA small RNA dysfunctions in disease reveal key roles for noncoding RNA modifications in hematopoietic stem cell differentiation. *Cell Rep* **3**, 1493-1502

19. McMahon, M., Contreras, A., and Ruggero, D. (2015) Small RNAs with big implications: new insights into H/ACA snoRNA function and their role in human disease. *Wiley interdisciplinary reviews. RNA* **6**, 173-189

20. Stumpf, C. R., and Ruggero, D. (2011) The cancerous translation apparatus. *Curr Opin Genet Dev* **21**, 474-483

21. Nachmani, D., Bothmer, A. H., Grisendi, S., Mele, A., Bothmer, D., Lee, J. D., Monteleone, E., Cheng, K., Zhang, Y., Bester, A. C., Guzzetti, A., Mitchell, C. A., Mendez, L. M., Pozdnyakova, O., Sportoletti, P., Martelli, M. P., Vulliamy, T. J., Safra, M., Schwartz, S., Luzzatto, L., Bluteau, O., Soulier, J., Darnell, R. B., Falini, B., Dokal,

I., Ito, K., Clohessy, J. G., and Pandolfi, P. P. (2019) Germline NPM1 mutations lead to altered rRNA 2'-O-methylation and cause dyskeratosis congenita. *Nat Genet*

22. Gonzales, B., Henning, D., So, R. B., Dixon, J., Dixon, M. J., and Valdez, B. C. (2005) The Treacher Collins syndrome (TCOF1) gene product is involved in pre-rRNA methylation. *Hum Mol Genet* **14**, 2035-2043

23. Massenet, S., Bertrand, E., and Verheggen, C. (2017) Assembly and trafficking of box C/D and H/ACA snoRNPs. *RNA Biol* **14**, 680-692

24. Rothe, B., Saliou, J. M., Quinternet, M., Back, R., Tiotiu, D., Jacquemin, C., Loegler, C., Schlotter, F., Pena, V., Eckert, K., Morera, S., Dorsselaer, A. V., Branlant, C., Massenet, S., Sanglier-Cianferani, S., Manival, X., and Charpentier, B. (2014) Protein Hit1, a novel box C/D snoRNP assembly factor, controls cellular concentration of the scaffolding protein Rsa1 by direct interaction. *Nucleic Acids Res* **42**, 10731-10747

25. Verheggen, C., Pradet-Balade, B., and Bertrand, E. (2015) SnoRNPs, ZNHIT proteins and the R2TP pathway. *Oncotarget* **6**, 41399-41400

26. Bragantini, B., Tiotiu, D., Rothe, B., Saliou, J. M., Marty, H., Cianferani, S., Charpentier, B., Quinternet, M., and Manival, X. (2016) Functional and Structural Insights of the Zinc-Finger HIT protein family members Involved in Box C/D snoRNP Biogenesis. *J Mol Biol* **428**, 2488-2506

27. Bizarro, J., Charron, C., Boulon, S., Westman, B., Pradet-Balade, B., Vandermoere, F., Chagot, M. E., Hallais, M., Ahmad, Y., Leonhardt, H., Lamond, A., Manival, X., Branlant, C., Charpentier, B., Verheggen, C., and Bertrand, E. (2014) Proteomic and 3D structure analyses highlight the C/D box snoRNP assembly mechanism and its control. *J Cell Biol* **207**, 463-480

28. Watkins, N. J., Dickmanns, A., and Luhrmann, R. (2002) Conserved stem II of the box C/D motif is essential for nucleolar localization and is required, along with the 15.5K protein, for the hierarchical assembly of the box C/D snoRNP. *Mol Cell Biol* **22**, 8342-8352

29. Anttonen, A. K., Laari, A., Kousi, M., Yang, Y. J., Jaaskelainen, T., Somer, M., Siintola, E., Jakkula, E., Muona, M., Tegelberg, S., Lonnqvist, T., Pihko, H., Valanne, L., Paetau, A., Lun, M. P., Hastbacka, J., Kopra, O., Joensuu, T., Katsanis, N., Lehtinen, M. K., Palvimo, J. J., and Lehesjoki, A. E. (2017) ZNHIT3 is defective in PEHO syndrome, a severe encephalopathy with cerebellar granule neuron loss. *Brain* **140**, 1267-1279

30. Ounap, K., Muru, K., Oiglane-Shlik, E., Ilves, P., Pajusalu, S., Kuus, I., Wojcik, M. H., and Reimand, T. (2020) PEHO syndrome caused by compound heterozygote variants in ZNHIT3 gene. *Eur J Med Genet* **63**, 103660

31. Somer, M. (1993) Diagnostic criteria and genetics of the PEHO syndrome. *J Med Genet* **30**, 932-936

32. Salonen, R., Somer, M., Haltia, M., Lorentz, M., and Norio, R. (1991) Progressive encephalopathy with edema, hypsarrhythmia, and optic atrophy (PEHO syndrome). *Clin Genet* **39**, 287-293

33. Sabaie, H., Ahangar, N. K., Ghafouri-Fard, S., Taheri, M., and Rezazadeh, M. (2020) Clinical and genetic features of PEHO and PEHO-Like syndromes: A scoping review. *Biomedicine & pharmacotherapy = Biomedecine & pharmacotherapie* **131**, 110793

34. Õunap, K., Muru, K., Õiglane-Shlik, E., Ilves, P., Pajusalu, S., Kuus, I., Wojcik, M. H., and Reimand, T. (2019) PEHO syndrome caused by compound heterozygote variants in ZNHIT3 gene. *Eur J Med Genet*

35. Ryan, O. W., Poddar, S., and Cate, J. H. (2016) CRISPR-Cas9 Genome Engineering in Saccharomyces cerevisiae Cells. *Cold Spring Harb Protoc* **2016**

36. Grzechnik, P., Szczepaniak, S. A., Dhir, S., Pastucha, A., Parslow, H., Matuszek, Z., Mischo, H. E., Kufel, J., and Proudfoot, N. J. (2018) Nuclear fate of yeast snoRNA is determined by co-transcriptional Rnt1 cleavage. *Nat Commun* **9**, 1783

37. Bragantini, B., Tiotiu, D., Rothé, B., Saliou, J.-M., Marty, H., Cianférani, S., Charpentier, B., Quinternet, M., and Manival, X. (2016) Functional and Structural Insights of the Zinc-Finger HIT protein family members Involved in Box C/D snoRNP Biogenesis. *Journal of Molecular Biology* **428**, 2488-2506

38. Quinternet, M., Chagot, M. E., Rothé, B., Tiotiu, D., Charpentier, B., and Manival, X. (2016) Structural Features of the Box C/D snoRNP Pre-assembly Process Are Conserved through Species. *Structure* **24**, 1693-1706

39. Chagot, M. E., Boutilliat, A., Kriznik, A., and Quinternet, M. (2022) Structural Analysis of the Plasmodial Proteins ZNHIT3 and NUFIP1 Provides Insights into the Selectivity of a Conserved Interaction. *Biochemistry* **61**, 479-493

40. Henras, A. K., Plisson-Chastang, C., O'Donohue, M. F., Chakraborty, A., and Gleizes, P. E. (2015) An overview of pre-ribosomal RNA processing in eukaryotes. *Wiley Interdiscip Rev RNA* **6**, 225-242

41. Kos, M., and Tollervey, D. (2010) Yeast pre-rRNA processing and modification occur cotranscriptionally. *Mol Cell* **37**, 809-820

42. Osheim, Y. N., French, S. L., Keck, K. M., Champion, E. A., Spasov, K., Dragon, F., Baserga, S. J., and Beyer, A. L. (2004) Pre-18S ribosomal RNA is structurally compacted

into the SSU processome prior to being cleaved from nascent transcripts in Saccharomyces cerevisiae. *Mol Cell* **16**, 943-954

43. Mills, E. W., and Green, R. (2017) Ribosomopathies: There's strength in numbers. *Science* **358**

44. Sulima, S. O., Hofman, I. J. F., De Keersmaecker, K., and Dinman, J. D. (2017) How Ribosomes Translate Cancer. *Cancer Discov* **7**, 1069-1087

45. Erales, J., Marchand, V., Panthu, B., Gillot, S., Belin, S., Ghayad, S. E., Garcia, M., Laforets, F., Marcel, V., Baudin-Baillieu, A., Bertin, P., Coute, Y., Adrait, A., Meyer, M., Therizols, G., Yusupov, M., Namy, O., Ohlmann, T., Motorin, Y., Catez, F., and Diaz, J. J. (2017) Evidence for rRNA 2'-O-methylation plasticity: Control of intrinsic translational capabilities of human ribosomes. *Proc Natl Acad Sci U S A* **114**, 12934-12939

46. Baxter-Roshek, J. L., Petrov, A. N., and Dinman, J. D. (2007) Optimization of ribosome structure and function by rRNA base modification. *PLoS One* **2**, e174

47. Baudin-Baillieu, A., Fabret, C., Liang, X. H., Piekna-Przybylska, D., Fournier, M. J., and Rousset, J. P. (2009) Nucleotide modifications in three functionally important regions of the Saccharomyces cerevisiae ribosome affect translation accuracy. *Nucleic Acids Res* **37**, 7665-7677

48. Liang, X. H., Liu, Q., and Fournier, M. J. (2009) Loss of rRNA modifications in the decoding center of the ribosome impairs translation and strongly delays pre-rRNA processing. *RNA* **15**, 1716-1728

49. Liang, X. H., Liu, Q., and Fournier, M. J. (2007) rRNA modifications in an intersubunit bridge of the ribosome strongly affect both ribosome biogenesis and activity. *Mol Cell* **28**, 965-977

50. Cheung, Y. N., Maag, D., Mitchell, S. F., Fekete, C. A., Algire, M. A., Takacs, J. E., Shirokikh, N., Pestova, T., Lorsch, J. R., and Hinnebusch, A. G. (2007) Dissociation of eIF1 from the 40S ribosomal subunit is a key step in start codon selection in vivo. *Genes Dev* **21**, 1217-1230

51. Keeling, K. M., Lanier, J., Du, M., Salas-Marco, J., Gao, L., Kaenjak-Angeletti, A., and Bedwell, D. M. (2004) Leaky termination at premature stop codons antagonizes nonsense-mediated mRNA decay in S. cerevisiae. *RNA* **10**, 691-703

52. Salas-Marco, J., and Bedwell, D. M. (2005) Discrimination between defects in elongation fidelity and termination efficiency provides mechanistic insights into translational readthrough. *J Mol Biol* **348**, 801-815

53. Landry, D. M., Hertz, M. I., and Thompson, S. R. (2009) RPS25 is essential for translation initiation by the Dicistroviridae and hepatitis C viral IRESs. *Genes Dev* **23**, 2753-2764

54. Garreau de Loubresse, N., Prokhorova, I., Holtkamp, W., Rodnina, M. V., Yusupova, G., and Yusupov, M. (2014) Structural basis for the inhibition of the eukaryotic ribosome. *Nature* **513**, 517-522

55. Marchand, V., Blanloeil-Oillo, F., Helm, M., and Motorin, Y. (2016) Illumina-based RiboMethSeq approach for mapping of 2'-O-Me residues in RNA. *Nucleic Acids Res* **44**, e135

56. Beltrame, M., and Tollervey, D. (1995) Base pairing between U3 and the pre-ribosomal RNA is required for 18S rRNA synthesis. *EMBO J* **14**, 4350-4356

57. Li, H. D., Zagorski, J., and Fournier, M. J. (1990) Depletion of U14 small nuclear RNA (snR128) disrupts production of 18S rRNA in Saccharomyces cerevisiae. *Mol Cell Biol* **10**, 1145-1152

58. Khoshnevis, S., Dreggors, R. E., Hoffmann, T. F. R., and Ghalei, H. (2019) A conserved Bcd1 interaction essential for box C/D snoRNP biogenesis. *J Biol Chem* **294**, 18360-18371

59. Sharma, S., Marchand, V., Motorin, Y., and Lafontaine, D. L. J. (2017) Identification of sites of 2'-O-methylation vulnerability in human ribosomal RNAs by systematic mapping. *Sci Rep* **7**, 11490

60. Krogh, N., Jansson, M. D., Hafner, S. J., Tehler, D., Birkedal, U., Christensen-Dalsgaard, M., Lund, A. H., and Nielsen, H. (2016) Profiling of 2'-O-Me in human rRNA reveals a subset of fractionally modified positions and provides evidence for ribosome heterogeneity. *Nucleic Acids Res* **44**, 7884-7895

61. Buchhaupt, M., Sharma, S., Kellner, S., Oswald, S., Paetzold, M., Peifer, C., Watzinger, P., Schrader, J., Helm, M., and Entian, K. D. (2014) Partial methylation at Am100 in 18S rRNA of baker's yeast reveals ribosome heterogeneity on the level of eukaryotic rRNA modification. *PLoS One* **9**, e89640

62. Motorin, Y., Quinternet, M., Rhalloussi, W., and Marchand, V. (2021) Constitutive and variable 2'-O-methylation (Nm) in human ribosomal RNA. *RNA Biol*, 1-10

63. Aquino, G. R. R., Krogh, N., Hackert, P., Martin, R., Gallesio, J. D., van Nues, R. W., Schneider, C., Watkins, N. J., Nielsen, H., Bohnsack, K. E., and Bohnsack, M. T. (2021)

RNA helicase-mediated regulation of snoRNP dynamics on pre-ribosomes and rRNA 2'-O-methylation. *Nucleic Acids Res* **49**, 4066-4084

64. Zaher, H. S., and Green, R. (2009) Fidelity at the molecular level: lessons from protein synthesis. *Cell* **136**, 746-762

65. Kimura, S., and Suzuki, T. (2010) Fine-tuning of the ribosomal decoding center by conserved methyl-modifications in the Escherichia coli 16S rRNA. *Nucleic Acids Res* **38**, 1341-1352

66. Datta, M., Pillai, M., Modak, M. J., Liiv, A., Khaja, F. T., Hussain, T., Remme, J., and Varshney, U. (2021) A mutation in the ribosomal protein uS12 reveals novel functions of its universally conserved PNSA loop. *Mol Microbiol* **115**, 1292-1308

67. Jack, K., Bellodi, C., Landry, D. M., Niederer, R. O., Meskauskas, A., Musalgaonkar, S., Kopmar, N., Krasnykh, O., Dean, A. M., Thompson, S. R., Ruggero, D., and Dinman, J. D. (2011) rRNA pseudouridylation defects affect ribosomal ligand binding and translational fidelity from yeast to human cells. *Mol Cell* **44**, 660-666

68. Rodriguez, C. M., Chun, S. Y., Mills, R. E., and Todd, P. K. (2019) Translation of upstream open reading frames in a model of neuronal differentiation. *BMC Genomics* **20**, 391

69. Higa-Nakamine, S., Suzuki, T., Uechi, T., Chakraborty, A., Nakajima, Y., Nakamura, M., Hirano, N., and Kenmochi, N. (2012) Loss of ribosomal RNA modification causes developmental defects in zebrafish. *Nucleic Acids Res* **40**, 391-398

Figures

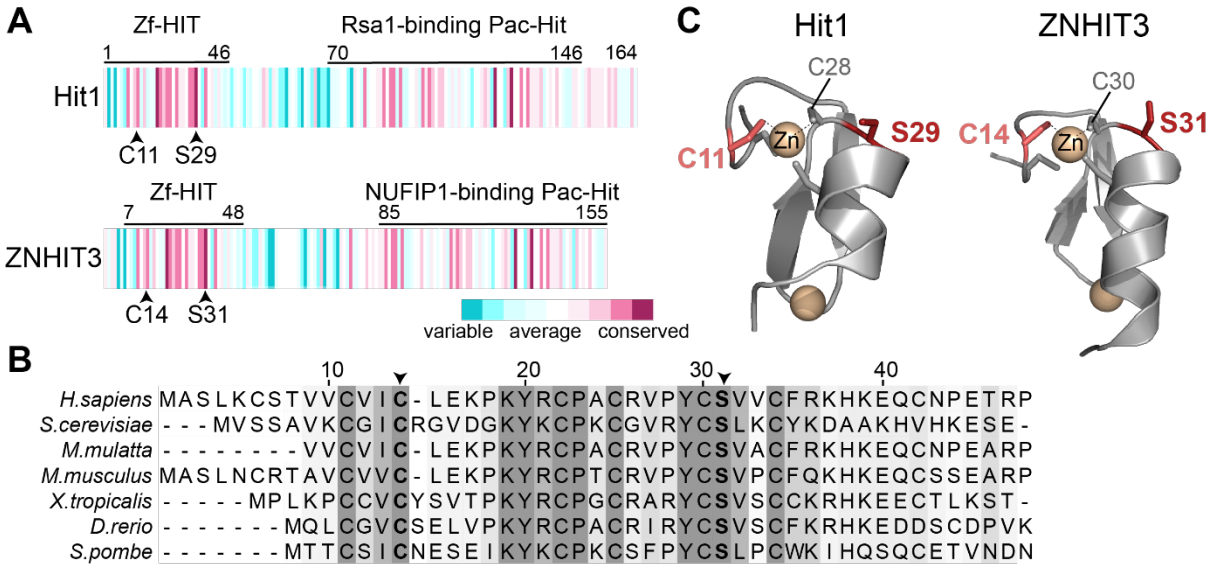

Figure 1. PEHO syndrome variations in the evolutionarily conserved protein Hit1. (A) Domain organization of yeast Hit1 and human ZNHIT3 showing the conserved residues mutated in PEHO syndrome. The figure was generated using ConSurf. **(B)** Multiple sequence alignment of the Zf-Hit domains generated with Clustal Omega and colored in Jalview. Shaded amino acids are conserved. Darker shades of gray show higher conservation. The PEHO-associated conserved cysteine and serine residues are in bold and marked with an arrow. **(C)** The structure of the Zf-HIT domain of Hit1 (PDB ID: 2N95) and ZNHIT3 (PDB ID: 2YQQ) highlighting the conserved residues mutated in PEHO syndrome.

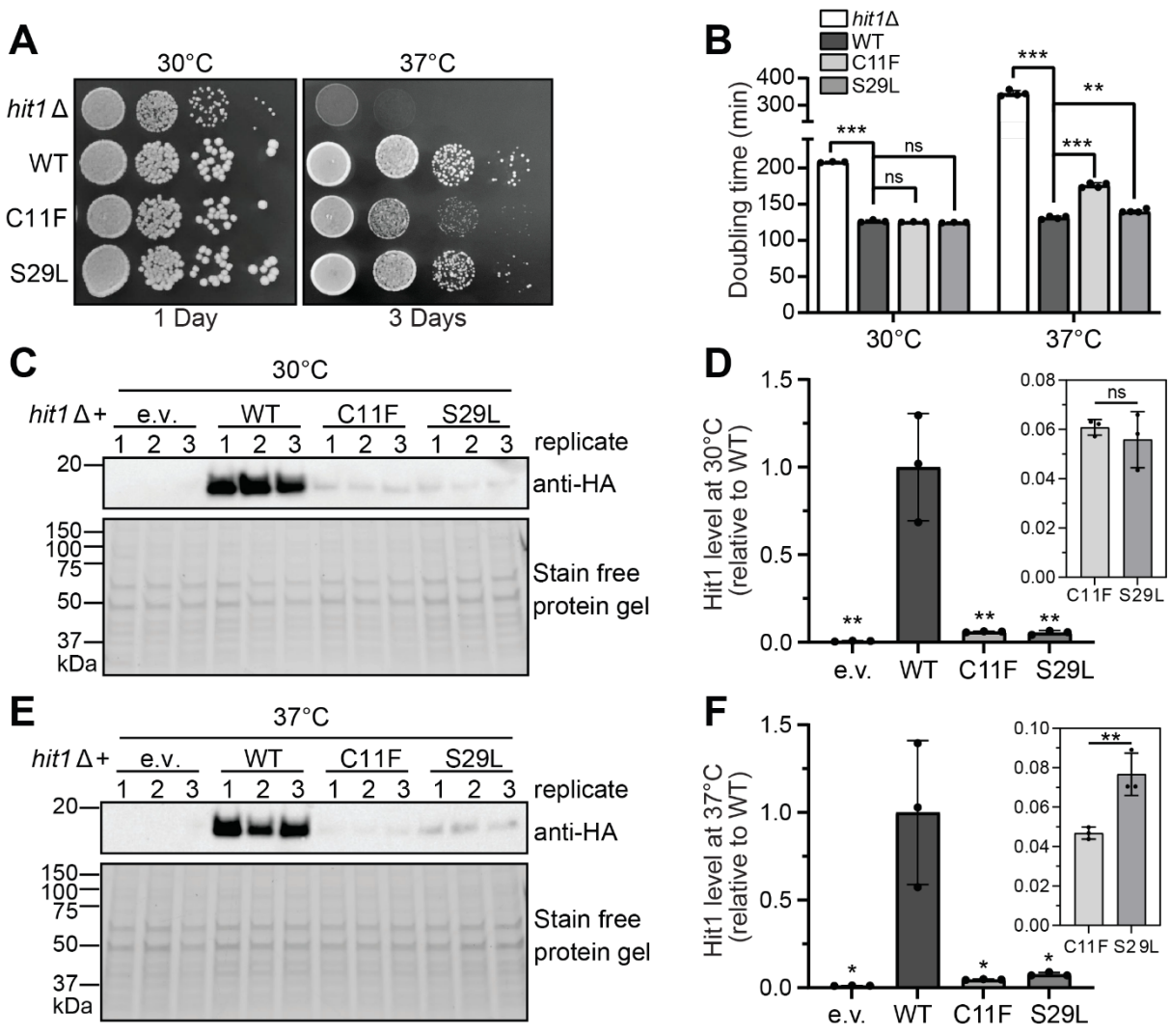

Figure 2. PEHO syndrome-associated amino acid variations in Hit1 protein cause temperature-sensitive slow-growth phenotypes and result in significant loss of Hit1 protein. **(A)** Growth of *hit1*Δ, wild-type (WT), *hit1-C11F*, and *hit1-S29L* yeast strains on complete solid medium at 30ºC and 37ºC. **(B)** Doubling times of *hit1*Δ, wild-type (WT), *hit1-C11F*, and *hit1-S29L* yeast strains at 30ºC and 37ºC in a complete liquid medium. **(C)** Western blot analysis of steady-state protein levels in total cell lysates of *hit1*Δ cells expressing N-terminally HA-tagged Hit1 (WT), Hit1-C11F, or Hit1-S29L at 30ºC. **(D)** Quantification of blots shown in panel C normalized to total protein signal relative to WT. Significance was determined using an unpaired

t-test compared to WT. Box shows a zoomed-in view of the relative steady-state protein levels in *hit1-C11F* and -*S29L* cells. **(E)** Western blot analysis of steady-state protein levels in total cell lysates of *hit1*Δ cells expressing N-terminally HA-tagged Hit1 (WT), Hit1-C11F, or Hit1-S29L at 37ºC. **(F)** Quantification of blots shown in panel C normalized to total protein signal relative to WT. Significance was determined using an unpaired t-test compared to WT. Box shows a zoomed-in view of the relative steady-state protein levels in *hit1-C11F* and -*S29L* cells. For all graphs, bars represent the mean and standard deviation of 3 biological replicates. ns: not significant; *: $P<0.05$; **: $P<0.01$; ***: $P<0.001$.

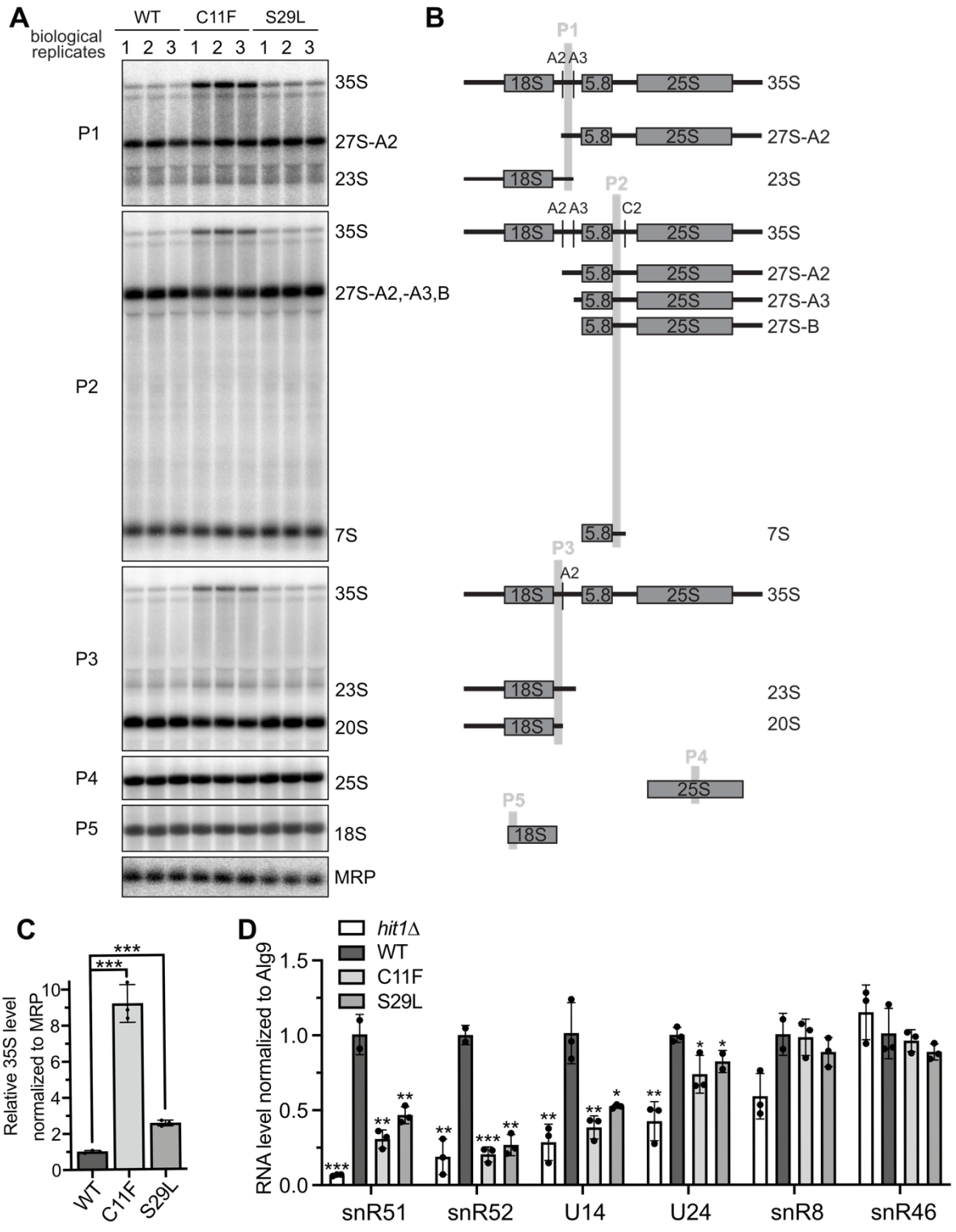

Figure 3. PEHO syndrome mutations result in defective rRNA processing and a reduction of steady-state box C/D snoRNA levels. (A) Northern blot analysis of steady-state levels of

precursor rRNA levels in *hit1*Δ, wild-type control (WT), *hit1-C11F*, and *hit1-S29L* yeast grown at 37ºC. Each set represents an independent biological replicate. **(B)** Schematic of the yeast 35S precursor rRNA showing the binding sites of probes (P1-P5) used in panel A. **(C)** Quantification on the blots shown in panel A. 35S signal is shown normalized to MRP signal and relative to WT. **(D)** RT-qPCR quantification of steady-state snoRNA levels in *hit1*Δ, wild-type control (WT), *hit1-C11F*, and *hit1-S29L* yeast grown at 37ºC. The levels of four box C/D snoRNAs and two H/ACA snoRNAs (controls) are shown. For all graphs, bars represent the mean and SD of 2-4 biological replicates. Significance was determined using an unpaired t-test compared to WT. n.s.: *: $P<0.05$; **: $P<0.01$; ***: $P<0.001$.

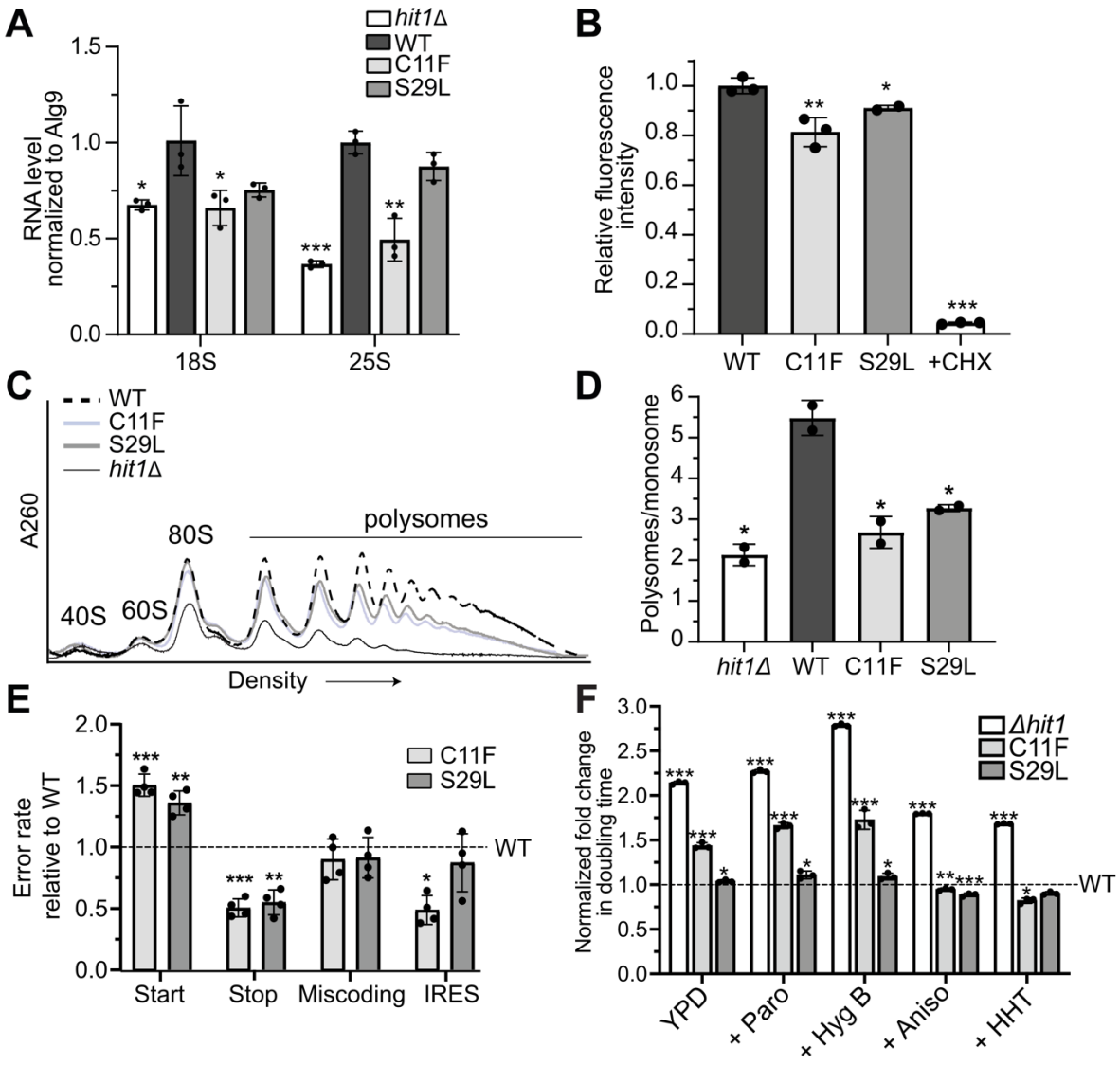

Figure 4. PEHO syndrome mutations cause translation defects. (A) RT-qPCR quantification of steady-state mature rRNA levels in *hit1*Δ, wild-type control (WT), *hit1-C11F*, and *hit1-S29L* yeast grown at 37ºC. **(B)** Quantification of nascent protein synthesis by Click-iT HPG in wild-type control and *hit1-C11F* cells**. (C)** Polysome profiles of *hit1*Δ yeast cells expressing wild-type HA-Hit1, HA-Hit1-C11F, HA-Hit1-S29L or an empty plasmid grown at 37°C. Clarified cell extracts were resolved on a sucrose gradient and scanned at 260 nm. **(D)** The ratios of polysomes to monosomes (P/M) determined by polysome profiling and area under the curve analysis of two biological replicates are indicated. **(E)** Expression of Firefly and Renilla luciferase was measured

in wild-type, *hit1-C11F* or *hit1-S29L* yeast harboring dual-luciferase plasmids (listed in table S3). The ratio of Firefly luciferase to Renilla luciferase is shown normalized to their respective control plasmids and relative to WT. **F)** Doubling times of *hit1*Δ, *hit1-C11F*, and *hit1-S29L* yeast in liquid media in the presence of translation inhibitors: Paromomycin (Paro), hygromycin B (Hyg B), anisomycin (Aniso) and homoharringtonine (HHT). The fold change is calculated by dividing the doubling time of *hit1*Δ*, hit1-C11F,* or *hit1-S29L* cells by the mean wild-type doubling time in each condition. Bars represent the mean and SD of 2-4 biological replicates. Significance was determined relative to wild-type using an unpaired t-test. *, $P < 0.05$; **, $P < 0.01$; ***, $P < 0.001$.

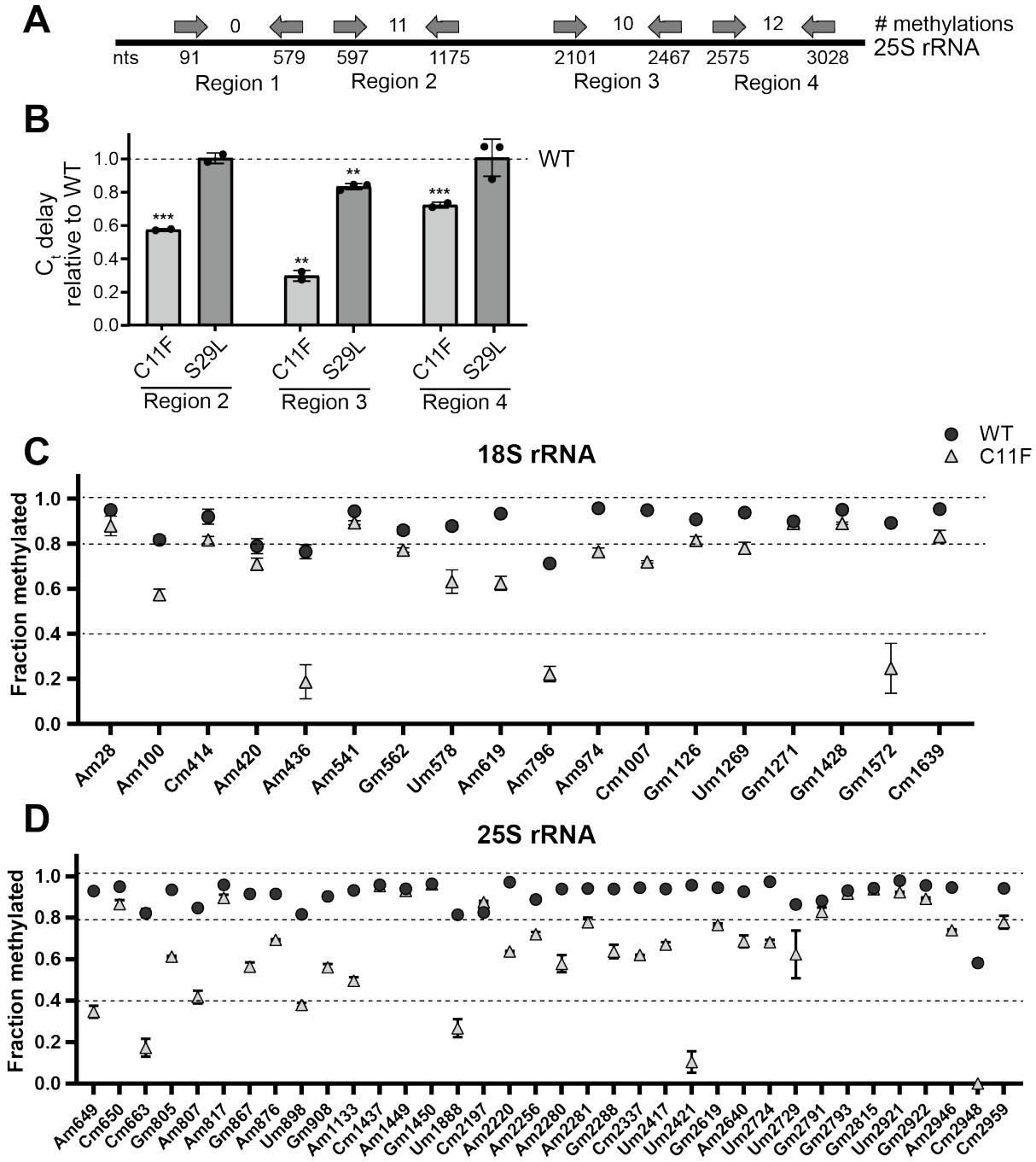

Figure 5. The *hit1-C11F* mutation results in site-specific reductions of 2'-O-methylation levels of polysomal rRNAs. A) Schematic of regions of 25S probed in B. **B)** Total RNA from wild-type control, *hit1-C11F*, and *hit1-S29L* cells were extracted, and three regions of 25S rRNA

(regions 2-4) were probed for their 2'-O-methylation levels by reverse transcription at low dNTP concentration followed by qPCR in biological triplicate. Region 1 was used for normalization. Bars represent the mean and SD of 2-3 biological replicates. Significance was determined relative to wild-type using an unpaired t-test. **, $P < 0.01$; ***, $P < 0.001$. **C-D)** RiboMethSeq analysis of polysomal RNA extracted from wild-type control and *hit1-C11F* cells grown at 37ºC. MethScores of 18S rRNA (**C**) and 25S rRNA 2'-O-methylated nucleotides (**D**). Data indicate the mean and SD of three biological replicates.

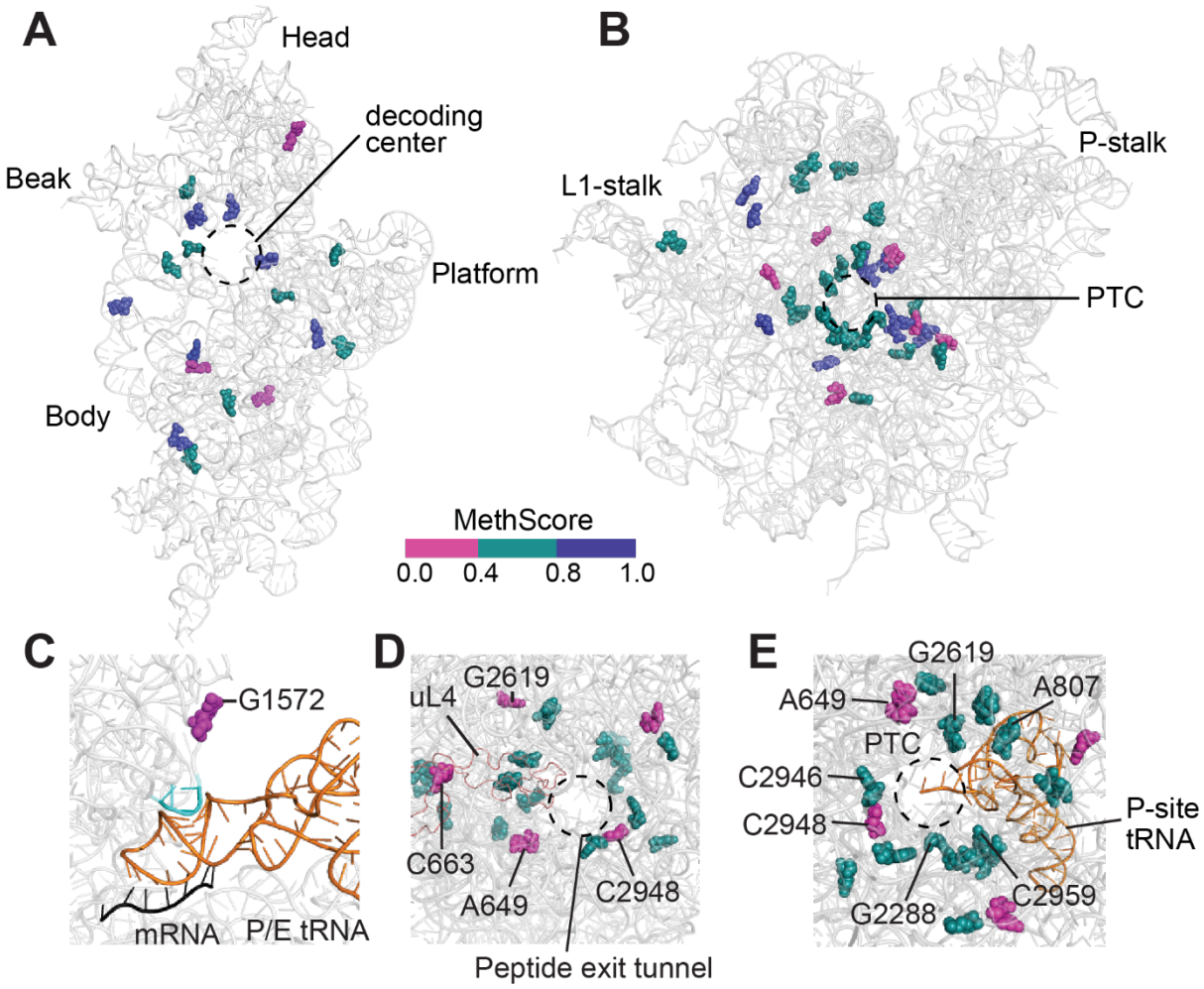

Figure 6. The *hit1-C11F* mutant impacts 2′-O-Methylation of nucleotides at key ribosome positions. A) The position of each rRNA 2'-O-methylation site is marked on the structure of 18S rRNA (PDB ID: 6GQV). **B)** The position of each rRNA 2'-O-methylation site is marked on the structure of 25S rRNA (PDB ID: 6GQV). In panels A and B, MethScores > 0.8 indicate stably methylated sites and are shown in the dark blue; MethScores between 0.4 and 0.8 are considered variable sites and shown in teal green; MethScores below 0.4 indicate hypo 2'-O-methylated sites and are in magenta. **C)** View of the small ribosomal subunit showing variable and hypo 2'-O-methylated sites near the decoding center. The critical and conserved ridge (nucleotides 1575-1578), which forms a steric block between the P- and E-site tRNA, is located near the hypo 2'-O-

methylated site G1572 and is shown in light blue. tRNA is colored in orange and mRNA in black (PDB ID: 3j78). Views of peptide exit tunnel (**D**) and peptidyl transferase center (**E**) show numerous variable and hypo 2'-O-methylated sites located at or near these functionally important regions.

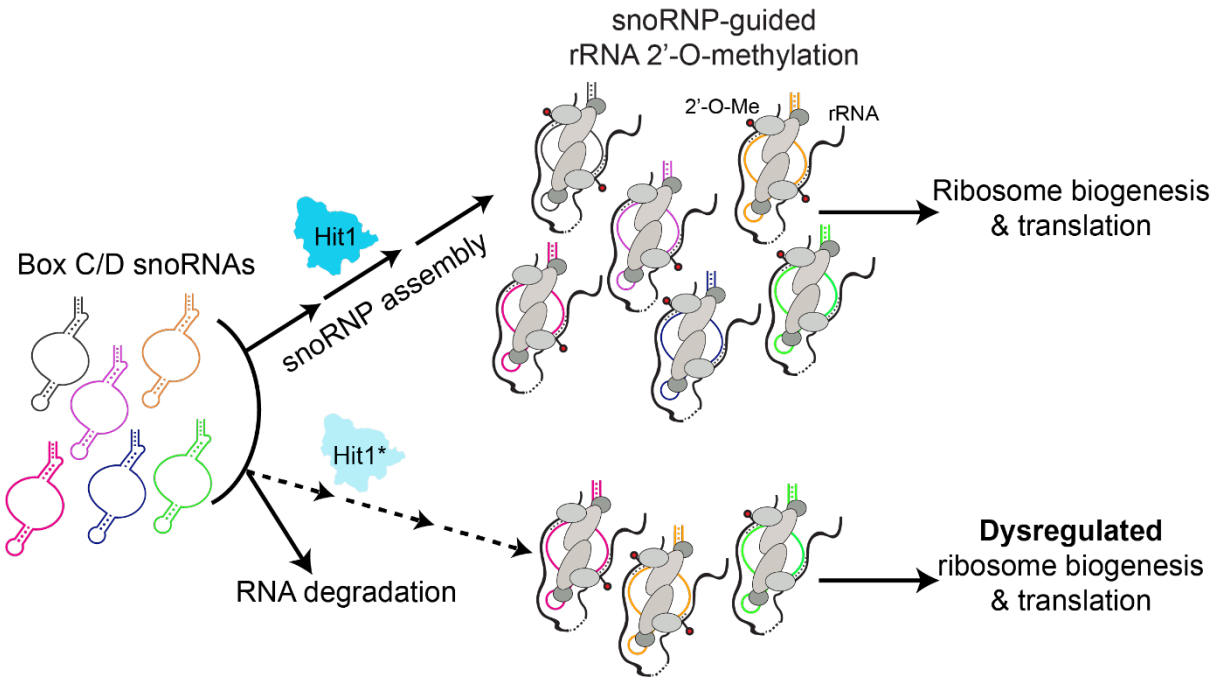

Figure 7. Model of the molecular mechanism of cellular defects caused by PEHO syndrome-associated Hit1 variants. Hit1 is an assembly factor critical for the formation of box C/D snoRNPs. The steady-state levels of Hit1 regulate the cellular box C/D snoRNA levels, the accuracy of rRNA 2'-O-methylation pattern, ribosome biogenesis and translation. PEHO-linked *hit1* mutant yeast cells have lower steady-state Hit1 levels that result in lower levels of box C/D snoRNAs and negatively impact snoRNP assembly, which leads to impaired ribosome biogenesis and rRNA 2'-O-methylation, ultimately altering the cellular translational program.

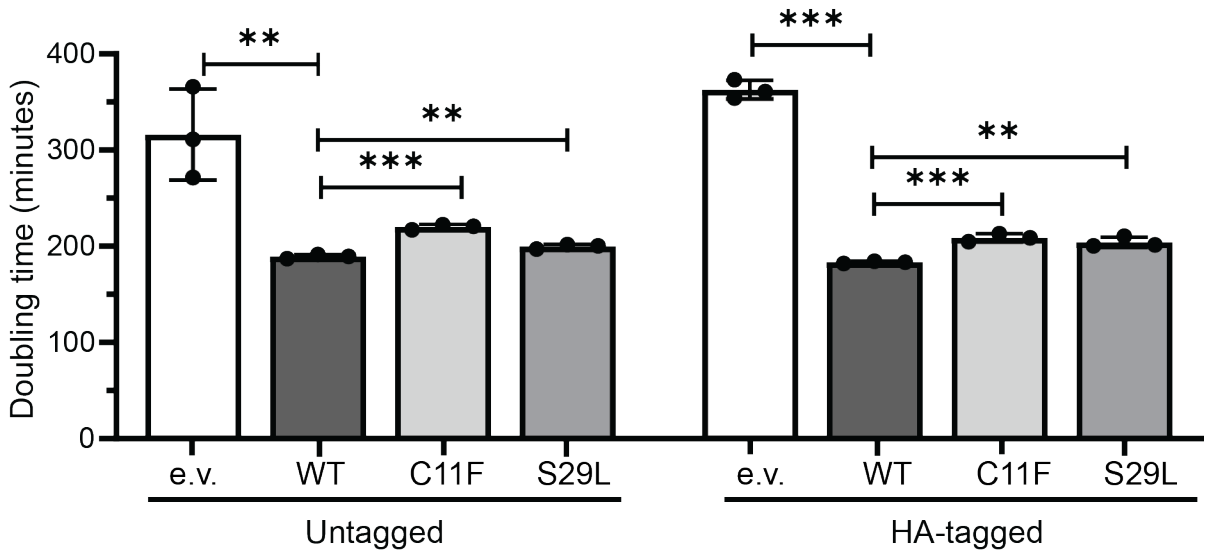

Figure S1. HA-tagged *HIT1* mutant yeast have the same slow-growth phenotype as untagged *HIT1* mutant yeast. Doubling times of *hit1*Δ yeast expressing 3xHA-tagged or untagged *Hit1*, *hit1-C11F*, *hit1-S29L*, or an empty vector is shown for cells grown in minimal media at 37ºC. Bars represent the mean and standard deviation of 3 biological replicates. Significance was determined using an unpaired t-test. **: P<0.01; ***: P<.001.

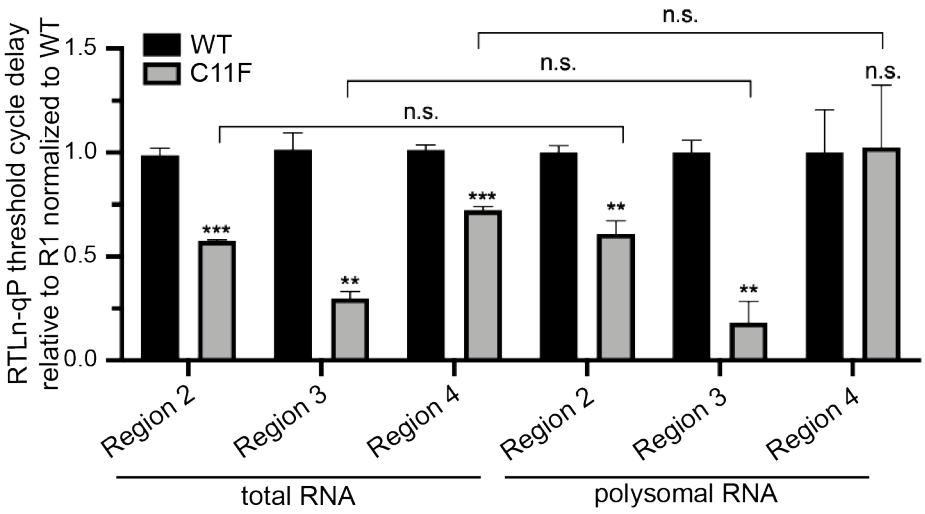

Figure S2. Ribosomal RNA 2'-O-methylation is not significantly altered between the total and polysomal RNA pools. Total RNA or polysomal RNA from wild-type control and *hit1-C11F* cells were extracted, and three regions of 25S rRNA were probed for their 2'-O-methylation levels by reverse transcription at low dNTP concentration followed by qPCR in biological triplicate. Bars represent the mean and SD of 2-3 biological replicates. Significance is shown relative to wild-type control. n.s.: not significant; **: $p<0.01$; ***: $p<0.001$.

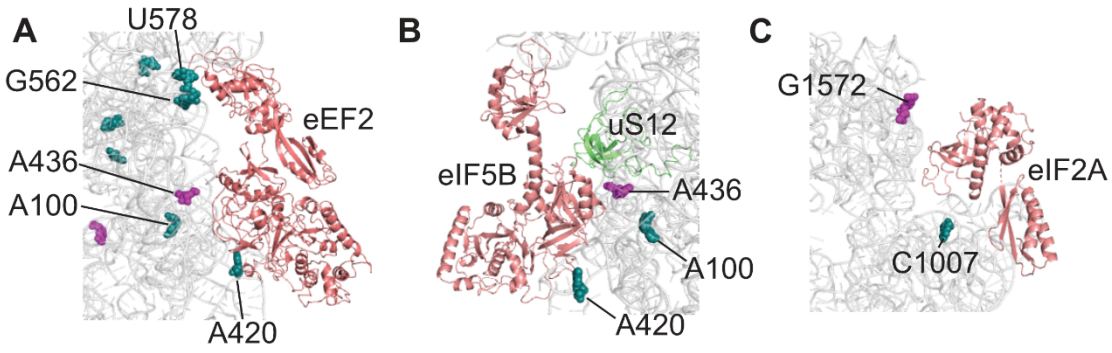

Figure S3. Views of the small ribosomal subunit showing variable and hypo 2'-O-methylated sites near eEF2 (**A**), eIF5B (**B**), eIF2A (**C**) binding sites. Translation factors located near hypo 2'-O-methylated sites are colored in salmon red (PDB IDs: 6GQV, 4V8Z, 6FYX), and the ribosomal protein uS12, located near the hypo 2'-O-methylated site A436, is colored in lime green.

Chapter 3. A conserved Bcd1 interaction essential for box C/D snoRNP biogenesis

Summary

Using mutational screening, we identified an N-terminal motif of Bcd1 which is necessary for Bcd1 binding with Snu13 and snoRNAs. We uncovered that these interactions are critical for snoRNP assembly, unveiling a novel step in the hierarchical box C/D snoRNP assembly pathway. I contributed to this work by performing northern blots for both small and large RNAs, uncovering the decreased box C/D snoRNA levels and rRNA processing impairments in *bcd1-D72A* cells. I also generated the *bcd1-D72A* mutations endogenously using CRISPR-Cas9 mediated genome editing.

S. Khoshnevis, R. E. Dreggors, T. F. R. Hoffmann, H. Ghalei, A conserved Bcd1 interaction essential for box C/D snoRNP biogenesis. *J Biol Chem* **294**, 18360-18371 (2019).

These findings were published in *Journal of Biological Chemistry* on November 29, 2019. Supplemental tables can be found online at: https://www.jbc.org/article/S0021-9258(20)30698-0/fulltext

Abstract

Precise modification and processing of rRNAs are required for the production of ribosomes and accurate translation of proteins. Small nucleolar ribonucleoproteins (snoRNPs) guide the folding, modification, and processing of rRNAs and are thus critical for all eukaryotic cells. Bcd1, an essential zinc finger HIT protein functionally conserved in eukaryotes, has been implicated as an early regulator for biogenesis of box C/D snoRNPs and controls steady-state levels of box C/D snoRNAs through an unknown mechanism. Using a combination of genetic and biochemical approaches, here we found a conserved N-terminal motif in Bcd1 from *Saccharomyces* cerevisiae that is required for interactions with box C/D snoRNAs and the core snoRNP protein, Snu13. We show that both the Bcd1-snoRNA and Bcd1-Snu13 interactions are critical for snoRNP assembly and ribosome biogenesis. Our results provide mechanistic insight into Bcd1 interactions that likely control the early steps of snoRNP maturation and contribute to the essential role of this protein in maintaining the steady-state levels of snoRNAs in the cell.

Introduction

Ribosomes are essential and conserved macromolecular machines that catalyze the production of proteins in all cells. Ribosome integrity is extensively monitored through its biogenesis in a highly regulated process that involves nearly 200 assembly factors (1, 2). A critically important class of assembly factors for ribosome biogenesis is small nucleolar ribonucleoproteins (snoRNPs)[3] that ensure the proper folding, modification, and processing of ribosomal RNAs for the coordinated binding of ribosomal proteins (3, 4). snoRNPs fall into two major groups based on their conserved RNA elements: box H/ACA snoRNPs direct the isomerization of uridines into pseudouridines, whereas box C/D snoRNPs guide the 2′-*O*-methylation of target RNAs. In these complexes, a small nucleolar RNA (snoRNA) binds to a set of essential core proteins to form the catalytically

active snoRNP (5).

Eukaryotic box C/D snoRNPs contain four core proteins: Snu13, Nop56, Nop58, and the methyltransferase Nop1 in yeast (SNU13, NOP56, NOP58, and FBL/fibrillarin in humans). These proteins are proposed to assemble on the snoRNA in a hierarchal manner (6–9), in a process that is regulated by the action of several assembly factors (10). In yeast, these assembly factors include the Hsp90/R2TP (Rvb1, Rvb2, Tah1, and Pih1) chaperone/co-chaperone system and the proteins Rsa1, Hit1, and Bcd1 (11–20). However, how these assembly factors drive the biogenesis of snoRNPs is not understood.

Among the assembly factors linked to box C/D snoRNP biogenesis, Bcd1 is essential and specific to this process, whereas others are implicated in the biogenesis of other RNPs (16, 21–23). Examples are the involvement of Rsa1 in assembly of the large ribosomal subunits (24) and the participation of R2TP in diverse cellular processes including transcription, chromatin remodeling, phosphatidylinositol-3 kinase-related protein kinase (PIKK) signaling, mitotic spindle assembly, and apoptosis (25–27).

The importance of Bcd1 as a factor required for box C/D snoRNA accumulation was first revealed using a *tetO7* shutoff allele of the essential *BCD1* gene in a microarray screen that was designed to monitor the abundance and processing of noncoding RNAs (22, 23). Later, RNAi-mediated depletion of the human homologue of *BCD1*, *ZNHIT6* indicated the conservation of Bcd1/ZNHIT6 function for maintaining box C/D snoRNA levels in human cells (11). Several more recent studies have identified the network of binding proteins for Bcd1 and ZNHIT6 (11–13, 21) including Rvb2, Pih1, Rsa1, Nop58, and Snu13 in yeast cells (11, 12) and RUVBL1/RUVBL2, PIH1, NUFIP, ZNHIT3, NOP58, and SNU13 in human cells (13). However, the mechanism of these interactions and the chronology of the binding events remain largely unclear.

Bcd1/ZNHIT6 are thought to be involved at early steps during the assembly of box C/D snoRNPs (13, 21). Using quantitative proteomics in human cell lines, ZNHIT6 was identified as part of an early protein-only complex together with assembly factors RUVBL1/2, NUFIP, ZNHIT3, and the core proteins SNU13 and NOP58 (13). More recently, depletion of Bcd1 was shown to result in a significant loss of interactions between Rsa1 and Nop58, suggesting that Bcd1 participates in loading of Nop58 into an early pre-snoRNP complex (21). Furthermore, Bcd1 controls the interaction of several snoRNP-related proteins with C/D snoRNAs (21). Although depletion of *BCD1* was shown to have minimal effect on the amount of Snu13 and Nop56 associated with box C/D snoRNAs, it significantly reduced the snoRNA association of assembly factors Rvb2, Pih1 and Rsa1, and the core proteins Nop58 and Nop1 (21). It is unclear how Bcd1 coordinates all these protein-protein and protein-RNA interactions and regulates the steady-state level of snoRNAs. Intriguingly, Bcd1 is reported to interact with RNAs directly in a nonspecific manner, and to bind to longer RNAs with higher affinity (16). Together, how Bcd1 gains specificity for assembly of box C/D snoRNPs and the significance of Bcd1-RNA interaction for maintaining snoRNA levels remain unclear.

Here we define the domain organization of Bcd1/ZNHIT6 and use a combination of genetic and biochemical approaches to show that Bcd1 interacts with snoRNAs and Snu13 via a conserved element near its N-terminal region. Further, we demonstrate that perturbation of these interactions leads to a significant decrease in steady-state levels of box C/D snoRNAs as well as defects in ribosome biogenesis. Together, our data provide insights into Bcd1-mediated interactions with box C/D snoRNAs and reveal their significance for snoRNP production and ribosome biogenesis.

Materials and methods

Yeast strains and plasmids

S. cerevisiae strains used in this study are listed in Table S1. Oligonucleotides and plasmids used in this study are listed in Table S2 and Table S3, respectively.

Making bcd1-D72A yeast strain using CRISPR-Cas9

Genome editing was carried out as described previously (58). A primer was designed for guide recognition sequence mutagenesis (Table S2) and used to amplify the pCAS9 vector (Addgene 60847) (59). A double-stranded 160-mer repair DNA was generated using oligos listed in Table S2. The D72A CRISPR was carried out by transforming pCAS9-Bcd1 and the PCR product into the WT BY4741 strain. Transformants were plated onto G418 and allowed to grow for 72 h at 37 °C. Individual colonies were selected and restreaked onto YPD. Mutations in individual colonies were confirmed by PCR and sequencing.

Yeast growth assays

tetO7::BCD1 cells containing ZNHIT6 or Bcd1 expression plasmids were grown to saturation in synthetic glucose liquid culture lacking histidine (His^-). Cultures were diluted in sterile water to a final concentration of 10^7 cells/ml, followed by four successive cascade dilutions in a 1:10 ratio. Dilutions were spotted onto synthetic His^- medium plates with and without doxycycline and grown at 30 °C.

Protein expression and purification

All proteins were expressed in *Escherichia coli* Rosetta2 (DE3) cells (Novagen). Cells were grown at 37 °C to A_{600} of 0.6 in 2× YT media supplemented with the appropriate antibiotics and then transferred to 18 °C. Protein expression was induced by addition of 0.3 mm or 1 mm isopropyl β-D-1-thiogalactopyranoside (IPTG) for pGEX-6-P2 or pET23/pSV272 harboring cells, respectively. Cultures were harvested 18 h after induction.

Bcd1 and Bcd1-D72A were expressed as His-tagged proteins and purified on Ni-NTA resin in buffer A. The protein was eluted with 250 mm imidazole. The tag was cleaved overnight and the protein was further purified over a MonoS ion exchange column in buffer B and eluted with a linear gradient of 150 mm to 1 mNaCl over 20 column volumes. Final purification was performed on a Superdex S-200 gel filtration column (GE Healthcare) equilibrated in 150 mm NaCl, 20 mm Tris/HCl, pH 7.5, 5% glycerol, 40 μm $ZnCl_2$, and 1 mm DTT. His-MBP–tagged Bcd1 and Bcd1-D72A were purified on Ni-NTA in buffer A and eluted as above. The proteins were buffer exchanged overnight in buffer B and further purified over MonoQ and Superdex 200 columns and stored in 150 mm NaCl, 20 mm Tris/HCl, pH 7.5, 5% glycerol and 40 μm $ZnCl_2$ and 1 mm DTT. Rvb1/2 were expressed and purified as published previously (60). MBP-Rsa1/GST-Hit1 were co-expressed and purified using Ni-NTA in 200 mm NaCl, 50 mm HEPES/NaOH, pH 7.5, 5% glycerol. The complex was eluted by increasing the concentration of imidazole to 200 mm, and further purified on a GSH Sepharose column (GE Healthcare). The GST tag of Hit1 was removed overnight using PreScission protease (GE Healthcare) in buffer B. The GST tag and the protease were removed using a MonoQ ion exchange column. The complex was further polished using a Superdex 200 gel filtration column equilibrated in 200 mm NaCl, 20 mm HEPES/NaOH, 5% glycerol, and 1 mm DTT. GST-Snu13 was purified using GSH Sepharose in buffer C. The protein was further purified using a Superdex 75 gel filtration column in buffer D. $Nop58^{1–437}$ was purified as a GST-tagged protein in buffer C. The GST-tag was cleaved off overnight using PreScission protease in 150 mm NaCl, 30 mm Tris/HCl, pH 7.5, 5% glycerol, and 2 mm 2-mercaptoethanol. Both GST-tagged and untagged proteins were further purified using MonoQ and Superdex 200 and stored in buffer D. Tah1 and His-tagged Pih1 were co-expressed and purified on Ni-NTA resin in 100 mm NaCl, 25 mm sodium phosphate, 5% glycerol, and 30 mm imidazole. The complex

was eluted by increasing the concentration of imidazole to 200 mm. The His tag of Pih1 was cleaved overnight using tobacco etch virus protease in 100 mm NaCl, 25 mm sodium phosphate, and 10% glycerol. The uncleaved His-Pih1 and the tobacco etch virus protease were removed by a second step of Ni-NTA. The complex was further purified using a Superdex 200 gel filtration column equilibrated in 100 mmNaCl, 25 mm sodium phosphate, 5% glycerol, and 1 mm DTT. GST-tagged Tah1 and His-MBP–tagged Pih1 were co-expressed and purified as above with the exception that after the first Ni-NTA, the complex was further purified on GSH Sepharose. His-MBP tag was cleaved overnight. The complex was polished on S-200 gel filtration column.

In vitro interaction studies

5 μm of the untagged proteins were mixed with 3 μm tagged protein (or control) in 150 mm NaCl and 20 mm Tris/HCl, pH 7.5, 5% glycerol, and 40 μm $ZnCl_2$, and preincubated on ice for 15 min. 10% of the reaction was set aside as the input control before addition of 25 μl of equilibrated amylose resin (New England Biolabs) or GSH Sepharose. The mixture was incubated for 30 min at 4 °C, washed, and eluted with binding buffer supplemented with either 20 mm maltose (amylose resin) or reduced glutathione (GSH Sepharose). Input, final wash, and the eluate from each binding study were analyzed on a SDS-PAGE.

In vitro RNA-protein–binding assay

In vitro transcribed RNA was labeled using [γ-^{32}P]ATP. Trace amount of labeled RNA was folded and mixed with appropriate protein and incubated for 20 min in 20 mm Tris, pH 7.5, 100 mm KCl, 5 mm $MgCl_2$at 30 °C before mixing with the heparin loading dye (1 mg/ml final concentration) and loading on a running 8% acrylamide/TBE gel at 4 °C. Protein-bound and unbound fractions were quantified using Quantity One (Bio-Rad), and data were fit to a single binding isotherm using Prism (GraphPad).

Measuring the thermal stability of Bcd1 and its variant

3 μm of Bcd1-WT or D72A variant were loaded as triplicates into glass capillaries (NanoTemper Technologies) and intrinsic protein fluorescence at 330 and 350 nm was monitored between 35 and 95 °C in the Tycho instrument (NanoTemper Technologies). Temperature inflection values (Ti) were obtained by automated data analysis using the accompanying software.

Analysis of the steady-state levels of snoRNAs

Cells were grown in selective media in the presence of doxycycline, to $A_{600} \sim 0.6$. Total RNA from three biological replicates of each strain was isolated using the hot phenol method. snoRNAs were separated on 10% acrylamide/urea gels, transferred to Hybond nylon membrane (GE Healthcare) and probed as indicated. Bands were quantified using Image Lab software (Bio-Rad).

Analysis of the steady-state levels of pre-rRNAs

BY4741 or *bcd1-D72A* cells were grown in YPD to mid-log phase. Total RNAs from three biological samples of each yeast strain were isolated using the hot phenol method. rRNAs were separated on a 1% agarose/formaldehyde gel and transferred by capillarity overnight in 20× saline sodium citrate on a nylon membrane (GE Healthcare). Membranes were probed as indicated. Band were quantified using Image Lab software (Bio-Rad).

Pulldown assay from yeast cells

tetO7::BCD1 yeast cells were grown for 16 h in YPD while constitutively expressing a twin-Strep–tagged Bcd1 from a TEF promoter. Strep-tagged protein was purified using Strep-Tactin (IBA Lifesciences) in 150 mm NaCl, 50 mm Tris/HCl, pH 7.5, 5% glycerol, and 5 mm $MgCl_2$, and eluted in the same buffer supplemented with 2.5 mm desthiobiotin. Eluted proteins were analyzed by Western blotting. Eluted RNA was precipitated and analyzed by Northern blotting as described above with the exception that 1 fmol of an *in vitro* transcribed random RNA was spiked

into each tube to serve as the control for precipitation efficiency.

Twin-Strep–Snu13 was expressed from GPD promoter in *tetO7::BCD1* cells expressing endogenous Bcd1 as well as HA-tagged WT or D72A variant of Bcd1. Strep purification and data analysis were performed as described above.

Sucrose density gradient analysis

Yeast cells were grown to mid log phase in YPD supplemented with 10 mg/liter doxycycline and harvested after addition of 0.1 mg/ml cycloheximide, washed, and lysed in ice-cold gradient buffer (20 mm HEPES, pH 7.4, 5 mm $MgCl_2$, 100 mm NaCl, and 3 mm DTT) supplemented with 0.1 mg/ml cycloheximide and cOmplete Protease Inhibitor mixture (Roche). Lysate was cleared by 10 min of centrifugation at 10,000 × *g*, applied to 10–50% sucrose gradients in gradient buffer, and centrifuged for 2 h at 40,000 rpm in a SW 41 Ti rotor. Gradients were fractionated and scanned by UV 260 nm absorbance. Fractions were analyzed for their protein content by Western blotting.

Antibodies

HRP-conjugated anti-rabbit and anti-mouse secondary antibodies were obtained from Rockland Immunochemicals. The Utp13, Rrp5, and Rps10 antibodies (a gift from K. Karbstein, Scripps, FL) and the Rvb2 (a gift from W. Houry) were raised in rabbits. Bcd1 was detected using an anti-HA antibody obtained from BioLegend or HRP-conjugated anti-Strep (IBA Bioscience). Rpl3 was detected by an antibody obtained from the Developmental Studies Hybridoma Bank, The University of Iowa, deposited by J.R. Warner.

Results

Bcd1 and ZNHIT6 share similar domains that are arranged differently

Yeast Bcd1 is an essential protein (22, 28) with a zinc finger HIT domain (Zf-HIT) at its N terminus (residues 1–45) which has high structural homology to the Zf-HIT domain of Hit1 (16).

The Zf-HIT domain is important for the stability of Bcd1 (16) and mediates the interaction of ZNHIT6 with RUVBL1/2 (29). We reasoned that because deletion of Zf-HIT domain of Bcd1 is not lethal in yeast (16), additional elements must contribute to the essential function of the protein. To identify the important domains of Bcd1, we first performed a sequence alignment across eukaryotes using Clustal Omega, followed by a domain analysis using IUPred and Phyre2 (30–32). Bcd1 proteins fall into two groups (Fig. 1*A*): the first group, exemplified by human Bcd1 (ZNHIT6), contains an intrinsically disordered region (IDR) at its N terminus (residues 1 to ∼70 of ZNHIT6), a Zf-HIT domain in the middle (residues 215–258), and a wheel domain (residues 304–452). The wheel domain consists of a twisted five-stranded β sheet surrounded by several α helices and was predicted based on homology to a newly identified domain in Cns1, an essential Hsp90 co-chaperone (33). The second group, exemplified by yeast Bcd1 (Fig. 1*A*), contains a Zf-HIT domain at its N terminus (residues 1–45) (16), followed by a wheel domain (123–288) and an intrinsically disordered region at the C terminus (310–366). Thus, Bcd1 and ZNHIT6 share similar domains that are organized differently.

A conserved region in the N terminus of Bcd1 is essential for yeast viability

Previous studies showed that expression of the Zf-HIT domain of Bcd1 (residues 1–45) alone does not support the growth of yeast depleted of endogenous *BCD1* (16). However, a fragment encompassing residues 1–96 of Bcd1 is sufficient to maintain cell viability in the absence of *BCD1* (21). To investigate the reason for this growth rescue, we first checked the expression of Bcd1 fragments lacking either the Zf-HIT domain (*bcd1*$^{47–366}$) or residues 1–97 (*bcd1*$^{97–366}$) in cells depleted of the endogenous *BCD1* via a doxycycline-repressible promoter (*tetO7::BCD1*). As expected, the expression of *bcd1*$^{47–366}$ partially rescued the lethality of *BCD1*-depleted cells. Cells expressing *bcd1*$^{97–366}$ grew similarly to cells expressing an empty vector, implicating that Bcd1

residues 47–97 are important for cell viability (Fig. 1*B*). To confirm that the observed growth defects are not because of lack of protein expression, we assayed the expression of the two variant proteins ($Bcd1^{47–366}$ and $Bcd1^{97–366}$) by Western blotting (Fig. 1*C*). These data indicated that the two Bcd1 variants were expressed and their levels were similar to WT Bcd1.

To identify which Bcd1 residues are critical for function, we individually mutated highly conserved amino acids within this region to alanine (Fig. S1) and checked the effect of each mutation on the growth of yeast cells depleted of their endogenous *BCD1* and supplemented with a plasmid expressing the variant protein. Of all the conserved residues tested, the alanine substitution of Asp-72 (*bcd1-D72A*) showed a strong growth phenotype that resembled the growth defect observed in cells expressing vector only (Fig. 1*D*). Mutation of Leu-76 to alanine (L76A) also conferred a growth phenotype, albeit to a much lesser extent than D72A, indicating the overall importance of the region-spanning residues 72–76 (Fig. 1*D*). It is noteworthy that mutating the highly conserved residue Tyr-73 within this region did not show any effect on cell growth (Fig. 1*D*), indicating the specific importance of Asp-72, and to a lesser extent, Leu-76 for Bcd1 function. Because the effect from D72A mutation on cell growth was much greater than L76A, we focused on this residue for further analyses.

To check whether the observed phenotype in cells expressing Bcd1-D72A was a result of protein destabilization because of the mutation, we compared the expression levels of WT and D72A proteins by Western blotting. These analyses confirmed that the protein variant was expressed to similar levels as WT Bcd1 (Fig. 1*E*). To compare the stability of the D72A variant and WT Bcd1 proteins, we overexpressed and purified each protein and measured their thermal unfolding (Fig. 1*F*). Bcd1 and Bcd1-D72A show similar apparent melting temperatures (ΔTi 2.6 °C, Fig. 1*F*), suggesting the D72A mutation does not lead to a global destabilization of the protein and instead

likely affects Bcd1 function.

D72A disrupts the Bcd1 binding to the core snoRNP protein, Snu13

Bcd1 interacts with core box C/D snoRNP proteins Nop58 and Snu13 and assembly factors Rvb2, Pih1, and Rsa1 (11, 12). The interaction network of Bcd1/ZNHIT6 has been established using *in vitro* pulldown experiments and quantitative proteomic studies in cell culture (13). However, the coordination of the events remains largely unknown (10). We reasoned that if Bcd1 interactions with its binding partners are essential, the growth defect observed upon expression of Bcd1-D72A may arise from disruption of these important interactions. To test this, we performed pulldown assays to compare the binding interaction of WT and D72A variant of Bcd1 to its known binding partners (Fig. 2). We purified the core proteins individually and co-purified Rvb1 with Rvb2, Tah1 with Pih1, and MBP-tagged Rsa1 with Hit1 (removal of the MBP moiety renders the Rsa1/Hit1 complex unstable). Because the C terminus of Nop58 is highly charged and intrinsically disordered, we could not purify the protein to high purity and yield and therefore used a Nop58 variant that lacks the last 73 amino acids of the protein ($Nop58^{1–437}$).

First, the complex of MBP-Rsa1/Hit1 was immobilized on amylose resin and incubated with excess of either WT or D72A variant of Bcd1. After extensive washing of the resin, the retained proteins were eluted and analyzed on SDS-PAGE. We did not observe any significant difference in the binding of the D72A variant *versus* WT Bcd1 to MBP-Rsa1/Hit1 (Fig. 2*A*). We next immobilized MBP-tagged Bcd1 or Bcd1-D72A on amylose resin and incubated it with either Rvb1/Rvb2 complex (Fig. 2*B*), Tah1/Pih1 complex (Fig. 2*C*), or $Nop58^{1–438}$ (Fig. 2*D*). Rvb1/Rvb2 and Tah1/Pih1 demonstrated robust binding to either MBP-Bcd1 WT or D72A (Fig. 2, *B* and *C*). In contrast, $Nop58^{1–437}$ bound weakly to both (Fig. 2*D*). To confirm these findings, we performed the reciprocal pulldown by immobilizing GST-$Nop58^{1–437}$ or GST-Tah1/Pih1 or GST alone on

GSH Sepharose beads and incubated them WT and D72A variant of Bcd1. As expected, both WT and D72A variant of Bcd1 were pulled down by GST-Nop58$^{1–437}$ or GST-Tah1/Pih1 but not by GST alone (Fig. S2, *A* and *B*). We did not perform the reciprocal pulldown with Rvb1/2 as tagging these proteins can interfere with their oligomeric state (34). Strikingly, when Bcd1 or Bcd1-D72A were tested for their interaction with GST-Snu13, no binding was observed for Bcd1-D72A (Fig. 2*E*). In the reciprocal pulldown, untagged Snu13 did not bind to either WT MBP-Bcd1 or D72A variant (data not shown). It is likely that the N-terminal region of Bcd1 is responsible for establishing its transient interaction with Snu13 and hence a large tag such as MBP could hinder this interaction. Collectively, these *in vitro* binding assays indicate that the Bcd1-D72A variant abolishes binding to Snu13, but does not impact interactions with Rvb1/2, Tah1/Pih1, or Nop58.

To confirm these results further, we expressed N-terminally Strep-tagged BCD1 or Bcd1-D72A in yeast cells and purified the protein from mid-log phase yeast total lysates and analyzed the proteins that co-eluted using Western blotting. Although WT Bcd1 co-purified both Rvb2 and Snu13 (Fig. 3*A*), the Bcd1-D72A variant bound to Rvb2 but failed to co-purify Snu13 (Fig. 3*A*), further corroborating the results of pulldown assays performed using recombinant proteins (Fig. 2*E*). To further support this finding, we performed the reciprocal pulldown using an N-terminally Strep-tagged Snu13 overexpressed in cells expressing HA-tagged WT or D72A variant of Bcd1. Analysis of the eluted proteins by Western blotting revealed that Strep-Snu13 can pull down Bcd1 from WT, but not *bcd1-D72A* cells (Fig. S2*C*). Taken together, these data confirm the results of *in vitro* binding assays that D72A variant fails to interact with Snu13.

Bcd1-D72A variant is impaired in binding to RNA

Bcd1 interacts with RNAs in a nonspecific manner (16), yet it contributes specifically to the maintenance of box C/D snoRNA levels in the cell (22, 23). To test if the severe growth defect

observed upon expression of Bcd1-D72A may partially arise from the loss of interaction of Bcd1 with RNA, we compared the RNAs co-purified with WT Strep-tagged Bcd1 and D72A variants (see above) using Northern blotting. Although the levels of purified WT Bcd1 and Bcd1-D72A are similar, significantly less U3 and U24 snoRNAs were bound to Bcd1-D72A as compared with Bcd1-WT (Fig. 3, *A* and *B*). To corroborate this *in vivo* finding, we *in vitro* transcribed a box C/D snoRNA (snR51) and compared its affinity for Bcd1 and Bcd1-D72A using EMSAs. Although WT Bcd1 binds to snR51 with a K_d of 0.47 ± 0.05 μm, the D72A variant binds more weakly (K_d 3.90 ± 0.79 μm) (Fig. 3, *C* and *D*). Taken together, these data suggest that Bcd1 Asp-72 affects the ability of the protein to interact with snoRNAs.

Bcd1D72A abolishes production of box C/D snoRNAs

Bcd1 is essential for the maintenance of box C/D snoRNA levels (22, 23). We therefore reasoned that the severe growth phenotype observed upon expressing Bcd1-D72A may be a result of perturbing box C/D snoRNA levels. To test this hypothesis, we used Northern blotting to analyze the steady-state levels of six box C/D snoRNAs in mid-log phase cells expressing WT *BCD1*, *bcd1-D72A*, or an empty vector (Fig. 4, *A*and *B*). These were compared with levels of scR1, the RNA component of the signal recognition particle, and three box H/ACA snoRNAs as controls (Fig. 4). As previously observed in the cells depleted of *BCD1*(21–23), lower levels of the tested box C/D snoRNAs, and unchanged levels of H/ACA snoRNAs and scR1 RNA were observed when an empty vector was expressed (Fig. 4). Similarly, in the cells expressing Bcd1-D72A, the levels of the tested box C/D snoRNAs decreased (Fig. 4). This change was unique to box C/D snoRNAs as the three box H/ACA snoRNAs tested did not show significant variations in cells expressing Bcd1-D72A. Because the expression level of Bcd1 and Bcd1-D72A is similar (Fig. 1*E*), the significant drop in the level of box C/D snoRNAs strongly suggests that the

conserved Bcd1 Asp72 is critical for maintaining the cellular levels of box C/D snoRNAs.

Dysregulation of Bcd1 impairs ribosome biogenesis

Box C/D snoRNAs are active players in the assembly of ribosomes and direct the folding, processing, and 2′-*O*-methylation of rRNAs during transcription and ribosomal protein binding (5). Because of their critical role in ribosome assembly, alteration of snoRNA levels can have profound effects on cell viability, especially in rapidly dividing cells such as cancer cells (35, 36). To assess the significance of Bcd1 interactions with Snu13 and snoRNAs for snoRNP biogenesis and ribosome production, we grew cells expressing Bcd1 or the Bcd1-D72A variant to mid-log phase and stalled translation by addition of cycloheximide. Polysome profiles on 10–50% sucrose gradients revealed a significant decrease in polysomes and an increase in the amount of free 60S subunit in cells expressing Bcd1-D72A compared with WT (Fig. 5*A*). Western blot analysis of gradient fractions (Fig. 5*B*) revealed that in WT cells, RpS10, a small ribosomal subunit (SSU) protein, was mainly in fractions corresponding to the monosomes and the polysomes. Rpl3, a large ribosomal subunit protein, was also found mostly in fractions corresponding to the monosomes and the polysomes. Utp13, a ribosome assembly factor and a subunit of the UTPB complex, which is involved in the biogenesis of SSU processome (37) was found in fractions corresponding to 90S. Rrp5, a protein involved in the assembly of both 40S and 60S subunits (38), was found in fractions corresponding to maturing 60S as well as SSU processome. However, in *bcd1-D72A*cells RpS10 was mainly found in 40S and 80S fractions (Fig. 5*B*). There was also a significant decrease in RpS10 in the polysomes, indicating a drop in the pool of translating ribosomes. Similarly, RpL3 was mostly found in 60S and 80S fractions. Some Rpl3 was also detected in early polysome fractions, albeit to a much lesser extent than WT. Interestingly, both Utp13 and Rrp5 shifted toward lighter fractions in cells expressing Bcd1-D72A, indicating a defect in the formation of SSU

processome and perturbation of ribosome assembly.

To reveal how this mutation impairs ribosome biogenesis, we analyzed rRNA processing in WT and *bcd1-D72A* cells. To avoid possible effects from the addition of doxycycline on rRNA processing, we used CRISPR-Cas9 genome engineering to introduce *bcd1-D72A* mutation into BY4741 yeast strain. We isolated total RNA from BY4741 or *bcd1-D72A* cells in the log phase and subjected them to Northern blotting.

In yeast the majority of rRNA processing occurs co-transcriptionally (39, 40), where A_0 and A_1 cleavages in 5′-ETS are followed by the A_2 cleavage in ITS1, resulting in the formation of 20S as the major 18S precursor (reviewed in Ref. 41). In an alternative pathway, shown to happen under unfavorable growth conditions, 35S is cleaved further downstream of the A_2 site at the so-called A_3 site, resulting in the formation of 23S (40–47). Our analysis revealed a reduction in the levels of both 18S and 25S rRNAs in *bcd1-D72A* cells (Fig. 6), explaining the decrease in their polysome levels (Fig. 5). The levels of 20S and 27S A_2, the products of the A_2 cleavage in ITS1 were also lowered in *bcd1-D72A* cells compared with WT. This reduction was accompanied by an increase in the unprocessed 35S as well as 23S suggesting a switch from co-transcriptional A_2 processing to posttranscriptional A_3 processing pathway.

Collectively, these data indicate the critical role of Bcd1-mediated interactions during snoRNP assembly and their impact on ribosome biogenesis.

Discussion

snoRNAs regulate the biogenesis and modification of ribosomes and are thus critically important for control of the cellular translational output. Despite their importance, little is currently known about how snoRNA levels are controlled posttranscriptionally. This is an important question because snoRNA level changes can lead to a decrease in ribosome biogenesis as well as the

alteration of the rRNA modification pattern, which impacts translation fidelity and the choice of mRNAs translated (48–51). Indeed, alteration of snoRNA levels is commonly observed in various human cancers, including breast, brain, lung, and prostate cancers (35).

The abundance of snoRNAs is controlled by the binding to a set of core proteins for the formation of catalytically active snoRNPs. Complex formation protects snoRNAs from degradation by nucleases, thus regulating their turnover rate (10, 52). Assembly factors assist in binding of the core proteins to snoRNAs, but their mechanism of function is poorly understood (10). Here, we show that the interactions of the assembly factor Bcd1 with the core protein Snu13 and snoRNAs are critical for maintaining box C/D snoRNA levels. Furthermore, our mutational analyses revealed a critical region of Bcd1 (residues 72–76) which is important for the essential function of the protein for interaction with Snu13 and snoRNAs.

Based on previous proteomic experiments in human cell lines, a model for snoRNP assembly was suggested (13). In this model, ZNHIT6 associates with an early protein-only pre-snoRNP complex and is proposed to stay bound during maturation to be part of a complex that recruits the box C/D snoRNAs. ZNHIT6 is thought to leave the maturing pre-snoRNP concomitantly with the binding of fibrillarin and Nop56 (13). Whether ZNHIT6 presence is required for snoRNA recruitment and how it controls the steady-state level of box C/D snoRNAs has so far remained elusive.

In yeast, an N-terminal fragment (residues 1–97) of Bcd1 is sufficient for growth and maintenance of steady-state expression levels of box C/D snoRNAs, although it associates poorly with snoRNAs (21). *In vitro*, full-length Bcd1 and a viable N-terminally truncated form of Bcd1 that lacks the Zf-HIT domain (residues 1–45) interact with snoRNAs but their binding can be competed out in presence of longer RNAs (16). These data suggested that the key function of Bcd1 is independent of its ability to bind to RNA (16, 21). Our mutational screening approach enabled us

to define the effect of single amino acid substitutions in the region of Bcd1 that is associated with its essential function (residues 45–97) and to reassess the ability of the protein to interact with RNAs in its full-length form. We show that the D72A mutation significantly weakens the binding of Bcd1 to RNA and Snu13, causing a severe growth defect in yeast cells and altering the steady-state levels of snoRNAs. Our data strongly suggest that the ability of Bcd1 to interact with Snu13 and snoRNAs is important for its essential function in snoRNP assembly and for maintenance of box C/D snoRNA steady-state levels.

Secondary structure prediction of Bcd1-D72A using PSIPRED and its comparison to the WT protein indicates that Asp-72 is located in a short loop between two helices (Fig. S1). The D72A mutation could result in the disappearance of the short loop and formation of a long helix by combining the two helices. Thus, we suggest that the Bcd1-D72A mutation weakens the interaction of the protein with Snu13 and RNA by a conformational change between the Zf-HIT and wheel domains of the protein. Structural analysis of Bcd1 will be essential to clarify its interactions that are critically important for its role in snoRNP biogenesis.

Discussion

snoRNAs are produced as larger precursors that are trimmed by exonucleases for maturation in a process that is linked to the assembly of the snoRNP core proteins (52). The conserved box C/D RNA elements, which form Kink(K)-turns, are essential for snoRNP assembly and serve as the binding site for the recruitment of Snu13 that is followed by ordered recruitment of other core proteins (9, 53–55). Thus, the association of Snu13 with pre-snoRNAs is required for establishing the hierarchy of binding of the other core proteins and is thought to be the first step in commitment of snoRNAs to assembly (10). Similarly, Bcd1 is found to associate with pre-snoRNAs at an early stage, and likely co-transcriptionally (21). We therefore anticipate that our identified Bcd1-

mediated contacts with Snu13 and snoRNAs will be essential and critical for early engagement of the snoRNP assembly machinery to protect snoRNAs from rapid turnover.

Eukaryotes transcribe their major ribosomal RNAs (18S, 5.8S, and 25S/28S) as a large polycistronic precursor (35S) (1). In yeast, this precursor can undergo processing either co-transcriptionally (~70%) or posttranscriptionally (~30%) (39). The hallmark of the co-transcriptional route is the cleavage at site A_2within ITS1, resulting in the formation of 20S and $27SA_2$, whereas the posttranscriptional route is marked by the production of 35S precursor and the A_3 cleavage, resulting in the formation of 23S and $27SA_3$. It was shown that under stress, yeast cells switch their rRNA processing toward posttranscriptional route (40, 46, 47). This route is considered for most part to be nonproductive (46). However, there is evidence of 23S processing to make new 18S rRNA (47). The *bcd1-D72A* cells, which are impaired in snoRNP biogenesis, show the features of posttranscriptional rRNA processing: accumulation of 35S accompanied by an increase in 23S and a drop in 20S levels. They grow and make new ribosomes, albeit at a lower rate. It is therefore tempting to speculate that hypomethylation of the rRNA pushes the balance between co-transcriptional and posttranscriptional rRNA processing toward the latter. It remains to be examined whether or not the new ribosomes made in these cells are the products of the A_3 cleavage pathway or the co-transcriptional pathway.

Bcd1 is conserved from yeast to human. Because the Bcd1 mutation analyzed in this study is conserved in ZNHIT6, we used the cBioPortal (56, 57) to investigate the common cancer mutations in ZNHIT6 (Fig. S3). Interestingly, the most common form of mutation observed in ZNHIT6 is a truncation at residue Arg-258, which likely results in the production of a truncated form of the protein that lacks the conserved region encompassing Asp-277, and thus fails to interact with Snu13 and snoRNAs. Thus, modulation of the Bcd1/ZNHIT6 essential interactions by a

single point mutation may be exploited by cancer cells and effectively contribute to the alteration of snoRNA levels and perturbation of ribosome biogenesis. This may be an effective means to unbalance the level of snoRNAs in cancer cells, or perhaps modulate the cellular translational program under certain stress conditions. Confirmation of this awaits the future analyses of ZNHIT6 function in human cells.

Acknowledgements

We thank J. A. Ball for purification of Nop58$^{1–437}$ and GST-Snu13, and K. Araki for help with gradient fractionation. We also thank K. P. Hopfner for the Rvb1/2 expression plasmid; W. Houry and K. Karbstein for antibodies; and G. L. Conn, C. M. Dunham, D. Reines, and members of the Ghalei lab for comments on the manuscript.This work was supported by Department of Biochemistry at Emory School of Medicine startup funds (to H. G.).

References

1. Woolford J. L. Jr., and Baserga S. J. (2013) Ribosome biogenesis in the yeast *Saccharomyces cerevisiae*. *Genetics* 195, 643–681 10.1534/genetics.113.153197

2. Klinge S., and Woolford J. L. Jr. (2019) Ribosome assembly coming into focus. *Nat. Rev. Mol. Cell Biol*. 20, 116–131 10.1038/s41580-018-0078-y

3. Sloan K. E., Warda A. S., Sharma S., Entian K. D., Lafontaine D. L. J., and Bohnsack M. T. (2017) Tuning the ribosome: The influence of rRNA modification on eukaryotic ribosome biogenesis and function. *RNA Biol*. 14, 1138–1152 10.1080/15476286.2016.1259781

4. Decatur W. A., and Fournier M. J. (2003) RNA-guided nucleotide modification of ribosomal and other RNAs. *J. Biol. Chem*. 278, 695–698 10.1074/jbc.R200023200

5. Watkins N. J., and Bohnsack M. T. (2012) The box C/D and H/ACA snoRNPs: Key players in the modification, processing and the dynamic folding of ribosomal RNA. *Wiley Interdiscip. Rev. RNA* 3, 397–414 10.1002/wrna.117

6. Watkins N. J., Dickmanns A., and Lührmann R. (2002) Conserved stem II of the box C/D motif is essential for nucleolar localization and is required, along with the 15.5K protein, for the hierarchical assembly of the box C/D snoRNP. *Mol. Cell. Biol*. 22, 8342–8352 10.1128/mcb.22.23.8342-8352.2002

7. Omer A. D., Ziesche S., Ebhardt H., and Dennis P. P. (2002) In vitro reconstitution and activity of a C/D box methylation guide ribonucleoprotein complex. *Proc. Natl. Acad. Sci. U.S.A*. 99, 5289–5294 10.1073/pnas.082101999

8. Tran E. J., Zhang X., and Maxwell E. S. (2003) Efficient RNA 2′-*O*-methylation requires juxtaposed and symmetrically assembled archaeal box C/D and C′/D′ RNPs. *EMBO J*. 22, 3930–3940 10.1093/emboj/cdg368

9. Watkins N. J., Segault V., Charpentier B., Nottrott S., Fabrizio P., Bachi A., Wilm M., Rosbash M., Branlant C., and Luhrmann R. (2000) A common core RNP structure shared between the small nucleolar box C/D RNPs and the spliceosomal U4 snRNP. *Cell* 103, 457–466 10.1016/s0092-8674(00)00137-9

10. Massenet S., Bertrand E., and Verheggen C. (2017) Assembly and trafficking of box C/D and H/ACA snoRNPs. *RNA Biol*. 14, 680–692 10.1080/15476286.2016.1243646

11. McKeegan K. S., Debieux C. M., Boulon S., Bertrand E., and Watkins N. J. (2007) A dynamic scaffold of pre-snoRNP factors facilitates human box C/D snoRNP assembly. *Mol. Cell. Biol*. 27, 6782–6793 10.1128/MCB.01097-07

12. McKeegan K. S., Debieux C. M., and Watkins N. J. (2009) Evidence that the AAA+ proteins TIP48 and TIP49 bridge interactions between 15.5K and the related NOP56 and NOP58 proteins during box C/D snoRNP biogenesis. *Mol. Cell. Biol*. 29, 4971–4981 10.1128/MCB.00752-09

13. Bizarro J., Charron C., Boulon S., Westman B., Pradet-Balade B., Vandermoere F., Chagot M. E., Hallais M., Ahmad Y., Leonhardt H., Lamond A., Manival X., Branlant C., Charpentier B., Verheggen C., and Bertrand E. (2014) Proteomic and 3D structure analyses highlight the C/D box snoRNP assembly mechanism and its control. *J. Cell Biol*. 207, 463–480 10.1083/jcb.201404160

14. Boulon S., Marmier-Gourrier N., Pradet-Balade B., Wurth L., Verheggen C., Jády B. E., Rothé B., Pescia C., Robert M. C., Kiss T., Bardoni B., Krol A., Branlant C., Allmang C., Bertrand E., and Charpentier B. (2008) The Hsp90 chaperone controls the biogenesis of L7Ae RNPs through conserved machinery. *J. Cell Biol*. 180, 579–595 10.1083/jcb.200708110

15. Back R., Dominguez C., Rothé B., Bobo C., Beaufils C., Morera S., Meyer P., Charpentier B., Branlant C., Allain F. H., and Manival X. (2013) High-resolution structural analysis shows how Tah1 tethers Hsp90 to the R2TP complex. *Structure* 21, 1834–1847 10.1016/j.str.2013.07.024

16. Bragantini B., Tiotiu D., Rothé B., Saliou J. M., Marty H., Cianférani S., Charpentier B., Quinternet M., and Manival X. (2016) Functional and structural insights of the zinc-finger HIT protein family members involved in box C/D snoRNP biogenesis. *J. Mol. Biol*. 428, 2488–2506 10.1016/j.jmb.2016.04.028

17. Rothé B., Saliou J. M., Quinternet M., Back R., Tiotiu D., Jacquemin C., Loegler C., Schlotter F., Peña V., Eckert K., Moréra S., Dorsselaer A. V., Branlant C., Massenet S., Sanglier-Cianférani S., Manival X., and Charpentier B. (2014) Protein Hit1, a novel box C/D snoRNP assembly factor, controls cellular concentration of the scaffolding protein Rsa1 by direct interaction. *Nucleic Acids Res*. 42, 10731–10747 10.1093/nar/gku612

18. Kakihara Y., Makhnevych T., Zhao L., Tang W., and Houry W. A. (2014) Nutritional status modulates box C/D snoRNP biogenesis by regulated subcellular relocalization of the R2TP complex. *Genome Biology* 15, 404 10.1186/s13059-014-0404-4

19. Zhao R., Kakihara Y., Gribun A., Huen J., Yang G., Khanna M., Costanzo M., Brost R. L., Boone C., Hughes T. R., Yip C. M., and Houry W. A. (2008) Molecular chaperone Hsp90 stabilizes Pih1/Nop17 to maintain R2TP complex activity that regulates snoRNA accumulation. *J. Cell Biol*. 180, 563–578 10.1083/jcb.200709061

20. Prieto M. B., Georg R. C., Gonzales-Zubiate F. A., Luz J. S., and Oliveira C. C. (2015) Nop17 is a key R2TP factor for the assembly and maturation of box C/D snoRNP complex. *BMC Mol. Biol*. 16, 7 10.1186/s12867-015-0037-5

21. Paul A., Tiotiu D., Bragantini B., Marty H., Charpentier B., Massenet S., and Labialle S. (2019) Bcd1p controls RNA loading of the core protein Nop58 during C/D box snoRNP biogenesis. *RNA* 25, 496–506 10.1261/rna.067967.118

22. Peng W. T., Robinson M. D., Mnaimneh S., Krogan N. J., Cagney G., Morris Q., Davierwala

A. P., Grigull J., Yang X., Zhang W., Mitsakakis N., Ryan O. W., Datta N., Jojic V., Pal C., et al. (2003) A panoramic view of yeast noncoding RNA processing. *Cell* 113, 919–933 10.1016/s0092-8674(03)00466-5

23. Hiley S. L., Babak T., and Hughes T. R. (2005) Global analysis of yeast RNA processing identifies new targets of RNase III and uncovers a link between tRNA 5′ end processing and tRNA splicing. *Nucleic Acids Res*. 33, 3048–3056 10.1093/nar/gki608

24. Kressler D., Doère M., Rojo M., and Linder P. (1999) Synthetic lethality with conditional dbp6 alleles identifies rsa1p, a nucleoplasmic protein involved in the assembly of 60S ribosomal subunits. *Mol. Cell. Biol*. 19, 8633–8645 10.1128/mcb.19.12.8633

25. Kakihara Y., and Houry W. A. (2012) The R2TP complex: Discovery and functions. *Biochim. Biophys. Acta* 1823, 101–107 10.1016/j.bbamcr.2011.08.016

26. Nano N., and Houry W. A. (2013) Chaperone-like activity of the AAA+ proteins Rvb1 and Rvb2 in the assembly of various complexes. *Philos. Trans. R. Soc. Lond. B Biol. Sci*. 368, 20110399 10.1098/rstb.2011.0399

27. Snider J., Thibault G., and Houry W. A. (2008) The AAA+ superfamily of functionally diverse proteins. *Genome Biol*. 9, 216 10.1186/gb-2008-9-4-216

28. Giaever G., Chu A. M., Ni L., Connelly C., Riles L., Veronneau S., Dow S., Lucau-Danila A., Anderson K., Andre B., Arkin A. P., Astromoff A., El-Bakkoury M., Bangham R., Benito R., et al. (2002) Functional profiling of the *Saccharomyces cerevisiae* genome. *Nature* 418, 387–391 10.1038/nature00935

29. Cloutier P., Poitras C., Durand M., Hekmat O., Fiola-Masson E., Bouchard A., Faubert D., Chabot B., and Coulombe B. (2017) R2TP/Prefoldin-like component RUVBL1/RUVBL2 directly interacts with ZNHIT2 to regulate assembly of U5 small nuclear ribonucleoprotein. *Nat.*

Commun. 8, 15615 10.1038/ncomms15615

30. Sievers F., Wilm A., Dineen D., Gibson T. J., Karplus K., Li W., Lopez R., McWilliam H., Remmert M., Soding J., Thompson J. D., and Higgins D. G. (2011) Fast, scalable generation of high-quality protein multiple sequence alignments using Clustal Omega. *Mol. Syst. Biol*. 7, 539 10.1038/msb.2011.75

31. Dosztanyi Z., Csizmok V., Tompa P., and Simon I. (2005) IUPred: Web server for the prediction of intrinsically unstructured regions of proteins based on estimated energy content. *Bioinformatics* 21, 3433–3434 10.1093/bioinformatics/bti541

32. Kelley L. A., Mezulis S., Yates C. M., Wass M. N., and Sternberg M. J. E. (2015) The Phyre2 web portal for protein modeling, prediction and analysis. *Nat. Protoc*. 10, 845 10.1038/nprot.2015.053

33. Schopf F. H., Huber E. M., Dodt C., Lopez A., Biebl M. M., Rutz D. A., Muhlhofer M., Richter G., Madl T., Sattler M., Groll M., and Buchner J. (2019) The co-chaperone Cns1 and the recruiter protein Hgh1 link Hsp90 to translation elongation via chaperoning elongation factor 2. *Mol. Cell* 74, 73–87.e78 10.1016/j.molcel.2019.02.011

34. Cheung K. L., Huen J., Kakihara Y., Houry W. A., and Ortega J. (2010) Alternative oligomeric states of the yeast Rvb1/Rvb2 complex induced by histidine tags. *J. Mol. Biol*. 404, 478–492 10.1016/j.jmb.2010.10.003

35. Gong J., Li Y., Liu C. J., Xiang Y., Li C., Ye Y., Zhang Z., Hawke D. H., Park P. K., Diao L., Putkey J. A., Yang L., Guo A. Y., Lin C., and Han L. (2017) A pan-cancer analysis of the expression and clinical relevance of small nucleolar RNAs in human cancer. *Cell Rep*. 21, 1968–1981 10.1016/j.celrep.2017.10.070

36. Monaco P. L., Marcel V., Diaz J. J., and Catez F. (2018) 2′-*O*-methylation of ribosomal RNA:

Towards an epitranscriptomic control of translation? *Biomolecules* 8, E106 10.3390/biom8040106

37. Barandun J., Hunziker M., and Klinge S. (2018) Assembly and structure of the SSU processome—a nucleolar precursor of the small ribosomal subunit. *Curr. Opin. Struct. Biol*. 49, 85–93 10.1016/j.sbi.2018.01.008

38. Venema J., and Tollervey D. (1996) RRP5 is required for formation of both 18S and 5.8S rRNA in yeast. *EMBO J*. 15, 5701–5714

39. Kos M., and Tollervey D. (2010) Yeast pre-rRNA processing and modification occur cotranscriptionally. *Mol. Cell*37, 809–820 10.1016/j.molcel.2010.02.024

40. Osheim Y. N., French S. L., Keck K. M., Champion E. A., Spasov K., Dragon F., Baserga S. J., and Beyer A. L. (2004) Pre-18S ribosomal RNA is structurally compacted into the SSU processome prior to being cleaved from nascent transcripts in *Saccharomyces cerevisiae*. *Mol. Cell* 16, 943–954 10.1016/j.molcel.2004.11.031

41. Henras A. K., Plisson-Chastang C., O'Donohue M. F., Chakraborty A., and Gleizes P. E. (2015) An overview of pre-ribosomal RNA processing in eukaryotes. *Wiley Interdiscip. Rev. RNA* 6, 225–242 10.1002/wrna.1269

42. Dunbar D. A., Wormsley S., Agentis T. M., and Baserga S. J. (1997) Mpp10p, a U3 small nucleolar ribonucleoprotein component required for pre-18S rRNA processing in yeast. *Mol. Cell. Biol*. 17, 5803–5812 10.1128/mcb.17.10.5803

43. Venema J., and Tollervey D. (1999) Ribosome synthesis in *Saccharomyces cerevisiae*. *Annu. Rev. Genet*. 33, 261–311 10.1146/annurev.genet.33.1.261

44. Mullineux S. T., and Lafontaine D. L. (2012) Mapping the cleavage sites on mammalian pre-rRNAs: Where do we stand? *Biochimie* 94, 1521–1532 10.1016/j.biochi.2012.02.001

45. Kos-Braun I. C., and Kos M. (2017) Post-transcriptional regulation of ribosome biogenesis in yeast. *Microbial Cell* 4, 179–181 10.15698/mic2017.05.575

46. Kos-Braun I. C., Jung I., and Kos M. (2017) Tor1 and CK2 kinases control a switch between alternative ribosome biogenesis pathways in a growth-dependent manner. *PLoS Biol*. 15, e2000245 10.1371/journal.pbio.2000245

47. Talkish J., Biedka S., Jakovljevic J., Zhang J., Tang L., Strahler J. R., Andrews P. C., Maddock J. R., and Woolford J. L. Jr. (2016) Disruption of ribosome assembly in yeast blocks cotranscriptional pre-rRNA processing and affects the global hierarchy of ribosome biogenesis. *RNA* 22, 852–866 10.1261/rna.055780.115

48. Erales J., Marchand V., Panthu B., Gillot S., Belin S., Ghayad S. E., Garcia M., Laforets F., Marcel V., Baudin-Baillieu A., Bertin P., Coute Y., Adrait A., Meyer M., Therizols G., et al. (2017) Evidence for rRNA 2′-*O*-methylation plasticity: Control of intrinsic translational capabilities of human ribosomes. *Proc. Natl. Acad. Sci. U.S.A*. 114, 12934–12939 10.1073/pnas.1707674114

49. Baudin-Baillieu A., Fabret C., Liang X. H., Piekna-Przybylska D., Fournier M. J., and Rousset J. P. (2009) Nucleotide modifications in three functionally important regions of the *Saccharomyces cerevisiae* ribosome affect translation accuracy. *Nucleic Acids Res*. 37, 7665–7677 10.1093/nar/gkp816

50. Krogh N., Jansson M. D., Hafner S. J., Tehler D., Birkedal U., Christensen-Dalsgaard M., Lund A. H., and Nielsen H. (2016) Profiling of 2′-*O*-Me in human rRNA reveals a subset of fractionally modified positions and provides evidence for ribosome heterogeneity. *Nucleic Acids Res*. 44, 7884–7895 10.1093/nar/gkw482

51. Marcel V., Ghayad S. E., Belin S., Therizols G., Morel A. P., Solano-Gonzalez E., Vendrell J.

A., Hacot S., Mertani H. C., Albaret M. A., Bourdon J. C., Jordan L., Thompson A., Tafer Y., Cong R., et al. (2013) p53 acts as a safeguard of translational control by regulating fibrillarin and rRNA methylation in cancer. *Cancer Cell* 24, 318–330 10.1016/j.ccr.2013.08.013

52. Kufel J., and Grzechnik P. (2019) Small nucleolar RNAs tell a different tale. *Trends Genet*. 35, 104–117 10.1016/j.tig.2018.11.005

53. Szewczak L. B., DeGregorio S. J., Strobel S. A., and Steitz J. A. (2002) Exclusive interaction of the 15.5 kD protein with the terminal box C/D motif of a methylation guide snoRNP. *Chem. Biol*. 9, 1095–1107

54. Schultz A., Nottrott S., Watkins N. J., and Lührmann R. (2006) Protein-protein and protein-RNA contacts both contribute to the 15.5K-mediated assembly of the U4/U6 snRNP and the box C/D snoRNPs. *Mol. Cell. Biol*. 26, 5146–5154 10.1128/MCB.02374-05

55. Cahill N. M., Friend K., Speckmann W., Li Z. H., Terns R. M., Terns M. P., and Steitz J. A. (2002) Site-specific cross-linking analyses reveal an asymmetric protein distribution for a box C/D snoRNP. *EMBO J*. 21, 3816–3828 10.1093/emboj/cdf376

56. Cerami E., Gao J., Dogrusoz U., Gross B. E., Sumer S. O., Aksoy B. A., Jacobsen A., Byrne C. J., Heuer M. L., Larsson E., Antipin Y., Reva B., Goldberg A. P., Sander C., and Schultz N. (2012) The cBio cancer genomics portal: An open platform for exploring multidimensional cancer genomics data. *Cancer Discov*. 2, 401–404 10.1158/2159-8290.CD-12-0095

57. Gao J., Aksoy B. A., Dogrusoz U., Dresdner G., Gross B., Sumer S. O., Sun Y., Jacobsen A., Sinha R., Larsson E., Cerami E., Sander C., and Schultz N. (2013) Integrative analysis of complex cancer genomics and clinical profiles using the cBioPortal. *Sci. Signal*. 6, pl1 10.1126/scisignal.2004088

58. Ryan O. W., Poddar S., and Cate J. H. (2016) CRISPR-Cas9 genome engineering

in *Saccharomyces cerevisiae* cells. *Cold Spring Harb. Protoc*. 2016, pdb-prot086827 10.1101/pdb.prot086827

59. Ryan O. W., Skerker J. M., Maurer M. J., Li X., Tsai J. C., Poddar S., Lee M. E., DeLoache W., Dueber J. E., Arkin A. P., and Cate J. H. (2014) Selection of chromosomal DNA libraries using a multiplex CRISPR system. *eLife* 3, e03703 10.7554/eLife.03703

60. Zhou C. Y., Stoddard C. I., Johnston J. B., Trnka M. J., Echeverria I., Palovcak E., Sali A., Burlingame A. L., Cheng Y., and Narlikar G. J. (2017) Regulation of Rvb1/Rvb2 by a domain within the INO80 chromatin remodeling complex implicates the yeast Rvbs as protein assembly chaperones. *Cell Rep*. 19, 2033–2044 10.1016/j.celrep.2017.05.029

Figures

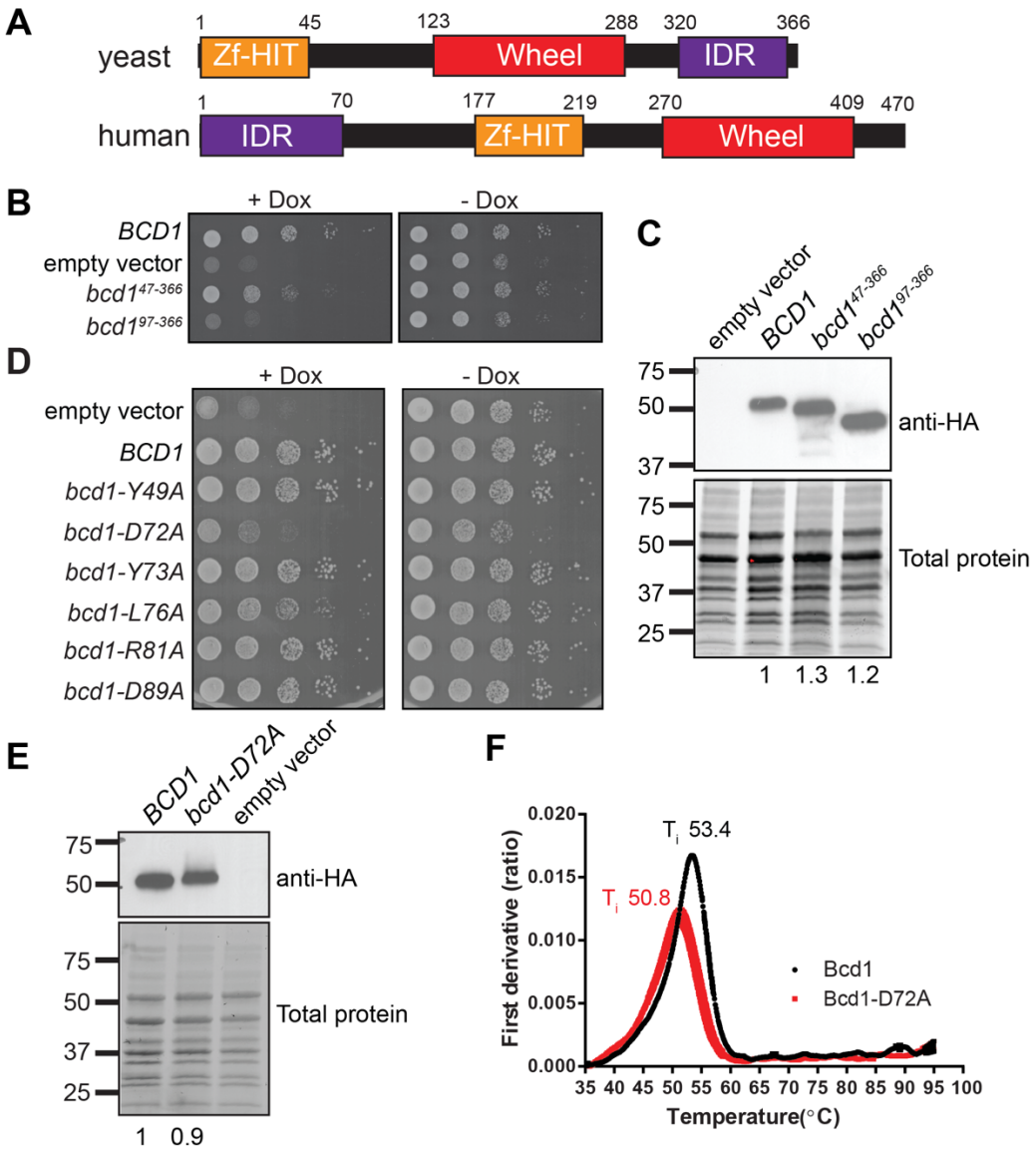

Figure 1. A conserved residue in the N-terminal region of Bcd1 is important for cell growth. *A*, domain organization of Bcd1 and ZNHIT6. *B*, serial dilution growth assay of yeast expressing *BCD1* under a doxycycline (*Dox*) repressible promoter (*tetO7::BCD1*), and supplemented with the indicated plasmids. *C*, Western blot analysis of Bcd1 and its variants. Total protein was resolved on a Mini-PROTEAN TGX Stain-Free gel (Bio-Rad) and imaged prior to the transfer to serves as loading control. Anti-HA intensity is normalized to the total protein and reported under each lane. *D*, serial dilution growth assay of *tetO7::BCD1* cells supplemented with the indicated plasmids.

E, Western blot analysis of Bcd1 and Bcd1-D72A. The anti-HA levels relative to the loading control is reported under each lane. *F*, the inflection temperature (Ti) of Bcd1 and Bcd1-D72A as a function of increasing temperature. The peaks in the first derivative view correspond to the Ti of the proteins.

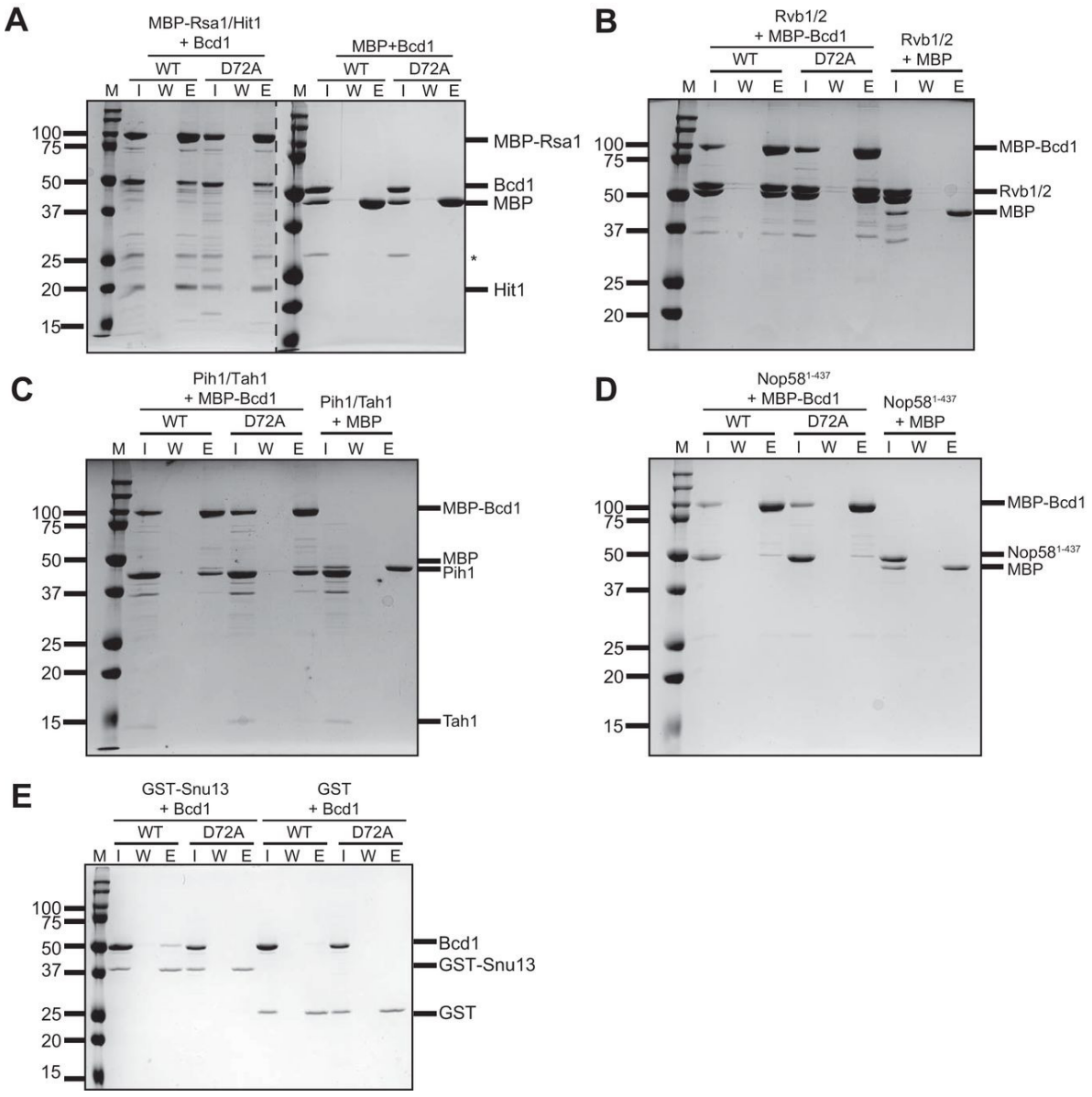

Figure 2. In vitro protein-binding assays testing the interaction network of Bcd1 with its binding partners. *A*, MBP-Rsa1/Hit1 immobilized on amylose resin can pull down WT and D72A variant Bcd1. *B–D*, MBP-Bcd1 (WT) or MBP-Bcd1-D72A (D72A) bound to amylose resin pulldowns Rvb1/2 (*B*), Nop58 (*C*), and Tah1/Pih1 (*D*). *E*, GST-Snu13 immobilized on GSH Sepharose resin can pull down WT but fails to interact with Bcd1-D72A. *M*, molecular weight marker (kDa); *I*, input; *W*, last wash; *E*, eluate; *, nonspecific contaminant.

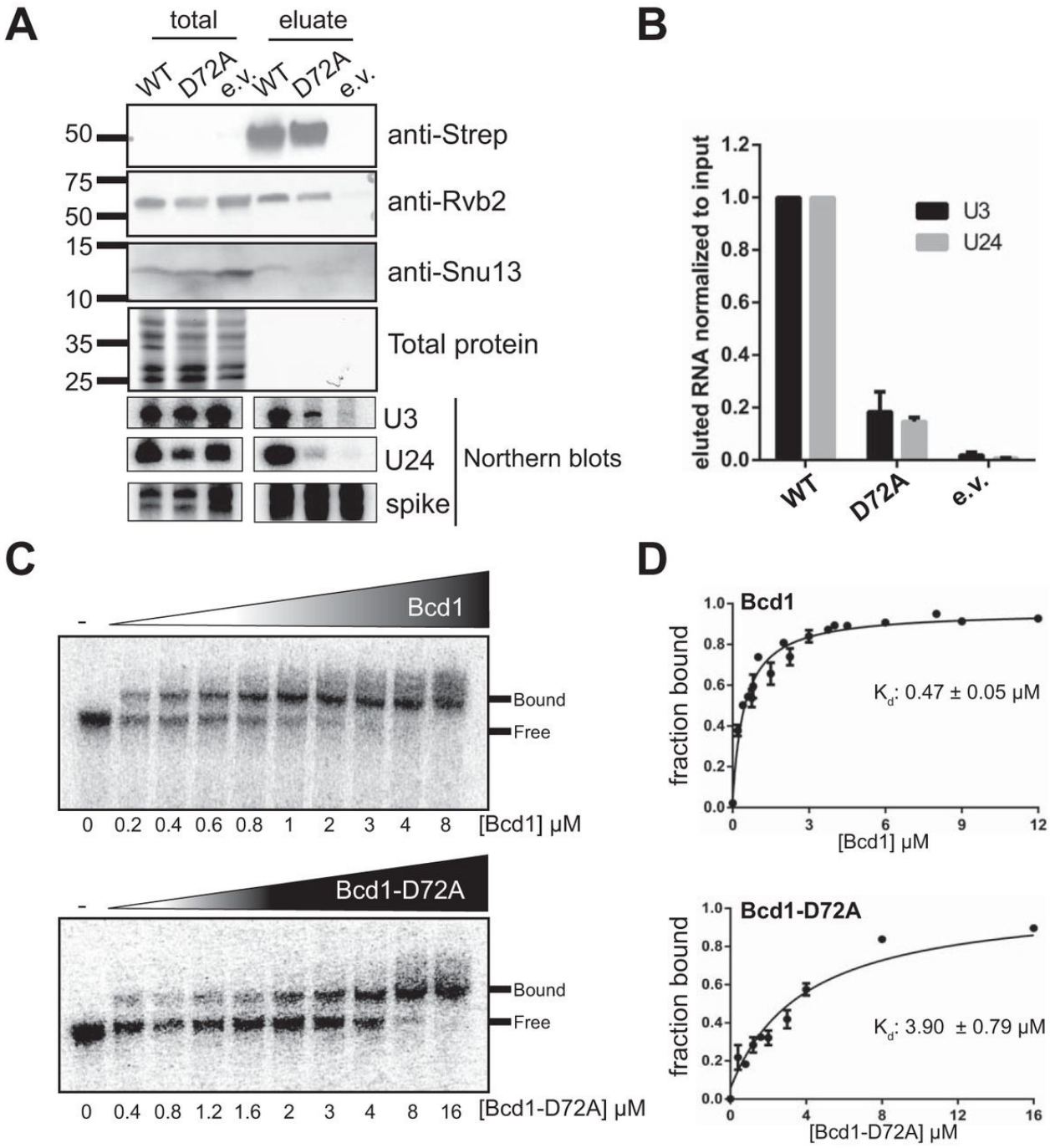

Figure 3. Mutation of a conserved residue of Bcd1 hampers the ability of the protein to interact with RNA. *A*, strep-tagged Bcd1 (WT) or Bcd1-D72A was used to pull down snoRNPs from yeast cells. Protein and RNA from input and eluates were analyzed by Western and Northern

blotting. *B*, quantification of the eluted RNA relative to input is shown in *A*. Data from two independent experiments were averaged. *Error bars* indicate mean +/- S.E. *C*, EMSA shows that Bcd1 binds to snR51 (a box C/D snoRNA), albeit weakly, whereas Bcd1-D72A binding to the snoRNA is weaker. *D*, quantification of the data shown in *C*. Data show averages from four independent experiments. *Errors bars* indicate mean +/- S.E.

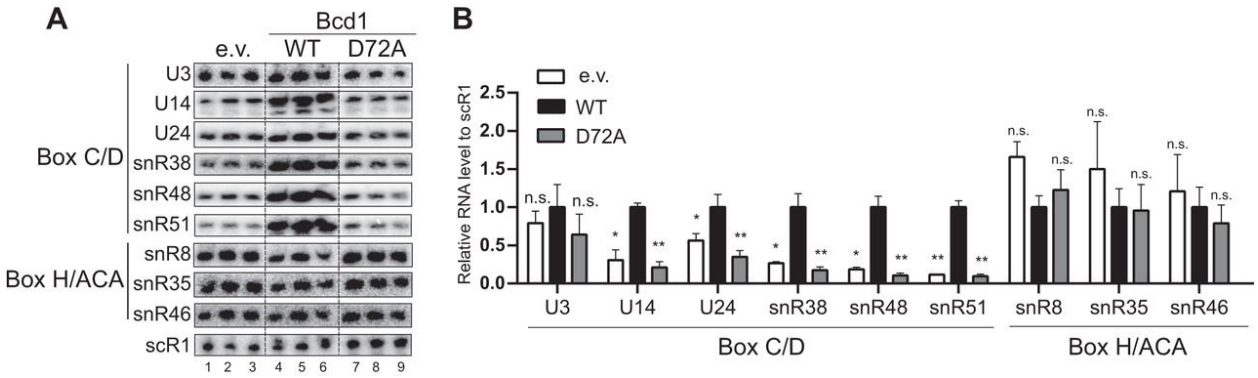

Figure 4. Bcd1-D72A variant abrogates the production of box C/D snoRNAs. *A*, Northern blotting analyses of steady-state expression levels of box C/D and box H/ACA snoRNAs in *tetO7::BCD1* cells treated with doxycycline and containing an empty vector (*lanes 1–3*), or a vector expressing Bcd1 (*lanes 4 – 6*), or Bcd1-D72A (*lanes 7–9*). *B*, quantification of data shown in *A* as normalized to scR1. *Lane 6* was excluded from data analyses. *Graph bars* represent the mean and S.D. from at least two biological replicates. Significance is relative to the WT and was determined using an unpaired *t* test. n.s., nonsignificant; $p > 0.05$; *, $p < 0.05$; **, $p < 0.01$.

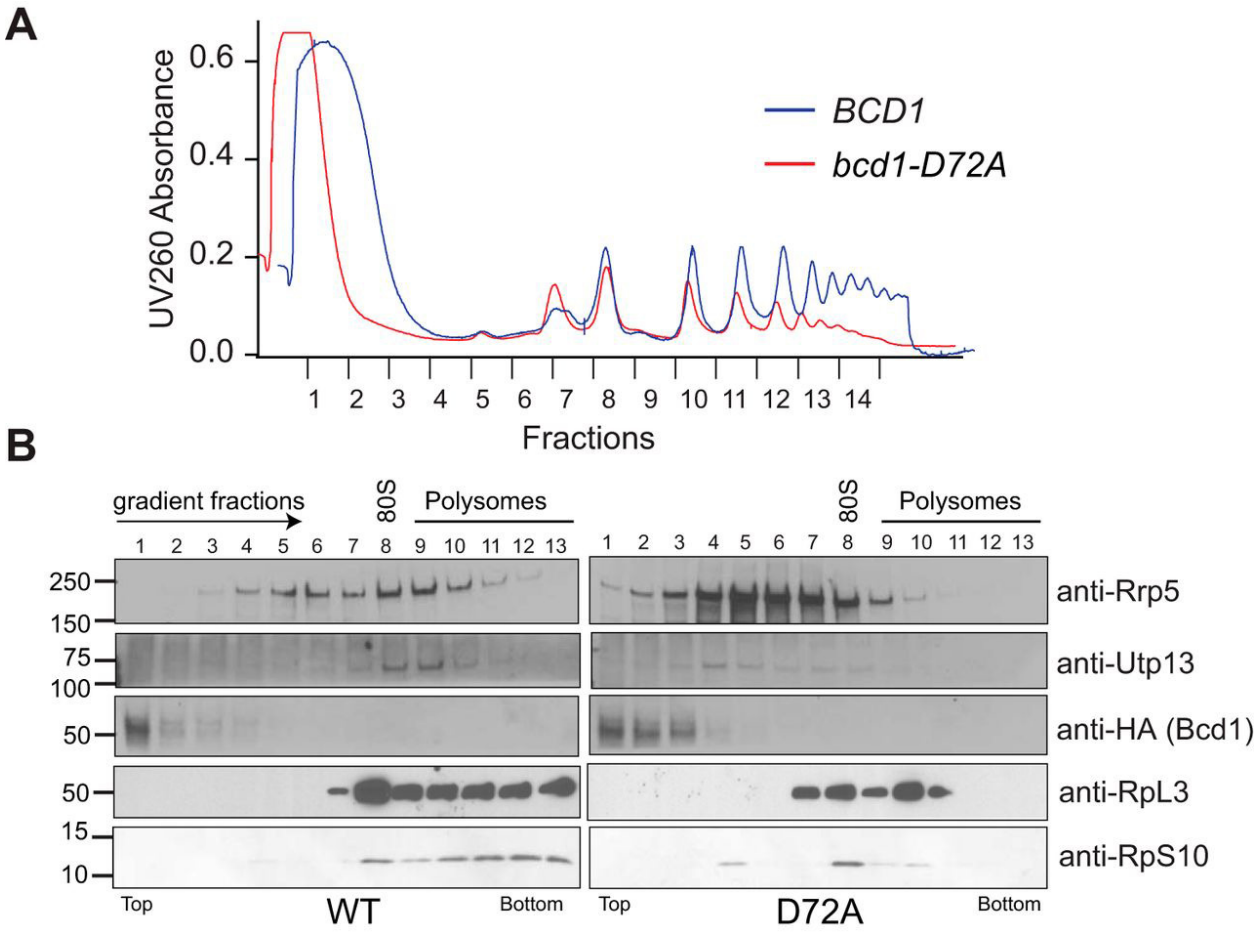

Figure 5. Ribosome biogenesis is impaired in cells expressing Bcd1-D72A. *A*, total lysate gradients of cells expressing either Bcd1 (WT) or Bcd1-D72A (D72A). *B*, Western blot analysis of gradient fractions shown in *A*.

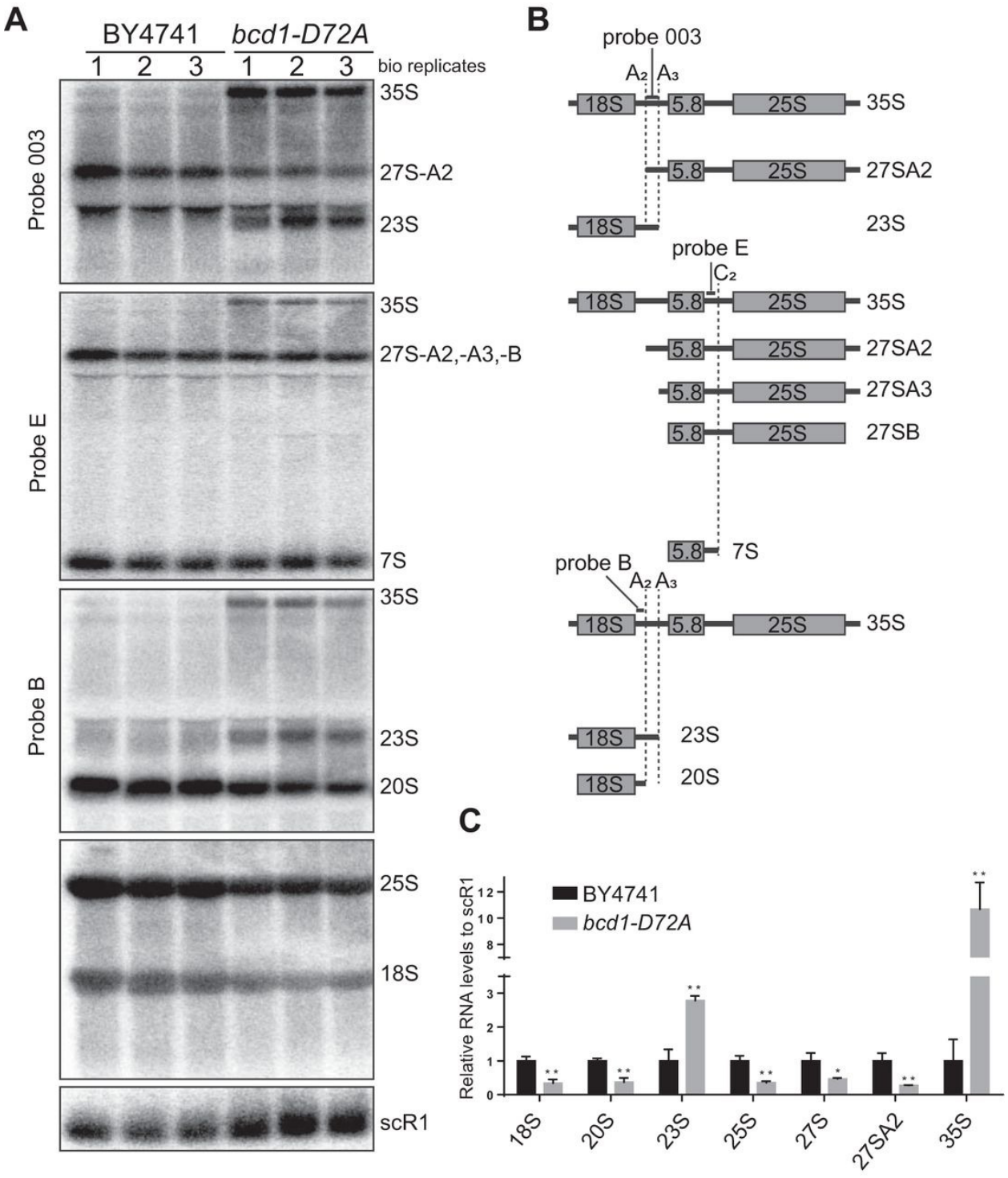

Figure 6. Alteration of rRNA processing in Bcd1-D72A cells. *A*, Northern blot analysis of the rRNA processing in BY4741 and *bcd1-D72A* cells. *B*, schematic of the binding sites for the probes

and the intermediates they detect. The positions of the cleavage sites are marked by *dashed lines*. *C*, quantification of data shown in *A*. Band intensities were normalized to scR1. *Graph bars* show averages from three biological replicates shown in *A*. Significance is relative to the WT and was determined using an unpaired *t* test. n.s., nonsignificant; $p > 0.05$; *, $p < 0.05$; **, $p < 0.01$.

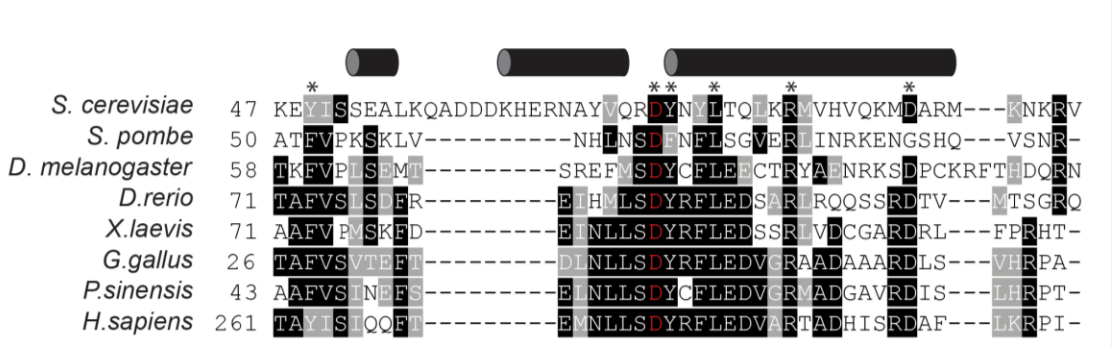

Figure S1. Sequence alignment of the fragments of Bcd1 corresponding to *S.cerevisiae* residues 47-97 from different organisms. Very conserved and less conserved residues are outlined in black and grey, respectively. The residues which were mutated in Figure 1D are marked with asterisks. The conserved Asp72 is colored in red. The secondary structure prediction of *S. cerevisiae* Bcd1 is shown on the top, with cylinders depicting alpha helices. This figure is related to Figure 1.

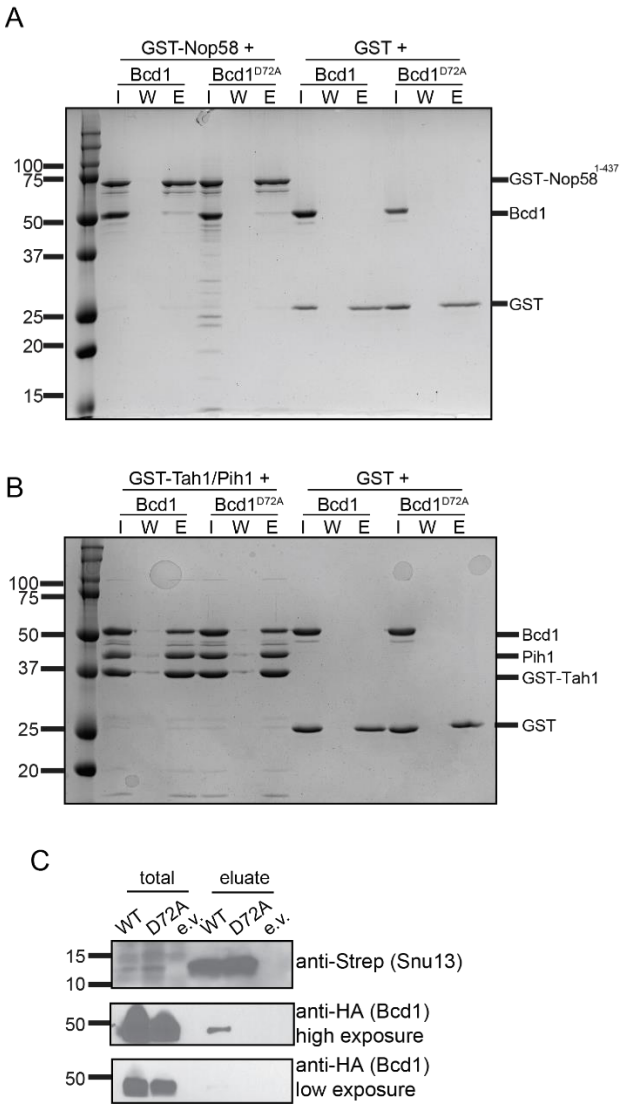

Figure S2. (A) Bcd1 and Bcd1-D72A variant bind to GST-Nop58$^{1-437}$ but not to GST alone. (B) Bcd1 and Bcd1-D72A bind to GST-Tah1/Pih1 but not to GST alone. (C) Strep-tagged Snu13 can pull down Bcd1 but not Bcd1-D72A variant from total yeast lysate. This figure is related to Figures 2 and 3.

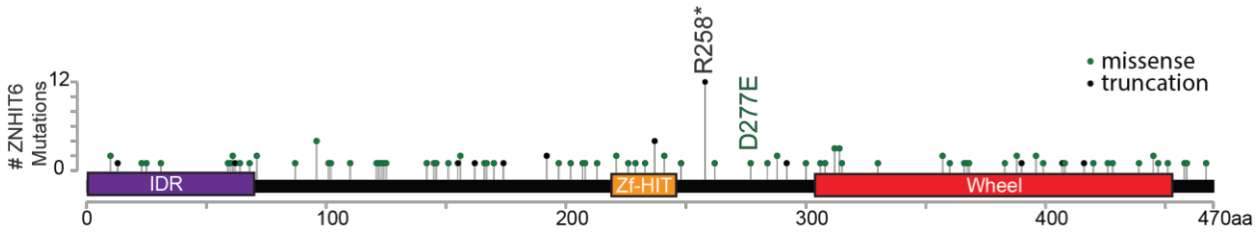

Figure S3. Analyses of ZNHIT6 cancer mutations. A stop mutation in ZNHIT6 which may result in ZNHIT6 protein lacking the conserved D277 and the wheel domain is associated with cancer.

Chapter 4. Ribosomal RNA 2'- O-methylations regulate translation by impacting ribosome dynamics

Summary

We used cells expressing the Bcd1-D72A variant as a tool and to uncover how global downregulation of box C/D snoRNAs impacts rRNA 2'-O-methylation and cellular translation. Despite a global downregulation of box C/D snoRNA levels and a global downregulation of translation in bcd1-D72A cells, we observe a site-specific change in the pattern of cellular rRNA 2'-O-methylations, specific impairments in translation fidelity, specific impairments in ribosomal ligand binding. We also reveal that hypo 2'-O-methylation impacts the ribosome dynamics by affecting the rotational status of ribosomes. I contributed to this work by generating the *bcd1-D72A* mutant strain used throughout this study using CRISPR-Cas9 mediated genome editing. Using an established reporter system, I performed dual luciferase assays uncovering that *bcd1-D72A* mutant has impaired translation fidelity. I also developed our lab's protocol used here for analyzing translation by HPG incorporation. Previous work in yeast detected newly synthesized HPG-labeled proteins in bulk using flow cytometry, but this work uses a modified protocol I refined for analyzing newly synthesized proteins by SDS-PAGE.

Khoshnevis, S., Dreggors-Walker, R.E., Marchand, V., Motorin, Y. and Ghalei, H. (2022) Ribosomal RNA 2'- O-methylations regulate translation by impacting ribosome dynamics. *Proc Natl Acad Sci U S A*, **119**, e2117334119.

These findings were published in *PNAS* on March 16, 2022. Supplemental tables can be found online at: https://www.pnas.org/doi/abs/10.1073/pnas.2117334119?url_ver=Z39.88-2003&rfr_id=ori%3Arid%3Acrossref.org&rfr_dat=cr_pub++0pubmed

Abstract

Protein synthesis by ribosomes is critically important for gene expression in all cells. Ribosomal RNAs (rRNAs) are marked by numerous chemical modifications. An abundant group of rRNA modifications, present in all domains of life, is 2'-O-methylation guided by box C/D small nucleolar RNAs (snoRNAs) which are part of small ribonucleoprotein complexes (snoRNPs). Although 2'-O-methylations are required for proper production of ribosomes, the mechanisms by which these modifications contribute to translation have remained elusive. Here, we show that a change in box C/D snoRNP biogenesis in actively growing yeast cells results in the production of hypo 2'-O-methylated ribosomes with distinct translational properties. Using RiboMethSeq for the quantitative analysis of 2'-O methylations, we identify site-specific perturbations of the rRNA 2'-O-methylation pattern and uncover sites that are not required for ribosome production under normal conditions. Characterization of the hypo 2'-O-methylated ribosomes reveals significant translational fidelity defects including frameshifting and near-cognate start codon selection. Using rRNA structural probing, we show that hypo 2'-O-methylation affects the inherent dynamics of the ribosomal subunits and impacts the binding of translation factor eIF1, thereby causing translational defects. Our data reveal an unforeseen spectrum of 2'-O-methylation heterogeneity in yeast rRNA and suggest a significant role for rRNA 2'-O-methylation in regulating cellular translation by controlling ribosome dynamics and ligand binding.

Introduction

RNA molecules are subject to co- and post-transcriptional modifications which expand their chemical and topological properties (1, 2). Methylation of the 2'-O position of the ribose moiety of nucleotides is a highly abundant RNA modification, found in all four types of ribonucleotides in both coding and non-coding RNAs in all domains of life (3). Ribosomal RNAs (rRNAs) are a

major target of ribose 2'-O methylations with fifty-five 2'-O-methylation sites identified in budding yeast and approximately 110 in humans. Although rRNA 2'-O-methylations are critical for the proper production of ribosomes and accurate protein translation, their precise molecular contributions and mechanism of function are unknown (3-8). The chemical properties of 2'-O-methylations and the observations made based on their contributions to the structure of the ribosome, have suggested a role for rRNA modifications in local and global stabilization of the rRNA structure (1, 6, 7, 9, 10). Moreover, rRNA modifications contribute to the interactions of ligands with the ribosome (11-13). Studies of modified nucleotides and RNA oligonucleotides have pointed to the importance of 2'-O-methylation in the stabilization of RNA structure by favoring the 3'-endo configuration of the ribose moiety and restricting the rotational freedom of the 3'-phosphate (14-19). However, how methylations of the rRNA backbone contribute to ribosome biogenesis and function remains largely unknown to date (4, 5, 20).

In eukaryotes and archaea, box C/D small nucleolar RNAs (snoRNAs) guide the 2'-O-methylation of rRNA sites by base pairing to specific segments of the rRNA (21-26). Methylation is carried out by the action of the methyltransferase Nop1 (fibrillarin in humans) as part of a small nucleolar ribonucleoprotein complex (snoRNP). In this complex, four core proteins (Snu13, Nop56, Nop58, and Nop1) assemble on a snoRNA in a stepwise manner (27). This evolutionarily conserved assembly process requires the action of several assembly factors that confer tight regulation of biogenesis and turnover of box C/D snoRNAs.

Recent quantitative studies have shown that 2'-O-methylations are not ubiquitously present on all of the cellular ribosomes, suggesting that these modifications may be an adjustable feature to fine tune the function of ribosomes (4, 28-36). However, because most rRNA 2'-O-methylations are deposited at an early stage during ribosome biogenesis, it is not clear how these modifications can

be adjusted or removed, and the source of rRNA 2'-O-methylation heterogeneity remains unknown (4, 5, 37). Attempts to investigate the repertoire of sub-stoichiometric 2'-O-methylation sites of rRNA include the study of natural variations between cell lines (32, 36), changes of rRNA 2'-O-methylations in primary human breast tumors (38), differential rRNA modifications during mouse development (39), changes of modifications in the presence or absence of the antitumor protein p53 (29, 35) which regulates the methyltransferase fibrillarin (40), changes caused by depletion of fibrillarin (28) and RNA helicase Dbp3 (41), and the use of a Nop1 mutant (42). Surprisingly, however, the methods used to study the effect of rRNA hypo 2'-O-methylation have not allowed identification of all potential variable modification sites. For example, mutating the active site of Nop1, which is expected to directly affect rRNA 2'-O-methylations, did not change the methylation pattern of the ribosome (42). The alternative approach of knocking down fibrillarin using siRNA in human cell lines (28), allowed researchers to identify a set of 2'-O-methylations which are specifically reduced in the presence of limiting amount of fibrillarin. However, because cells depleted of fibrillarin hardly divide or make any new ribosomes and likely rely on their already assembled ribosomes for survival (43-46), limited modification changes were observed using this strategy. Furthermore, which effects of fibrillarin knockdown are direct versus indirect was not discerned (47). Therefore, obtaining a comprehensive view of the rRNA sites that have the potential to be missed, removed or regulated has not been possible thus far.

To overcome this limitation, we present here a new strategy which involves decreasing the biogenesis of box C/D snoRNAs via a single mutation in an essential box C/D snoRNP assembly factor, Bcd1. Bcd1 is an evolutionarily conserved protein that cooperates with several other assembly factors to direct the assembly of box C/D snoRNAs into functional snoRNP complexes (27). Bcd1 controls the steady-state levels of box C/D snoRNAs by regulating the assembly of the

Nop58 protein into pre-snoRNPs and by mediating the interaction of Snu13 with snoRNAs (48-50). Using a variant of Bcd1 (*bcd1-D72A*), which causes a global box C/D snoRNA downregulation but allows cell growth and ribosome biogenesis (50), here, we reveal a wide spectrum of variable rRNA 2'-O-methylation sites in yeast ribosomes and identify their impact on translation. Strikingly, our data reveal that more than 70% of yeast rRNA 2'-O-methylation sites have the potential to be significantly hypo 2'-O-methylated. We also show that 2'-O-methylation affects the dynamics of the rRNA resulting in a change in the balance between different conformational states of the ribosomes required for translation. Finally, our data show that rRNA hypomethylation also impacts the binding of initiation factor 1 (eIF1) to the small ribosomal subunit. Together, these results allow us to dissect those rRNA 2'-O-methylation sites that are critical for ribosome biogenesis from those that are dispensable and may have other functional roles, and link rRNA 2'-O-methylation to specific features of the ribosomes.

Materials and methods

Plasmids and strains. Plasmids used in this study are listed in Table S2. All mutations were introduced by site-directed mutagenesis and confirmed by sequencing. Strains are listed in Table S3. All yeast strains were confirmed by PCR followed by sequencing, as well as western blotting when antibodies were available.

RiboMethSeq. RiboMethSeq was essentially performed as previously reported (32). Briefly, 150 ng total RNA was fragmented under denaturing conditions using an alkaline buffer (pH 9.4) to obtain average size of 20-40 nt. Fragments were end-repaired and ligated to adapters using NEBNext Small RNA kit for Illumina. Sequencing was performed on Illumina HiSeq1000. Reads were mapped to the yeast rDNA and snoRNA sequences, and the MethScore (fraction methylated) was calculated as MethScore (for +/- 2 nt) (93), equivalent to "ScoreC" in Birkedal et al. (31).

Statistical significance was determined using Student's t-test ($P < 0.05$). Data from RiboMethSeq analysis are deposited with European Nucleotide Archive (ENA) under accession number PRJEB49663.

HPG incorporation assay. BY4741 and *bcd1-D72A* cells were transformed with pRS411 and grown in synthetic media lacking methionine at 30°C to mid-log phase. L-Homopropargylglycine (HPG) was added to 10 mL cultures to a final concentration of 50 µM and cells were incubated at 30°C. At each indicated time point, 2 ml of the culture was removed, and cells were washed with cold water and frozen in liquid nitrogen. The cell pellets were resuspended in 100 µL of RIPA buffer (50mM Tris-HCl, pH 7.4, 150mM sodium chloride, 1mM EDTA, 1mM EGTA, 1% Triton X-100, 1% sodium deoxycholate and 0.1% SDS) supplemented with protease inhibitors, mixed with disruption beads, and lysed in a bead beater. After clearing the lysate, the protein concentration was measured using BCA assay (ThermoFisher), and an equal amount of protein was used for labeling by Alexa Fluor 488 using the Click-iT™ HPG Alexa Fluor™ 488 Protein Synthesis Assay Kit (ThermoFisher). Labeled proteins were resolved on 12% SDS gel and visualized on a ChemiDoc Imager (BioRad). Total protein was visualized after Coomassie staining and imaged using ChemiDoc.

Fidelity assay. Translation fidelity was measured using previously established dual-luciferase reporters (56-60). For measurements, 1 mL of BY4741 and *bcd1-D72A* cells expressing the dual luciferase plasmids were pelleted in the mid-log phase, washed, and frozen in liquid nitrogen. Luciferase activities were measured using the Promega Dual-Luciferase kit by resuspending cells in 100µL of 1X Passive Lysis Buffer and incubating for 10 min. The firefly activity was measured by mixing 10 µL lysates with 30 µL Luciferase Assay Reagent II in white, clear bottom 96W Microplates (Costar). For the same sample, the Renilla activity was measured by addition of 30

µL Stop&Glo Reagent. Measurements were performed using a Synergy Microplate reader (BioTek). For each sample, firefly luciferase activity was normalized against Renilla activity, and then values observed for *bcd1-D72A* were normalized against wild-type control.

***In vivo* RNA structure probing.** BY4741 and *bcd1-D72A* cells were grown to the mid-log phase at 30°C. SSU-G913 was probed using phenylglyoxal. The cultures were divided into two tubes, mixed with either phenylglyoxal (16 mM final concentration) or an equal volume of DMSO, and incubated for 5 min at 30°C before washing with water. RNA was extracted using phenol/chloroform and precipitated with ethanol. Precipitated RNA was resuspended in water and treated with DNase I (BioRad) and further purified with the Quick RNA miniprep kit (Zymo Research) before reverse transcription was performed using Superscript III (ThermoFisher) according to the manufacturer's protocol. To probe SSU-G913 in *nop1-ts* cells, experimental ts cells and wild-type control cells were grown to mid-log phase at 37°C before treatment with phenylglyoxal as before. Data were quantified using Image Lab Software (Biorad). The intensity of bands at the reverse transcription stops were normalized to all band intensities below the stop signal.

***In vitro* RNA structure probing.** 25 nM Purified 40S ribosomes from control or *bcd1-D72A* cells was mixed with 200 mM DMS or ethanol in 80 mM Hepes/NaOH (pH 7.4), 50 mM NaCl and 0.5 mM MgOAc. The mixture was incubated at 30°C for 5 minutes before quenching with 400 mM betamercaptoethanol/600 mM NaOAc. The RNA was precipitated with ethanol and further purified using a Quick RNA miniprep kit (Zymo Research) before reverse transcription was performed using Superscript III (ThermoFisher) according to the manufacturer's protocol. Data were quantified using Image Lab Software (Biorad). To quantify nucleotide accessibility and account for loading differences, the intensity of bands at the reverse transcription stops were

normalized to all band intensities below the stop signal.

***In vivo* ribosome binding assay.** *In vivo* crosslinking of the translation factors to the ribosome was done as previously described (94). Briefly, cells grown to mid-log phase were chilled by addition of crushed ice (25% of total culture volume) and crosslinked by addition of formaldehyde to a final concentration of 1% relative to the original volume of the culture. After 1 h incubation in ice bath, cells were pelleted by centrifugation, washed with chilled water and resuspend in the lysis buffer (20 mM Tris-HCl, pH 7.5, 100 mM KCl and 10 mM $MgCl_2$) supplemented with protease inhibitors and RNase inhibitor and froze in liquid Nitrogen. Cells were ruptured by grinding in cryogenic condition. To monitor eIF1 binding to 40S, the lysate was cleared by centrifugation and 20 units of OD_{260} were loaded on sucrose gradient (7.5%-30% sucrose in the lysis buffer) and centrifuged in SW41 rotor (Beckman Coulter) at 40,000 rpm for 5 h. Gradients were fractionated and analyzed by Western blot using eIF1 antibody (a gift from A. G. Hinnebusch). To assess the binding of eEF2 to the ribosomes, 20 OD_{260} of cleared lysate was loaded on 100 uL of sucrose cushion (1 M sucrose in lysis buffer) and spun down in TLA 100 (Beckman Coulter) for 2h at 400,000 xg. Pellet was resuspended in lysis buffer plus SDS loading dye and equal volumes of pellet and supernatant were analyzed by Western blot using antibodies against eEF2 (Kerafast) and Rpl3 (Developmental Studies Hybridoma Bank).

Purification of 40S and eIF1. 40S ribosomes from BY4741 and BCD1-D72A cells were purified as previously described (95). eIF1 was expressed as a HIS-tagged protein in Rosetta2(DE3) cells from the pET23-TEV-eIF1 plasmid. Protein expression was induced at OD_{600} ~0.6 by addition of 1 mM IPTG and the cultures were incubated for 16 hours at 18°C. eIF1 was purified on Ni-NTA resin in buffer A (500 mM NaCl, 50 mM HEPES-NaOH pH 7.5, 20 mM imidazole and 5% glycerol). The protein was eluted with 240 mM imidazole and further purified over a Superdex S-

75 gel filtration column (GE Healthcare) equilibrated in 150 mM NaCl, 20 mM HEPES-NaOH pH 7.5, 5 % glycerol, and 1 mM DTT.

eIF1-40S binding assay. His-eIF1 was labeled with NT650 fluorophore through non-covalent linkage to the His-tag moiety using the Monolith Protein Labeling Kit RED-tris-NTA 2nd generation (NanoTemper Technologies). 40S subunits (0.58 nM –1.2 μM) isolated from wild-type control or *bcd1-D72A* cells were incubated with 100 nM labeled eIF1. Fluorescence was measured using a Dianthus NT.23 Pico instrument (NanoTemper Technologies). Fluorescence values were baseline corrected and changes in fluorescence values were used to calculate bound fractions which were plotted against 40S concentration. Data were fitted with a non-linear regression model in GraphPad Prism 8.0.

Growth assay. Cells grown to mid-log phase in minimal media were diluted into fresh media and growth rates were measured in the Epoch2 microplate reader (BioTek) by recording OD_{600} every 20 min. For growth assays in the presence of translation inhibitors, the following concentrations were used: 500 μg/mL paromomycin, 1 mg/mL apramycin B, 250 μg/mL homoharringtonine and 3 μg/mL sordarin.

Analysis of the steady-state levels of snoRNAs. *NOP1* or *nop1-ts* cells were grown in YPD at 37°C to OD_{600} ~ 0.6. Total RNA from three biological replicates of each strain was isolated using the hot phenol method. snoRNAs were separated on 8% acrylamide/urea gels, transferred to Hybond nylon membrane (GE Healthcare), and probed as indicated. Bands were quantified using Image Lab software (Bio-Rad).

Results

Heterogeneity of rRNA 2'-O-methylation sites in yeast rRNA reveals sites that are dispensable for ribosome biogenesis.

To address which of the rRNA 2'-O-methylations sites are tunable in yeast and identify those that are dispensable for ribosome production in viable cells, we exploited a mutation in the modification machinery that alters the biogenesis of box C/D snoRNPs in actively growing yeast cells. For this purpose, we engineered the *bcd1-D72A* mutation in yeast cells using CRISPR/Cas9 genome editing (50). The introduction of this mutation into the genome ensures that all the ribosomes will be made in the presence of defective Bcd1, which causes cells to have low steady-state levels of box C/D snoRNAs (50). We then performed RiboMethSeq analysis (32) on RNAs isolated from actively growing wild-type control yeast cells and those expressing *bcd1*-D72A. Figure S1 shows the average MethScores (ScoreC) for all rRNA methylation sites in wild-type control and mutant *bcd1-D72A* cells. In line with the previous observations (31, 32), 47 of the 53 2'-O-methylation sites in wild-type control yeast cells are methylated at high levels (with MethScore > 0.8) and only a small fraction (6/53 sites) show MethScores below 0.8 (Figure S1). While the average MethScore for wild-type control is 0.85, analysis of data from *bcd1-D72A* cells reveal a much lower level of methylation (average MethScore 0.43). These data indicate that the majority of rRNA 2'-O-methylation positions are hypomethylated in *bcd1-D72A* cells.

Analysis of the 2'-O-methylation sites in the 18S rRNA of *bcd1-D72A* cells reveal 7 stable sites with similar methylation levels to the wild-type control (MethScore > 0.8), 8 variable sites (MethScore between 0.4 and 0.8), and 3 highly hypomethylated sites (MethScore < 0.4) (Figure 1A). The decoding center harbors stable modification sites (G1428 and C1639) (Figure 1B, C). In contrast, the hypo 2'-O-methylated sites within 18S rRNA do not cluster at a specific region within 40S subunit. For 25S rRNA, we identify 6 stable sites with near-complete methylation, 15 variable sites, and 14 hypo 2'-O-methylated sites (Figure 1D). With the exception of two stable modification sites (U2921 and C2959), the peptidyl transferase center (PTC) and the tRNA

accommodation corridor are devoid of 2'-O-methylated sites. However, several hypo 2'-O-methylated or variable sites neighbor these functional regions (Figure 1E, F).

Comparison of the rRNAs in *BCD1* and *bcd1-D72A* cells by northern blot using probes against 18S and 25S rRNAs does not reveal the presence of any rRNA processing intermediates (50), suggesting that although different rRNA processing intermediates accumulate in *bcd1-D72A* cells, their amounts are negligible compared to the fully processed mature rRNAs. Thus, RiboMethSeq analysis of the total RNA from *bcd1-D72A* is a good proxy for the 2'-O methylation levels in the mature ribosomes. To test if hypo 2'-O-methylated rRNAs assembled into functional mature ribosomes and validate the RiboMethSeq data, we tested whether the reduced methylation levels observed in *bcd1-D72A* cells are also present in mature purified ribosomes. To this end, we compared the 2'-O-methylation levels of a randomly selected variable site in each of the ribosomal subunits purified from *BCD1* or *bcd1-D72A* cells by reverse transcription at low concentration of dNTP combined with sequencing gel analysis (Figure S2A, B). This analysis shows that the 2'-O-methylation level of A974 in 18S rRNA isolated from purified hypo 2'-O-methylated 40S subunits is 0.4 relative to wild-type ribosomes, which is very similar to the estimated fraction methylated based on the Methscore value of 0.49. Similarly, analysis of fraction methylated at A2280 in 25S by quantification of stops in reverse transcription results in a value of 0.42, which is close to the measured MethScore of 0.39 for this site. Taken together, our RiboMethSeq data reveal that while 24% (13/53) of rRNA 2'-O-methylation sites are critical for ribosome biogenesis and function, other rRNA 2'-O-methylations can be variable (43%, 23/53) or even dispensable (34%, 18/53).

rRNA hypomethylation affects the fidelity of protein synthesis.

Ribosomal RNA modifications are critically important for the function and fidelity of ribosomes (7, 11, 51, 52). We, therefore, tested whether the change of rRNA 2'-O-methylation pattern in

bcd1-D72A cells affects the efficiency and accuracy of protein synthesis. To assess the translational efficiency of hypo 2'-O-methylated ribosomes, we analyzed the incorporation rate of L-homopropargylglycine (HPG), an amino acid analog of methionine containing an alkyne moiety that can be fluorescently modified, into newly synthesized peptides in rapidly dividing wild-type or *bcd1-D72A* cells. HPG-containing proteins were fluorescently labeled by the addition of Alexa Fluor 488 and separated from the unincorporated dye by SDS-PAGE (Figure 2A). Quantification of the levels of newly synthesized proteins relative to the total proteins in wild-type and *bcd1-D72A* cells reveal that while total protein synthesis is higher in wild-type control cells, the rate of HPG incorporation over time is not significantly different between the two strains (Figure 2B). However, we observe a higher fluorescent signal at each time point in control cells versus *bcd1-D72A* cells, suggesting a higher number of translating ribosomes in wild-type control cells in agreement with the ribosome biogenesis defects we had previously observed in *bcd1-D72A* cells (50).

To assess the quality of mature ribosomes in *bcd1-D72A* vs. wild-type control cells, we analyzed the purified 40S and 60S subunits from both cells by SDS-PAGE and western blots. This experiment did not reveal any apparent differences between the protein composition of ribosomes isolated from wild type and hypo 2'-O-methylated ribosomes (Figure S2C, D).

Because changes in ribosome number and/or composition can affect the accuracy of protein synthesis and impact the ability of ribosomes to initiate from internal ribosome entry sites (IRESs) (28, 53-55), we next assayed the fidelity of translation in wild-type control and *bcd1-D72A* cells. For this purpose, we used a set of established dual-luciferase reporter plasmids in which the translation of the firefly luciferase depends on a defect in translation fidelity including -1 and +1 programmed frameshifting, alternate start codon selection, stop codon readthrough, miscoding or

initiation from an IRES element (Figure 2C, (56-60)). Cells with lower translation fidelity will have higher expression of the firefly luciferase relative to the control cells. As an internal control, all plasmids contain a constitutively expressed Renilla luciferase used for normalization. For each plasmid reporter, the firefly luciferase activity was normalized against Renilla activity, and then values observed for *bcd1-D72A* were normalized against wild-type control. This analysis reveals that, compared to control ribosomes, ribosomes from *bcd1-D72A* cells have an increased rate of near-cognate start codon selection and frameshifting (Figure 2D). The data also reveal that the hypomodified ribosomes have reduced stop codon readthrough as well as IRES-mediated initiation. Thus, translation fidelity and IRES-dependent translation initiation are altered in *bcd1-D72A* cells.

To assess whether the translational defects in *bcd1-D72A* are due to structural changes in ribosomes, we used translation inhibitors that bind to the small (paromomycin and apramycin) or large (homoharringtonine) ribosomal subunits (61) and compared the growth of wild-type control and *bcd1-D72A* cells in liquid media in the absence or presence of sublethal doses of these drugs. This analysis reveals that *bcd1-D72A* cells are more sensitive than wild-type control cells to the addition of paromomycin and apramycin, aminoglycosides that specifically bind to the small ribosomal subunit at the decoding center. In the presence of these drugs, the fold change in doubling time of *bcd1-D72A* cells relative to wildtype control cells significantly increases (Figure 2E). In contrast, *bcd1-D72A* cells are hyposensitive to homoharringtonine, which binds in the large ribosomal subunit tRNA A-site (Figure 2E). These data suggest structural changes in both the small and large ribosomal subunits that can affect the biding between ribosome and ligands such as translational inhibitors, tRNAs or IRES elements.

rRNA hypo 2'-O-methylation impacts the rotational status of ribosomes.

Recent work has shown that mRNA structures that promote programmed frameshifting in bacteria change the reading frame of the ribosome by increasing the rotated-state pause (62-64), thus providing a link between ribosome dynamics and frameshifting. A pseudoknot in SARS-CoV2 mRNA also causes translation pausing prior to -1 frameshifting in mammalian ribosome by providing a bulky and well-structured obstacle wedged at the mRNA entry channel (65). Because 2'-O-methylation affects the flexibility of RNA, we hypothesized that the observed changes in mRNA frameshifting in *bcd1-D72A* cells could arise from altered dynamics of the ribosome. To address this question, we used RNA structure probing. Several key residues in both the small and large ribosomal subunits undergo detectable changes in conformation upon transition between rotated and non-rotated ribosomal states (66). The most prominent of these sites is G913 in 18S rRNA (SSU-G913) which is located at the inter-subunit bridge B7a. To compare the rotational dynamics of the wild-type control and hypomethylated ribosomes, we probed this nucleotide in wild-type and *bcd1-D72A* cells using phenylglyoxal (PGO) (Figure 3A). As a reference, we took advantage of two mutations in *RPL3* (*rpl3-W255C* and *rpl3-H256A*), that are known to stabilize ribosomes in non-rotated and rotated states, respectively (67). We then compared the rotational status of wild-type and hypo 2'-O-methylated ribosomes to the rotated and non-rotated ribosomes from *RPL3* mutant cells (Figure 3B).

Our analyses reveal that *in vivo*, the SSU-G913 nucleotide in *rpl3-W255C* ribosomes is protected and shows minor reactivity to PGO. In *rpl3-H256A* cells, however, in which the ribosomes are stabilized in the rotated state, the SSU-G913 nucleotide is more accessible when probed with PGO. Comparing the reactivity of SSU-G913 in wild-type control and *bcd1-D72A* cells with those of *rpl3-W255C* and *rpl3-H256A* reveal that the hypomethylated ribosomes from *bcd1-D72A* cells are at least as accessible to PGO as the rotated ribosomes from *rpl3-H256A* cells suggesting that the

majority of ribosomes from *bcd1-D72A* cells are in the rotated conformation relative to the wild-type control (Figure 3A, B). These data suggest that ribosomes from *bcd1-D72A* cells favor the rotated state and that the increased rate of frameshifting in hypomethylated ribosomes could be due to the increased time the hypo 2'-O-methylated ribosomes spend in the rotated state.

Elongation factor 2 (EF-G in bacteria and eEF2 in eukaryotes) binds to pre-translocation ribosomes and stabilizes the rotated state (68). Mutations in yeast ribosomes which stabilize the rotated conformation increase the affinity of eEF2 for ribosomes (66, 67). Overexpression of eEF2 causes stabilization of the rotated ribosomes by mass action and impairs yeast growth (Figure 3C, D). Therefore, we hypothesized that as the hypo 2'-O-methylated ribosomes preferentially assume the rotated conformation in the cell, the overexpression of eEF2 should have less deleterious effect on *bcd1-D72A* cells compared to the wild-type control. To test this, we compared the growth of wild-type control and *bcd1-D72A* yeast cells overexpressing eEF2 on solid media. While overexpression of eEF2 causes a severe growth defect in wild-type cells, as evident from the smaller colony size, it does not impact the growth of *bcd1-D72A* cells to the same extent (Figure 3C). To further quantify this growth difference, we measured the growth of wild-type control and *bcd1-D72A* yeast cells overexpressing eEF2 cells during their logarithmic phase of growth. The *bcd1-D72A* cells grow slower than wild-type control cells by 1.3-1.5 fold, depending on the plasmid they harbor and the media they are growing in. We observe that *bcd1-D72A* cells overexpressing eEF2 grow slower than *bcd1-D72A* cells harboring the empty vector (Figure 3D). However, because ribosomes in *bcd1-D72A* cells have a conformational bias towards the rotated state, these cells are affected to a lesser extent than wild-type control cells by overexpression of eEF2. These data indicate that *bcd1-D72A* cells are less sensitive to the overexpression of eEF2 than the control cells (Figure 3D). An alternative explanation is that reduced sensitivity of the

bcd1-D72A strain to eEF2 overexpression is due to a reduction of eEF2-ribosome affinity. To test this, we compared the binding of eEF2 to the ribosomes *in vivo*. To this end, *bcd1-D72A* and wild-type control cells were grown to mid-log phase and fixed with formaldehyde. The ribosome-bound and free eEF2 were then separated by centrifugation through a sucrose cushion. As shown in Figure 3E, we do not observe any difference between the ribosome-bound eEF2 fraction in *bcd1-D72A* and control cells. Thus, the lower sensitivity of *bcd1-D72A* cells to eEF2 overexpression is unlikely to be due to the reduced affinity of eEF2 for hypomethylated ribosomes.

To further test whether hypomethylated ribosomes spend more time in the rotated state, we measured the growth of *bcd1-D72A* and control cells in the presence of sordarin. Sordarin is an inhibitor of the eEF2 that binds to ribosome-bound eEF2 and prevents its domain movements which are required for translocation (69). We analyzed the effect of sordarin on the growth of *bcd1-D72A* and wild-type control cells and compared that to the growth of reference cells expressing wild-type *RPL3*, *rpl3-W255C,* or *rpl3-H256A*. Whereas cells expressing wildtype *RPL3* and *rpl3-W255C* show similar sensitivity to sordarin, *rpl3-H256A* and *bcd1-D72A* cells are both less sensitive to sordarin (Figure 3F, G). These data further support the notion that hypo 2'-O-methylated ribosomes, similar to *rpl3-H256A* harboring ribosomes, spend more time in the rotated state. Taken together, these data provide the first evidence that the 2'-O methylation status of rRNA affects the ribosomal rotation state. Importantly, because there are no 2'-O-methylation sites near the SSU-G913 nucleotide, our data suggest that the ribosome rotational changes observed in *bcd1-D72A* cells are due to long-range effects.

Recent studies have proposed a function for snoRNAs in chaperoning the folding of rRNA (70). The levels of box C/D snoRNAs are significantly lower in *bcd1-D72A* cells relative to wild-type control cells (48, 50). The changes we detect in the conformation of ribosomes could therefore

arise either directly from the lack of 2'-O-methylations or indirectly from the decreased levels of snoRNAs. To dissect the role of snoRNA binding and chaperoning from the effect of rRNA 2'-O-methylations on the ribosome structure, we took advantage of a temperature-sensitive (ts) mutation in the methyltransferase Nop1 (71). Cells harboring this mutation grow more slowly than wild-type control cells at 37°C, and have lower rRNA methylation levels but do not show any change in snoRNA levels (Figure S3). *In vivo* analysis of the SSU-G913 modification by PGO in *nop1-ts* cells compared to wild-type control cells show higher accessibility of SSU-G913 in *nop1-ts* cells, suggesting the stabilization of the rotated ribosomal conformation in the hypo 2'-O-methylated ribosomes (Figure 3H, I). Because the level of snoRNAs is similar to the wild-type control cells in the *nop1-ts* cells, these data indicate that the observed defects in the inherent dynamics of the ribosome in *bcd1-D72A* cells are more due to the decreased rRNA 2'-O-methylation rather than a decrease in snoRNA levels.

Binding of eIF1 to the hypo 2'-O-methylated small ribosomal subunit is weakened *in vivo* and *in vitro*.

Eukaryotic initiation factor 1 (eIF1) plays an important role in ensuring the selection of cognate start codon and antagonizing the near-cognate start codon selection by stabilizing the open, scanning-competent conformation of the small ribosomal subunit (40S) (72-74). Upon proper start codon selection, eIF1 is released from 40S allowing rearrangement of the ribosome from the open to closed conformation (57, 75). Because ribosomes from *bcd1-D72A* cells show an elevated level of near-cognate start codon recognition (Figure 2D), we hypothesized that the hypo 2'-O-methylated ribosomes from *bcd1-D72A* cells cannot bind to eIF1 as efficiently as wild-type ribosomes. To test this hypothesis, cells expressing wild-type or the D72A variant of Bcd1 were fixed with formaldehyde in the mid-log phase and ribosome-bound and free eIF1 were separated

by centrifugation on sucrose density gradients and quantified by western blotting. While ~25% of eIF1 co-migrates with the ribosomes in wild-type control cells, the binding of eIF1 to the hypo 2'-O-methylated ribosomes in *bcd1-D72A* cells is significantly reduced (Figure 4A).

To corroborate this finding, we next assessed the binding of eIF1 to 40S ribosomal subunits isolated from wild-type control and *bcd1-D72A* cells. For this purpose, we fluorescently labeled eIF1 at its N-terminus and determined its binding affinity for purified 40S subunits using Temperature-Related Intensity Change (TRIC) assay. Notably, the N-terminus of eIF1 is located away from the 40S, and therefore is unlikely to be affected by possible changes in the ribosome conformation around its binding site (Figure S4A). The results from these binding assays reveal that eIF1 binds to 40S subunits isolated from wild-type cells with a dissociation constant (K_d) of ~20 nM, comparable to previous reports (76). However, the affinity of eIF1 for hypo 2'-O-methylated 40S ribosomal subunits is lower by 3 fold (~60 nM) (Figure 4B). In line with this decrease in affinity, overexpression of eIF1, but not eIF1A, rescues the growth defects in *bcd1-D72A* cells to a great extent, while it does not affect the wild-type control cells (Figure 4C).

The biochemical and genetic data above suggest that rRNA 2'-O-methylations play a key role in regulating the binding of eIF1 thereby ensuring the stringency of start codon selection. A prediction from this finding is that other factors/mutants that antagonize the near-cognate start codon selection could at least partially rescue the slow growth phenotype of *bcd1-D72A* cells. To test this idea, we took advantage of two *rps3* missense mutants (R116D and R117D) that destabilize the closed conformation of the 48S pre-initiation complex (PIC) and antagonize the near-cognate start codon selection (77). First, we replaced the endogenous promoter of the *RPS3* gene with a galactose-inducible/glucose repressible promoter in wild-type control and *bcd1-D72A* cells. This allowed us to compare the impact of expression of wild-type and mutant versions of

RPS3 on the growth of wild-type control and *bcd1-D72A* cells by transforming in plasmids encoding these variants and turning off the expression of endogenous *RPS3*. Interestingly, expression of both variants of *RPS3* rescued the slow growth defect of *bcd1-D72A* cells (Figure 4D).

The 18S rRNA folds into distinct domains known as head, shoulder, and body (Figure S5). The mRNA binding site lies within a cleft between the head and body domains. In the open, scanning competent conformation, the head and body domains are farther apart from each other compared to the closed conformation, allowing the rapid movement of the 40S on the mRNA. In the closed conformation, the head and body come close to each other, locking the initiation codon in the P-site (78, 79). A distinct structural feature of the closed state is the appearance of the mRNA latch composed of elements in h18 in the body with h34 and Rps3 in the head domain (73). Comparing the latch nucleotides in the closed and open conformations (80) suggests that the A579 nucleotide is more solvent accessible in the open conformation and hence more likely to be modified by RNA structure probing reagents (Figure S5). To probe if the equilibrium between the open and closed conformations of 40S is affected in hypo 2'-O-methylated ribosomes, we treated 40S subunits isolated from control or *bcd1-D72A* cells with dimethyl sulfate (DMS) and analyzed the accessibility of the A579 nucleotide (Figure 4E). Our analysis shows a decreased reactivity of the A579 nucleotide towards DMS in *bcd1-D72A* cells relative to the control cells, suggesting that the mRNA latch is closed in a higher population of 40S ribosomes in *bcd1-D72A* relative to the wild-type control cells (Figure 4F).

Altogether, these data strongly suggest that rRNA hypo 2'-O-methylation changes the inherent conformational dynamics of ribosomes thereby impacting ribosome-factor interactions leading to translational errors. Thus, the deficiency in start codon selection in hypo 2'-O-methylated

ribosomes may be attributed to the weaker binding of the ribosome to eIF1 and changes in ribosome dynamics.

Discussion

snoRNA-guided ribose 2'-O methylation is an evolutionarily conserved common form of methylation in rRNA. Even though RNA 2'-O-methylation changes have been linked to a large number of human diseases (5, 8, 38, 40, 55, 81, 82), the role of rRNA 2'-O-methylations for the function of ribosomes is not understood to date. Recent findings indicate the plasticity of 2'-O-methylation in rRNA, proposing new avenues for fine-tuning the function of the ribosome (5, 28, 29, 36, 38, 39). Here, we describe a new strategy for surveying the repertoire of sub-stoichiometric rRNA 2'-O-methylation sites by exploiting a defect in box C/D snoRNP assembly. This approach allowed us to lower the overall level of box C/D snoRNAs thereby globally changing rRNA 2'-O methylations without severely affecting cell survival, enabling us to probe rRNA 2'-O-methylation changes that had remained elusive so far.

Interestingly, as suggested from previous studies of human snoRNAs (29), comparing the snoRNA levels to the fraction of modification of their corresponding 2'-O-methylation sites indicated that there was no direct correlation between the steady-state box C/D snoRNA levels and the methylation status of nucleotides. While the majority of box C/D snoRNA levels decreased by more than 60% in *bcd1-D72A* cells, in some cases we observed near complete 2'-O-methylation (Table S1). The observation that most stable methylation sites had their corresponding snoRNA levels reduced by 80-90%, suggests a threshold model for rRNA modification where the presence of even a small amount of snoRNAs is sufficient for 2'-O-methylation of the majority of transcribed rRNA.

Of the 53 2'-O-methylation sites in yeast rRNA, 38 are conserved between yeast and humans. The

potential of these conserved sites for variability in their methylation was assessed previously after knockdown of the methyltransferase fibrillarin (28). This study showed that 6/38 of the conserved sites between yeast and humans were less than 80% methylated and could be substantially altered. With our approach of manipulating snoRNA levels in yeast, we identified 25/38 conserved sites in yeast that were methylated in less than 80% of the rRNA population (Figure S6). Interestingly, all but one of the 6 variable conserved sites that were identified in human rRNA had their yeast equivalents also hypomodified in the *bcd1-D72A* mutants. The Cm2197 site in yeast rRNA is the only exception which remains fully methylated in *bcd1-D72A* cells, yet its human equivalent shows significant hypomethylation in fibrillarin depleted HeLa cells (28). We attribute this difference to the resistance of the guiding snoRNA, snR76, to *bcd1-D72A* mutation (Table S1) or the higher stability of this snoRNA. A possible explanation for the higher number of variable modifications in yeast rRNA compared to human rRNA could result from organismal differences. However, as opposed to cells depleted of fibrillarin, which undergo limited division and do not make new ribosomes, the *bcd1-D72A* yeast cells we have used in this study keep dividing and making new ribosomes (50). This can result in a higher rate of hypomodification and allow us to map sub-stoichiometric 2'-O-methylations in a more thorough way than was possible previously. While most of the box C/D snoRNAs in yeast guide the site-specific modification of rRNA, a few snoRNAs play a role in rRNA folding and processing (83). Recently, the box H/ACA snR35 was proposed to prevent the premature folding of helix31 in pre-40S, thereby contributing to rRNA folding in a manner distinct from its modifying role (70). Given the decrease in snoRNA levels in *bcd1-D72A* cells relative to wild-type control, we tested whether the changes in the dynamics of the ribosomes arise from the lack of methylation or decreased snoRNA levels. Our results show that altered inherent ribosomal dynamics can be caused by changes in rRNA 2'-O-methylation but

not by the loss of snoRNAs and their chaperoning effect. These findings corroborate previous work on several box C/D and H/ACA snoRNAs which point to the importance of rRNA modifications in addition to the chaperoning role of snoRNAs (52). However, further studies are required to dissect the potential role of snoRNAs in chaperoning rRNA folding and investigating the contributions from these events to rRNA dynamics.

Whereas deletion of most individual box C/D snoRNAs does not have a major effect on yeast cell growth under normal conditions (84-86), simultaneous deletion of groups of rRNA 2'-O-methylations or using a temperature-sensitive Nop1 severely affects cell growth and results in translation defects (4, 44, 87). For example, the absence of modifications in 25S H69 as well as around the decoding center and the A-site finger causes translational errors including stop-codon readthrough, +1 frameshifting, and -1 frameshifting (51, 87). Mapping 2′-O-methylation changes arising from fibrillarin knockdown onto the ribosome structure revealed that altered 2′-O-methylations can be found in several regions involved in intermolecular interactions, such as between tRNA and the A-site, inter-subunit bridges, or around the peptide exit tunnel (28). While these changes in 2'-O-methylation levels did not affect translation elongation, they affected the IRES-mediated translation initiation.

Our data reveal that changes in 2'-O-methylation levels can affect translation fidelity in multiple ways. In addition to modulating IRES-dependent translation initiation, similar to what was observed after fibrillarin knockdown, we also observe an increase in the rate of frameshifting and near-cognate start codon recognition. Frameshifting involves the pause of the ribosomal subunits in the rotated state prior to translocation (62-64). Our data indicate that hypo 2'-O-methylated ribosomes from *bcd1-D72A* cells favor the rotated state *in vivo* (Figure 3A-G). Because we observe a similar preference in rotational state of ribosomes in Nop1 deficient cells (Figure 3H, I), our data

suggest that the observed changes in rRNA dynamics are mainly due to the alteration of rRNA 2'-O-methylation pattern and not the rRNA folding defects resulting from the reduced snoRNA levels.

Previously, global pseudouridylation defects were shown to affect the binding of the A- and P-site tRNAs to the ribosome, explaining the increased frameshifting and decreased stop-codon readthrough rates of such ribosomes (11). Mapping of the hypomethylation sites around the E- and P-site tRNAs did not reveal dramatic changes in the methylation pattern, with the exception of two sites near the acceptor arm of each tRNA (Figure S4B, C). We also did not observe a change in the rate of HPG incorporation into newly synthesized proteins, despite its overall lower incorporation at any time point (Figure 2A), suggesting that the translation rate remains unchanged. These findings corroborate the previous observation that hypo 2'-O-methylation does not affect the elongation rate (28). Whether long-range effects from hypo 2'-O-methylated sites can also influence tRNA binding remains to be addressed.

To our knowledge, the effect of rRNA 2'-O-methylations on the near-cognate start codon selection was unknown to date. Here, we show that eIF1, a major antagonist of near-cognate start site selection, has a lower affinity for hypo 2'-O-methylated 40S than wild type 40S (Figure 4A-B). Interestingly, overexpression of eIF1, but not eIF1A, substantially suppresses the slow growth phenotype of *bcd1-D72A* cells without affecting the growth of wild-type control (Figure 4C). A point mutation in the *RPS3* gene which hampers the near-cognate start codon selection also substantially rescues the slow growth phenotype of *bcd1-D72A* (Figure 4D). Collectively, these results suggest that a major role of 2'-O-methylation of ribosomes is to support faithful translation initiation. The increased rate of near-cognate start site selection results in the production of peptides from many short open reading frames (88) or the production of proteins with extended

N-termini (89). Recently, near-cognate start site selection was also linked to the re-distribution of many proteins from the cytosol to mitochondria due to the gain of N-terminal mitochondrial targeting signals (90). It is not yet clear whether rRNA hypo 2'-O-methylation causes similar defects.

Based on the binding data presented, the eIF1 affinities for wild-type and hypomethylated ribosomes are 23 and 63 nM, respectively (Figure 4B). The observed 3-fold reduction in the eIF1-affinity for ribosome would not significantly reduce the fractional saturation of the binding interaction at physiological cellular concentrations of eIF1 (91). While the affinity of eIF1 for the wild-type 40S is very high, its affinity for the mRNA-bound 43S PIC is much lower (5-20 fold, depending on the nature of the P-site codon) (57). Therefore, we speculate that a 3-fold reduction in the binding affinity of eIF1 to hypo 2'-O-methylated 40S compared to the wild-type would significantly reduce the interaction of eIF1 to the mRNA-bound 40S at physiological cellular concentrations of eIF1 (91).

We noticed that, based on the accessibility of the nucleotide A579 of the mRNA latch, vacant hypo 2'-O-methylated 40S subunits assume a more closed conformation compared to the control ribosomes (Figure 4E, F). As we did not detect major changes in the 2'-O-methylation of rRNA in the vicinity of the eIF1 binding site (Figure S4A), we speculate that the decreased affinity of eIF1 for the ribosome is due to a change in the dynamics of the 40S ribosomal subunit (92). According to this model, in vacant 40S the head and body fluctuate relative to each other, and eIF1 preferentially binds and stabilizes the open conformation. In *bcd1-D72A* cells, the equilibrium between open and closed conformations is altered (Figure 4E, F), resulting in weaker binding of eIF1 to the 40S subunit. Future studies are needed to test this model.

Acknowledgments

This work was supported by startup funds from Emory University and NIH Grant 1R35GM138123 (to H.G.) and by ANR grant MetRibo2020 and Région Grand Est FRCR grant EpiARN (to Y.M.). R. E. D-W. was supported by an NSF Graduate Research Fellowship. We thank David Bedwell, John Dinman, Alan Hinnebusch, Katrin Karbstein and Sunnie Thompson for the gift of plasmids, strains and antibodies. We also thank members of the Ghalei lab, and Drs. Anita Corbett and Daniel Reines for comments on the manuscript.

References

1. M. Helm, Post-transcriptional nucleotide modification and alternative folding of RNA. *Nucleic acids research* **34**, 721-733 (2006).
2. I. A. Roundtree, M. E. Evans, T. Pan, C. He, Dynamic RNA Modifications in Gene Expression Regulation. *Cell* **169**, 1187-1200 (2017).
3. L. Ayadi, A. Galvanin, F. Pichot, V. Marchand, Y. Motorin, RNA ribose methylation (2'-O-methylation): Occurrence, biosynthesis and biological functions. *Biochim Biophys Acta Gene Regul Mech* **1862**, 253-269 (2019).
4. K. E. Sloan *et al.*, Tuning the ribosome: The influence of rRNA modification on eukaryotic ribosome biogenesis and function. *RNA Biol* **14**, 1138-1152 (2017).
5. P. L. Monaco, V. Marcel, J. J. Diaz, F. Catez, 2'-O-Methylation of Ribosomal RNA: Towards an Epitranscriptomic Control of Translation? *Biomolecules* **8** (2018).
6. S. K. Natchiar, A. G. Myasnikov, H. Kratzat, I. Hazemann, B. P. Klaholz, Visualization of chemical modifications in the human 80S ribosome structure. *Nature* **551**, 472-477 (2017).
7. W. A. Decatur, M. J. Fournier, rRNA modifications and ribosome function. *Trends Biochem Sci* **27**, 344-351 (2002).
8. D. G. Dimitrova, L. Teysset, C. Carre, RNA 2'-O-Methylation (Nm) Modification in Human Diseases. *Genes (Basel)* **10** (2019).
9. S. K. Natchiar, A. G. Myasnikov, I. Hazemann, B. P. Klaholz, Visualizing the Role of 2'-OH rRNA Methylations in the Human Ribosome Structure. *Biomolecules* **8** (2018).
10. Y. S. Polikanov, S. V. Melnikov, D. Söll, T. A. Steitz, Structural insights into the role of rRNA modifications in protein synthesis and ribosome assembly. *Nat Struct Mol Biol* **22**, 342-344 (2015).

11. K. Jack *et al.*, rRNA pseudouridylation defects affect ribosomal ligand binding and translational fidelity from yeast to human cells. *Mol Cell* **44**, 660-666 (2011).

12. J. Jiang, H. Seo, C. S. Chow, Post-transcriptional Modifications Modulate rRNA Structure and Ligand Interactions. *Acc Chem Res* **49**, 893-901 (2016).

13. M. McMahon *et al.*, A single H/ACA small nucleolar RNA mediates tumor suppression downstream of oncogenic RAS. *Elife* **8** (2019).

14. H. Abou Assi *et al.*, 2'-O-Methylation can increase the abundance and lifetime of alternative RNA conformational states. *Nucleic Acids Res* **48**, 12365-12379 (2020).

15. P. Auffinger, E. Westhof, Rules governing the orientation of the 2'-hydroxyl group in RNA. *J Mol Biol* **274**, 54-63 (1997).

16. G. Kawai *et al.*, Conformational rigidity of specific pyrimidine residues in tRNA arises from posttranscriptional modifications that enhance steric interaction between the base and the 2'-hydroxyl group. *Biochemistry* **31**, 1040-1046 (1992).

17. E. Malek-Adamian *et al.*, Adjusting the Structure of 2'-Modified Nucleosides and Oligonucleotides via C4'-α-F or C4'-α-OMe Substitution: Synthesis and Conformational Analysis. *J Org Chem* **83**, 9839-9849 (2018).

18. D. M. Cheng, R. H. Sarma, Nuclear magnetic resonance study of the impact of ribose 2'-O-methylation on the aqueous solution conformation of cytidylyl-(3' leads to 5')-cytidine. *Biopolymers* **16**, 1687-1711 (1977).

19. S. K. Mahto, C. S. Chow, Synthesis and solution conformation studies of the modified nucleoside N(4),2'-O-dimethylcytidine (m(4)Cm) and its analogues. *Bioorg Med Chem* **16**, 8795-8800 (2008).

20. C. S. Chow, T. N. Lamichhane, S. K. Mahto, Expanding the nucleotide repertoire of the

ribosome with post-transcriptional modifications. *ACS Chem Biol* **2**, 610-619 (2007).

21. Z. Kiss-Laszlo, Y. Henry, J. P. Bachellerie, M. Caizergues-Ferrer, T. Kiss, Site-specific ribose methylation of preribosomal RNA: a novel function for small nucleolar RNAs. *Cell* **85**, 1077-1088 (1996).

22. J. P. Bachellerie, J. Cavaillé, Guiding ribose methylation of rRNA. *Trends Biochem Sci* **22**, 257-261 (1997).

23. G. Yu, Y. Zhao, H. Li, The multistructural forms of box C/D ribonucleoprotein particles. *Rna* **24**, 1625-1633 (2018).

24. A. Lapinaite *et al.*, The structure of the box C/D enzyme reveals regulation of RNA methylation. *Nature* **502**, 519-523 (2013).

25. J. Lin *et al.*, Structural basis for site-specific ribose methylation by box C/D RNA protein complexes. *Nature* **469**, 559-563 (2011).

26. N. J. Watkins, M. T. Bohnsack, The box C/D and H/ACA snoRNPs: key players in the modification, processing and the dynamic folding of ribosomal RNA. *Wiley interdisciplinary reviews. RNA* **3**, 397-414 (2012).

27. S. Massenet, E. Bertrand, C. Verheggen, Assembly and trafficking of box C/D and H/ACA snoRNPs. *RNA Biol* **14**, 680-692 (2017).

28. J. Erales *et al.*, Evidence for rRNA 2'-O-methylation plasticity: Control of intrinsic translational capabilities of human ribosomes. *Proc Natl Acad Sci U S A* **114**, 12934-12939 (2017).

29. S. Sharma, V. Marchand, Y. Motorin, D. L. J. Lafontaine, Identification of sites of 2'-O-methylation vulnerability in human ribosomal RNAs by systematic mapping. *Sci Rep* **7**, 11490 (2017).

30. J. Yang *et al.*, Mapping of Complete Set of Ribose and Base Modifications of Yeast rRNA by RP-HPLC and Mung Bean Nuclease Assay. *PloS one* **11**, e0168873 (2016).

31. U. Birkedal *et al.*, Profiling of ribose methylations in RNA by high-throughput sequencing. *Angew Chem Int Ed Engl* **54**, 451-455 (2015).

32. V. Marchand, F. Blanloeil-Oillo, M. Helm, Y. Motorin, Illumina-based RiboMethSeq approach for mapping of 2'-O-Me residues in RNA. *Nucleic Acids Res* **44**, e135 (2016).

33. M. Taoka *et al.*, Landscape of the complete RNA chemical modifications in the human 80S ribosome. *Nucleic Acids Res* **46**, 9289-9298 (2018).

34. M. Taoka *et al.*, The complete chemical structure of Saccharomyces cerevisiae rRNA: partial pseudouridylation of U2345 in 25S rRNA by snoRNA snR9. *Nucleic acids research* **44**, 8951-8961 (2016).

35. N. Krogh *et al.*, Profiling of 2'-O-Me in human rRNA reveals a subset of fractionally modified positions and provides evidence for ribosome heterogeneity. *Nucleic Acids Res* **44**, 7884-7895 (2016).

36. Y. Motorin, M. Quinternet, W. Rhalloussi, V. Marchand, Constitutive and variable 2'-O-methylation (Nm) in human ribosomal RNA. *RNA Biol* 10.1080/15476286.2021.1974750, 1-10 (2021).

37. M. B. Ferretti, K. Karbstein, Does functional specialization of ribosomes really exist? *Rna* **25**, 521-538 (2019).

38. V. Marcel *et al.*, Ribosomal RNA 2'O-methylation as a novel layer of inter-tumour heterogeneity in breast cancer. *NAR Cancer* **2**, zcaa036 (2020).

39. J. Hebras, N. Krogh, V. Marty, H. Nielsen, J. Cavaillé, Developmental changes of rRNA ribose methylations in the mouse. *RNA Biol* **17**, 150-164 (2020).

40. V. Marcel *et al.*, p53 acts as a safeguard of translational control by regulating fibrillarin and rRNA methylation in cancer. *Cancer Cell* **24**, 318-330 (2013).

41. G. R. R. Aquino *et al.*, RNA helicase-mediated regulation of snoRNP dynamics on pre-ribosomes and rRNA 2'-O-methylation. *Nucleic acids research* **49**, 4066-4084 (2021).

42. Y. Zhao, J. Rai, H. Yu, H. Li, Pseudouridine-free Ribosome Exhibits Distinct Inter-subunit Movements. *bioRxiv* 10.1101/2021.06.02.446812, 2021.2006.2002.446812 (2021).

43. D. Tollervey, H. Lehtonen, M. Carmo-Fonseca, E. C. Hurt, The small nucleolar RNP protein NOP1 (fibrillarin) is required for pre-rRNA processing in yeast. *The EMBO journal* **10**, 573-583 (1991).

44. D. Tollervey, H. Lehtonen, R. Jansen, H. Kern, E. C. Hurt, Temperature-sensitive mutations demonstrate roles for yeast fibrillarin in pre-rRNA processing, pre-rRNA methylation, and ribosome assembly. *Cell* **72**, 443-457 (1993).

45. M. A. Amin *et al.*, Fibrillarin, a nucleolar protein, is required for normal nuclear morphology and cellular growth in HeLa cells. *Biochemical and biophysical research communications* **360**, 320-326 (2007).

46. F. J. LaRiviere, S. E. Cole, D. J. Ferullo, M. J. Moore, A late-acting quality control process for mature eukaryotic rRNAs. *Mol Cell* **24**, 619-626 (2006).

47. P. Tessarz *et al.*, Glutamine methylation in histone H2A is an RNA-polymerase-I-dedicated modification. *Nature* **505**, 564-568 (2014).

48. W. T. Peng *et al.*, A panoramic view of yeast noncoding RNA processing. *Cell* **113**, 919-933 (2003).

49. A. Paul *et al.*, Bcd1p controls RNA loading of the core protein Nop58 during C/D box snoRNP biogenesis. *RNA (New York, N.Y.)* **25**, 496-506 (2019).

50. S. Khoshnevis, R. E. Dreggors, T. F. R. Hoffmann, H. Ghalei, A conserved Bcd1 interaction essential for box C/D snoRNP biogenesis. *J Biol Chem* **294**, 18360-18371 (2019).

51. A. Baudin-Baillieu *et al.*, Nucleotide modifications in three functionally important regions of the Saccharomyces cerevisiae ribosome affect translation accuracy. *Nucleic acids research* **37**, 7665-7677 (2009).

52. X. H. Liang, Q. Liu, M. J. Fournier, rRNA modifications in an intersubunit bridge of the ribosome strongly affect both ribosome biogenesis and activity. *Mol Cell* **28**, 965-977 (2007).

53. E. W. Mills, R. Green, Ribosomopathies: There's strength in numbers. *Science* **358** (2017).

54. S. O. Sulima, I. J. F. Hofman, K. De Keersmaecker, J. D. Dinman, How Ribosomes Translate Cancer. *Cancer Discov* **7**, 1069-1087 (2017).

55. Y. Yi *et al.*, A PRC2-independent function for EZH2 in regulating rRNA 2'-O methylation and IRES-dependent translation. *Nat Cell Biol* **23**, 341-354 (2021).

56. J. W. Harger, J. D. Dinman, An in vivo dual-luciferase assay system for studying translational recoding in the yeast Saccharomyces cerevisiae. *RNA* **9**, 1019-1024 (2003).

57. Y. N. Cheung *et al.*, Dissociation of eIF1 from the 40S ribosomal subunit is a key step in start codon selection in vivo. *Genes Dev* **21**, 1217-1230 (2007).

58. K. M. Keeling *et al.*, Leaky termination at premature stop codons antagonizes nonsense-mediated mRNA decay in S. cerevisiae. *RNA* **10**, 691-703 (2004).

59. J. Salas-Marco, D. M. Bedwell, Discrimination between defects in elongation fidelity and termination efficiency provides mechanistic insights into translational readthrough. *J Mol Biol* **348**, 801-815 (2005).

60. D. M. Landry, M. I. Hertz, S. R. Thompson, RPS25 is essential for translation initiation by the Dicistroviridae and hepatitis C viral IRESs. *Genes Dev* **23**, 2753-2764 (2009).

61. N. Garreau de Loubresse *et al.*, Structural basis for the inhibition of the eukaryotic ribosome. *Nature* **513**, 517-522 (2014).

62. P. Qin, D. Yu, X. Zuo, P. V. Cornish, Structured mRNA induces the ribosome into a hyper-rotated state. *EMBO Rep* **15**, 185-190 (2014).

63. J. Choi, S. O'Loughlin, J. F. Atkins, J. D. Puglisi, The energy landscape of -1 ribosomal frameshifting. *Sci Adv* **6**, eaax6969 (2020).

64. J. Chen *et al.*, Dynamic pathways of -1 translational frameshifting. *Nature* **512**, 328-332 (2014).

65. P. R. Bhatt *et al.*, Structural basis of ribosomal frameshifting during translation of the SARS-CoV-2 RNA genome. *Science* **372**, 1306-1313 (2021).

66. S. O. Sulima *et al.*, Eukaryotic rpL10 drives ribosomal rotation. *Nucleic Acids Res* **42**, 2049-2063 (2014).

67. A. Meskauskas, J. D. Dinman, Ribosomal protein L3: gatekeeper to the A site. *Mol Cell* **25**, 877-888 (2007).

68. R. Belardinelli, H. Sharma, F. Peske, W. Wintermeyer, M. V. Rodnina, Translocation as continuous movement through the ribosome. *RNA Biol* **13**, 1197-1203 (2016).

69. M. C. Justice *et al.*, Elongation factor 2 as a novel target for selective inhibition of fungal protein synthesis. *J Biol Chem* **273**, 3148-3151 (1998).

70. H. Huang, K. Karbstein, Assembly factors chaperone ribosomal RNA folding by isolating helical junctions that are prone to misfolding. *Proc Natl Acad Sci U S A* **118** (2021).

71. M. Kofoed *et al.*, An Updated Collection of Sequence Barcoded Temperature-Sensitive

Alleles of Yeast Essential Genes. *G3 (Bethesda)* **5**, 1879-1887 (2015).

72. D. Maag, C. A. Fekete, Z. Gryczynski, J. R. Lorsch, A conformational change in the eukaryotic translation preinitiation complex and release of eIF1 signal recognition of the start codon. *Mol Cell* **17**, 265-275 (2005).

73. L. A. Passmore *et al.*, The eukaryotic translation initiation factors eIF1 and eIF1A induce an open conformation of the 40S ribosome. *Mol Cell* **26**, 41-50 (2007).

74. T. V. Pestova, V. G. Kolupaeva, The roles of individual eukaryotic translation initiation factors in ribosomal scanning and initiation codon selection. *Genes & development* **16**, 2906-2922 (2002).

75. J. S. Nanda *et al.*, eIF1 controls multiple steps in start codon recognition during eukaryotic translation initiation. *J Mol Biol* **394**, 268-285 (2009).

76. D. Maag, J. R. Lorsch, Communication between eukaryotic translation initiation factors 1 and 1A on the yeast small ribosomal subunit. *J Mol Biol* **330**, 917-924 (2003).

77. J. Dong *et al.*, Rps3/uS3 promotes mRNA binding at the 40S ribosome entry channel and stabilizes preinitiation complexes at start codons. *Proc Natl Acad Sci U S A* **114**, E2126-E2135 (2017).

78. A. G. Hinnebusch, The scanning mechanism of eukaryotic translation initiation. *Annu Rev Biochem* **83**, 779-812 (2014).

79. A. G. Hinnebusch, Structural Insights into the Mechanism of Scanning and Start Codon Recognition in Eukaryotic Translation Initiation. *Trends in biochemical sciences* **42**, 589-611 (2017).

80. J. L. Llácer *et al.*, Conformational Differences between Open and Closed States of the Eukaryotic Translation Initiation Complex. *Mol Cell* **59**, 399-412 (2015).

81. D. Nachmani *et al.*, Germline NPM1 mutations lead to altered rRNA 2'-O-methylation and cause dyskeratosis congenita. *Nat Genet* **51**, 1518-1529 (2019).

82. F. Zhou *et al.*, AML1-ETO requires enhanced C/D box snoRNA/RNP formation to induce self-renewal and leukaemia. *Nat Cell Biol* **19**, 844-855 (2017).

83. S. Ojha, S. Malla, S. M. Lyons, snoRNPs: Functions in Ribosome Biogenesis. *Biomolecules* **10** (2020).

84. S. Parker *et al.*, Large-scale profiling of noncoding RNA function in yeast. *PLoS Genet* **14**, e1007253 (2018).

85. L. N. Balarezo-Cisneros *et al.*, Functional and transcriptional profiling of non-coding RNAs in yeast reveal context-dependent phenotypes and in trans effects on the protein regulatory network. *PLoS Genet* **17**, e1008761 (2021).

86. J. Esguerra, J. Warringer, A. Blomberg, Functional importance of individual rRNA 2'-O-ribose methylations revealed by high-resolution phenotyping. *Rna* **14**, 649-656 (2008).

87. X. H. Liang, Q. Liu, M. J. Fournier, Loss of rRNA modifications in the decoding center of the ribosome impairs translation and strongly delays pre-rRNA processing. *RNA* **15**, 1716-1728 (2009).

88. S. D. Kulkarni *et al.*, Temperature-dependent regulation of upstream open reading frame translation in S. cerevisiae. *BMC Biol* **17**, 101 (2019).

89. F. Zhou, H. Zhang, S. D. Kulkarni, J. R. Lorsch, A. G. Hinnebusch, eIF1 discriminates against suboptimal initiation sites to prevent excessive uORF translation genome-wide. *RNA* **26**, 419-438 (2020).

90. G. Monteuuis *et al.*, Non-canonical translation initiation in yeast generates a cryptic pool of mitochondrial proteins. *Nucleic Acids Res* **47**, 5777-5791 (2019).

91. T. von der Haar, J. E. McCarthy, Intracellular translation initiation factor levels in Saccharomyces cerevisiae and their role in cap-complex function. *Mol Microbiol* **46**, 531-544 (2002).

92. D. Maag, M. A. Algire, J. R. Lorsch, Communication between eukaryotic translation initiation factors 5 and 1A within the ribosomal pre-initiation complex plays a role in start site selection. *Journal of molecular biology* **356**, 724-737 (2006).

93. F. Pichot *et al.*, Holistic Optimization of Bioinformatic Analysis Pipeline for Detection and Quantification of 2'-O-Methylations in RNA by RiboMethSeq. *Front Genet* **11**, 38 (2020).

94. L. Valásek, B. Szamecz, A. G. Hinnebusch, K. H. Nielsen, In vivo stabilization of preinitiation complexes by formaldehyde cross-linking. *Methods Enzymol* **429**, 163-183 (2007).

95. M. G. Acker, S. E. Kolitz, S. F. Mitchell, J. S. Nanda, J. R. Lorsch, Reconstitution of yeast translation initiation. *Methods Enzymol* **430**, 111-145 (2007).

Figures

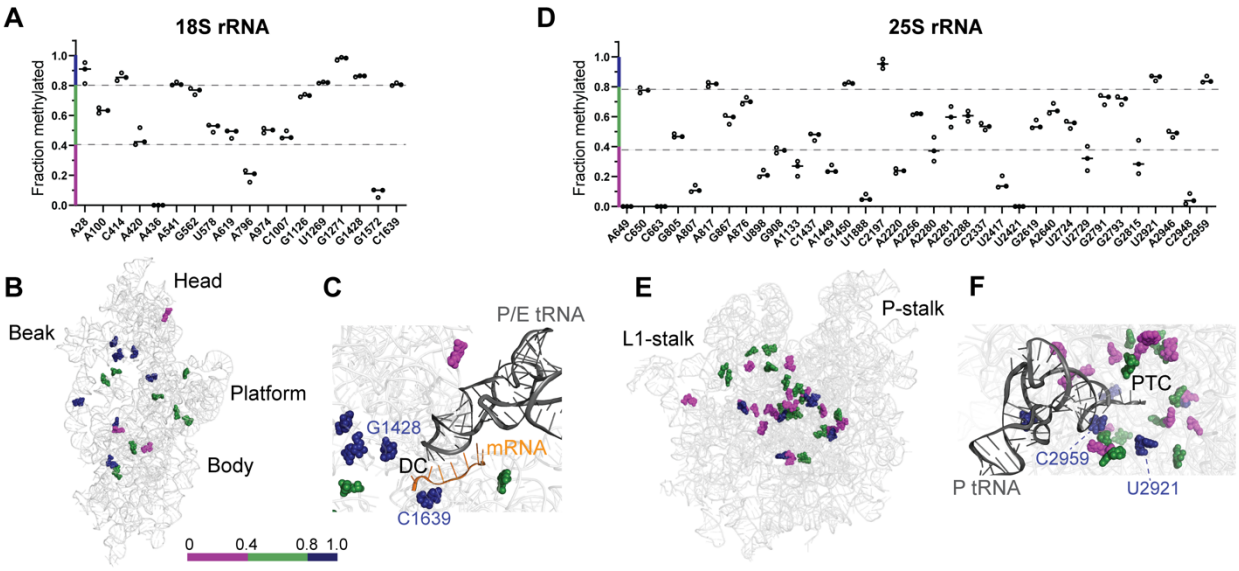

Figure 1. rRNA 2'-O-methylation sites change in a site-specific manner in *bcd1-D72A* cells. The fraction of 2′-O-methylation (MethScore) at each modification site in 18S (**A**) and 25S (**D**) rRNA in *bcd1-D72A* relative to wild-type control cells was evaluated by RiboMethSeq. Data are shown as mean MethScore values for 3 independent biological replicates. The position of each modification is marked on the 18S (**B**) and 25S (**E**) rRNA structure (PDB ID: 6GQV). The stable sites (MethScore >0.8) are colored in blue, the variable sites (0.4 < MethScore < 0.8) in green, and the hypo 2'-O-methylated sites (MethScore < 0.4) in magenta. (**C**) Modifications around the decoding center (DC) within 18S rRNA. (**F**) Modifications around the peptidyl transferase center (PTC) within 25S rRNA (PDB ID: 4V6I).

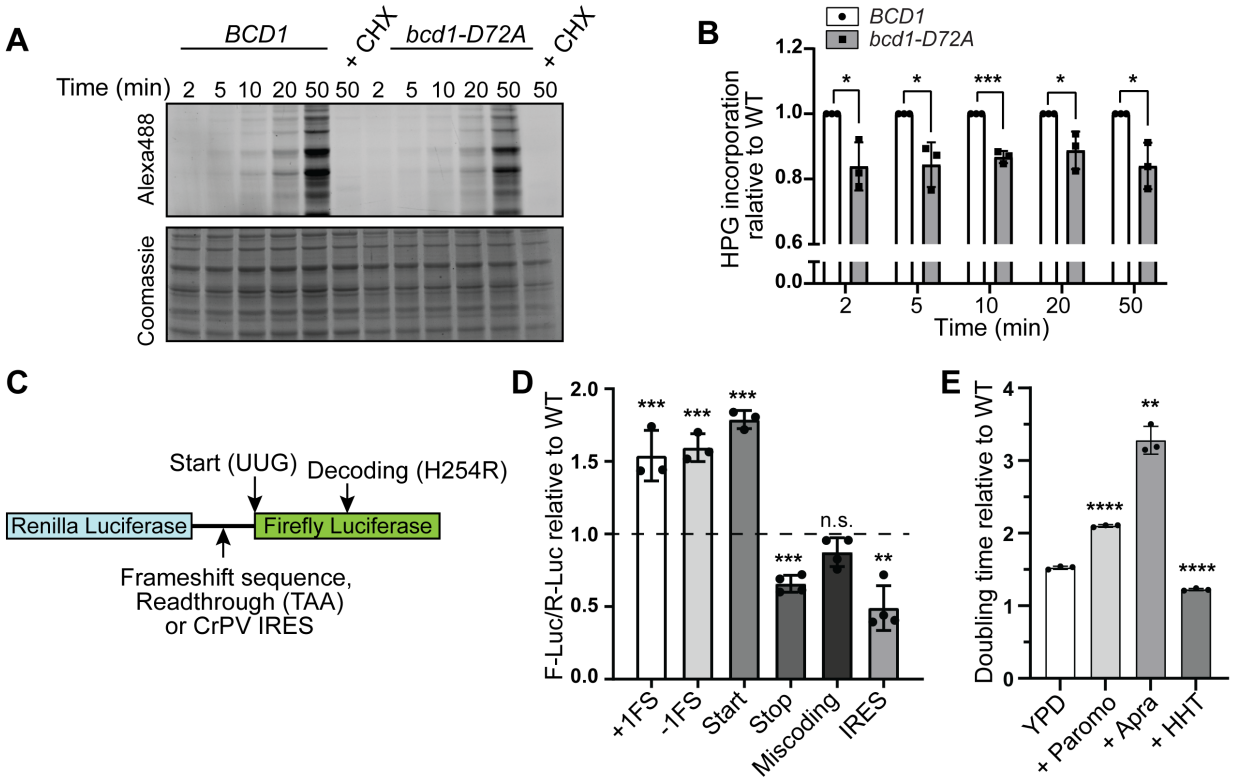

Figure 2. rRNA hypomethylation affects the function and fidelity of ribosomes. (**A**) Analysis of the incorporation rate of L-homopropargylglycine (HPG) into newly synthesized peptides in rapidly dividing yeast cells expressing wild-type or mutant Bcd1 over a time course (2-50 min). HPG-containing proteins were fluorescently labeled by addition of Alexa Fluor 488 and separated from unincorporated dye by SDS-PAGE and imaged (top) before staining with Coomassie blue for total protein detection (bottom). (**B**) Quantification of the data shown in panel A. At each time point, the ratio of the newly synthesized protein to the total protein for *bcd1-D72A* is normalized to the wild type. Three biological replicates were analyzed. (**C**) Schematic of the dual luciferase plasmids used in this study. For all plasmids, Renilla luciferase is constitutively expressed, while the expression of firefly luciferase is dependent on a specific translational defect/element. (**D**) Expression of firefly and Renilla luciferase was measured in wild-type control or *bcd1-D72A* yeast harboring the indicated plasmids. The ratio of firefly luciferase to Renilla luciferase was

normalized to the control plasmids and shown relative to wild-type. 3-4 biological replicates were analyzed. (**E**) Doubling times of wild-type control and *bcd1-D72A* cells were measured in media with or without translational inhibitors. The fold change, calculated by dividing the doubling time values of *bcd1-D72A* cells to wild-type control cells in each condition, is plotted. 3 biological replicates were analyzed. In panels B, D and E, column bars represent the mean values and the error bars depict the standard deviations. Significance was determined using a t-test. *$p \leq 0.05$; **$p \leq 0.01$; ***$p \leq 0.001$; ****$p \leq 0.0001$. n.s., non-significant.

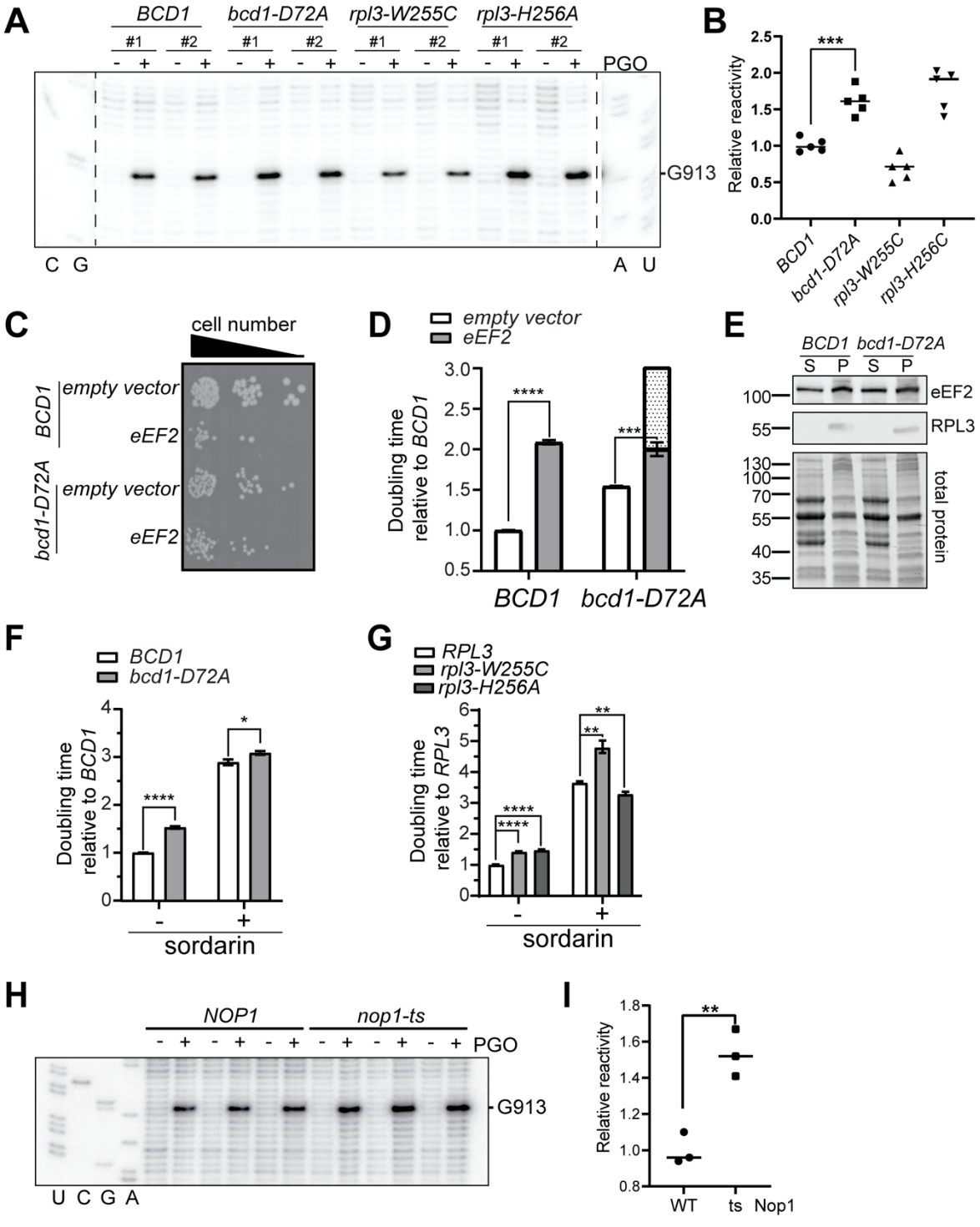

Figure 3. Hypo 2'-O-methylated ribosomes adopt a more rotated conformation *in vivo.* (A)

In vivo RNA structure probing of cells expressing either wild-type or D72A variant of Bcd1 with or without PGO treatment to probe the accessibility of SSU G913. Cells expressing W255C or H256A variants of Rpl3 were used as control for rotation status. Two biological replicates are shown in the figure. (**B**) Quantification of the SSU G913 modification by PGO. Five biological replicates were analyzed. (**C**) *bcd1-D72A* cells are less sensitive to the overexpression of eEF2 than wild type cells. Indicated cells were serially diluted on selective plate and grew for 48h at 30°C. **(D)** Quantification of the growth of *BCD1* and *bcd1-D72A* expressing eEF2. Dot pattern indicates the expected doubling time of *bcd1-D72A* if there was no rescue of eEF2 overexpression by the *bcd1-D72A* mutation. (**E**) Western blot against free (S; supernatant) and ribosome-bound (P; pellet) eEF2 from formaldehyde-fixed whole-cell extracts from *BCD1* or *bcd1-D72A* cells separated by centrifugation over a sucrose cushion. Rpl3 serves as an indicator of ribosome pelleting. (**F**) *bcd1-D72A* cells are less sensitive to sordarin (3 µg/mL) than wild type cells. (**G**) Whereas *rpl3-W255C* has the same sensitivity to sordarin as the wildtype, *rpl3-H256A* shows less sensitivity to sordarin. D, F, G; four biological replicates were analyzed. (**H**) Probing the accessibility of SSU G913 in *NOP1* and *nop1-ts* using PGO. Three biological replicates are shown in the figure. (**I**) Quantification of the SSU G913 modification by PGO. In panels B, D, F, G and I, bars represent the mean values. The error bars in panels D, F and G depict the standard deviations. Significance for all graphs was analyzed using a t-test. *$p \leq 0.05$; **$p \leq 0.01$; ***$p \leq 0.001$; ****$p \leq 0.0001$.

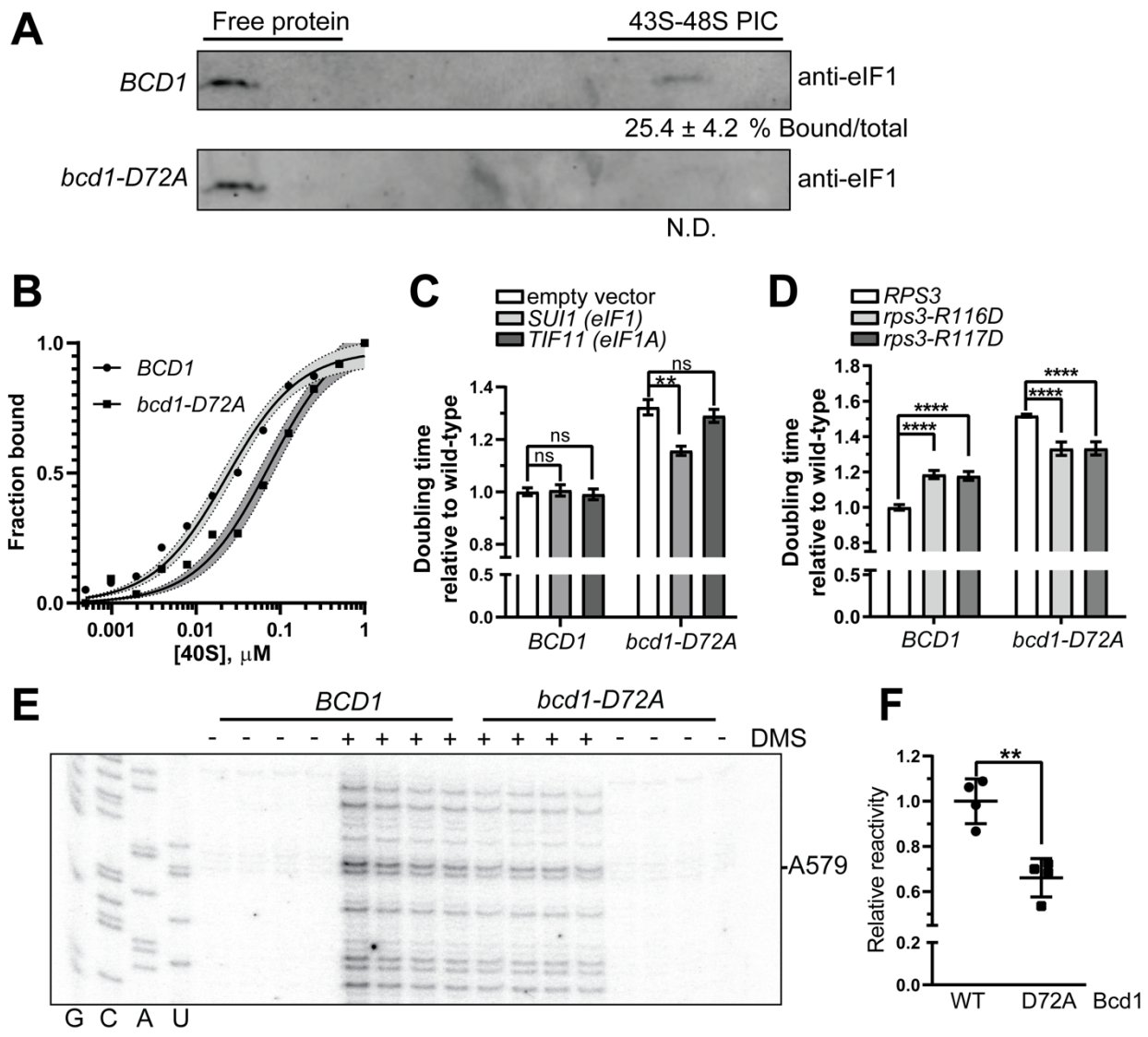

Figure 4. Binding of eIF1 to hypomethylated 40S is weakened *in vivo* and *in vitro*. (**A**) Western blot against eIF1 for the fractions of sucrose gradients of formaldehyde-fixed whole-cell extracts from *BCD1* (top) or *bcd1-D72A* (bottom). The ratio of eIF1 in 43-48S PIC relative to the total eIF1 is depicted under each blot. Two biological replicates were analyzed. (**B**) Fraction of eIF1 bound to 40S plotted against the 40S concentration. Data were fitted with a non-linear regression model in GraphPad Prism 8.0 to yield dissociation constants of 23 nM and 64 nM for wild type and hypo 2'-O-methylated ribosomes, respectively. 95% confidence levels are shown in shades of gray. (**C**)

Comparison of doubling times of *BCD1* and *bcd1-D72A* harboring either an empty vector or vectors expressing *SUI1* (eIF1) or *TIF11* (eIF1A) in minimal medium containing glucose. Four biological replicates were analyzed. (**D**) Comparison of doubling times of *BCD1* and *bcd1-D72A* in which the endogenous *RPS3* gene is deleted and either WT, R116D or R117D variant of *RPS3* are expressed from a plasmid. Four biological replicates were analyzed. (**E**) Probing the accessibility of SSU A579 in 40S ribosomal subunits purified from *BCD1* and *bcd1-D72A* cells using DMS. Four biological replicates are shown in the figure. (**F**) Quantification of data shown in panel E for the SSU A579 modification by DMS. In panels C, D and F, bars represent the mean values and the error bars depict the standard deviations. Significance was analyzed using a t-test. n.s., non-significant; **$p \leq 0.01$; ****$p \leq 0.0001$.

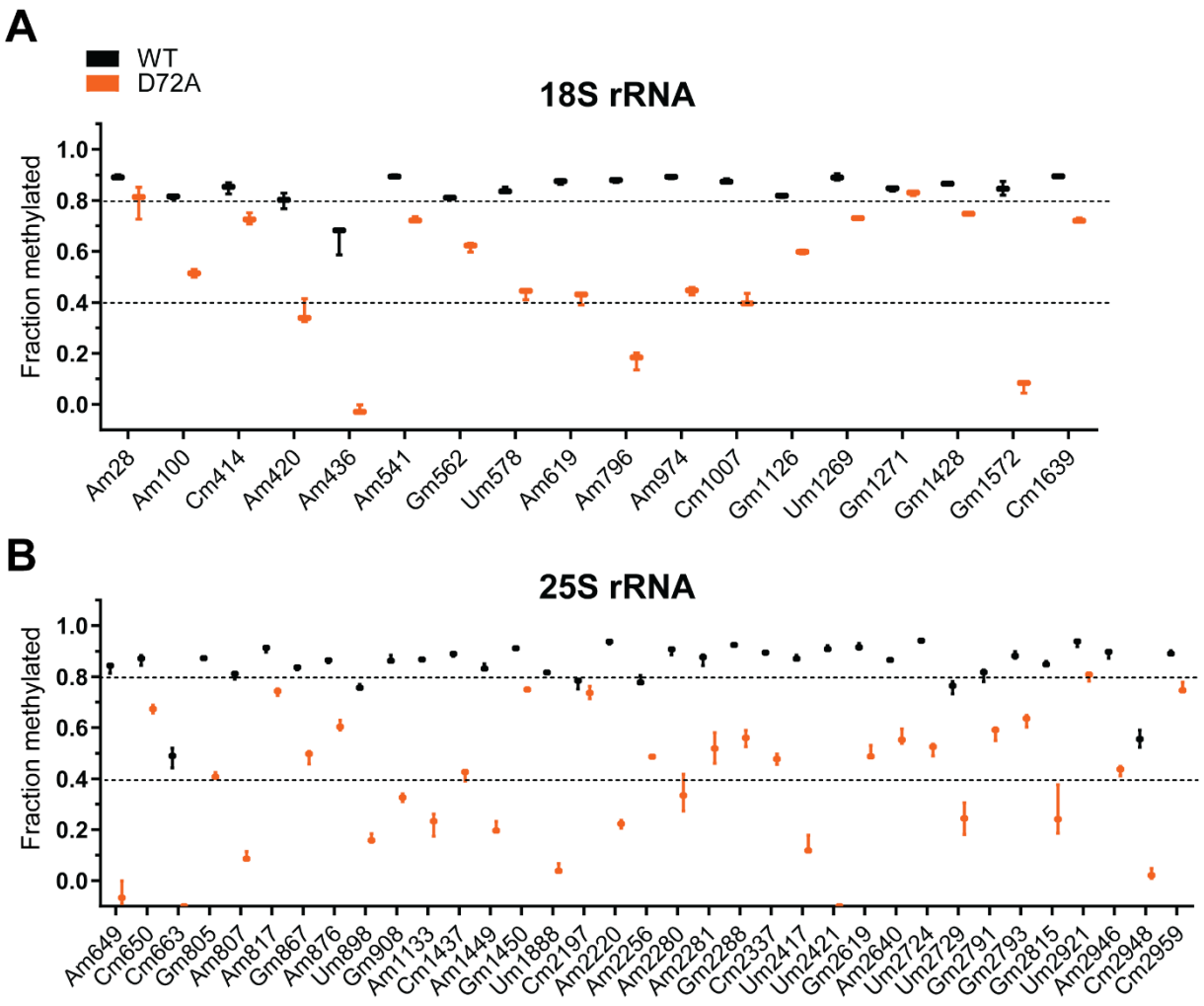

Figure S1. Comparison of the 2'-O-methylation sites. MethScores at each modified position of 18S **(A)** and 25S rRNA **(B)** are compared between wild-type control (WT) and *bcd1-D72A* (D72A) cells. RiboMethSeq was performed on three biological replicates. Box edges represent the interquartile range, midlines indicate the median, and lower and upper whiskers extend to the min and max, respectively.

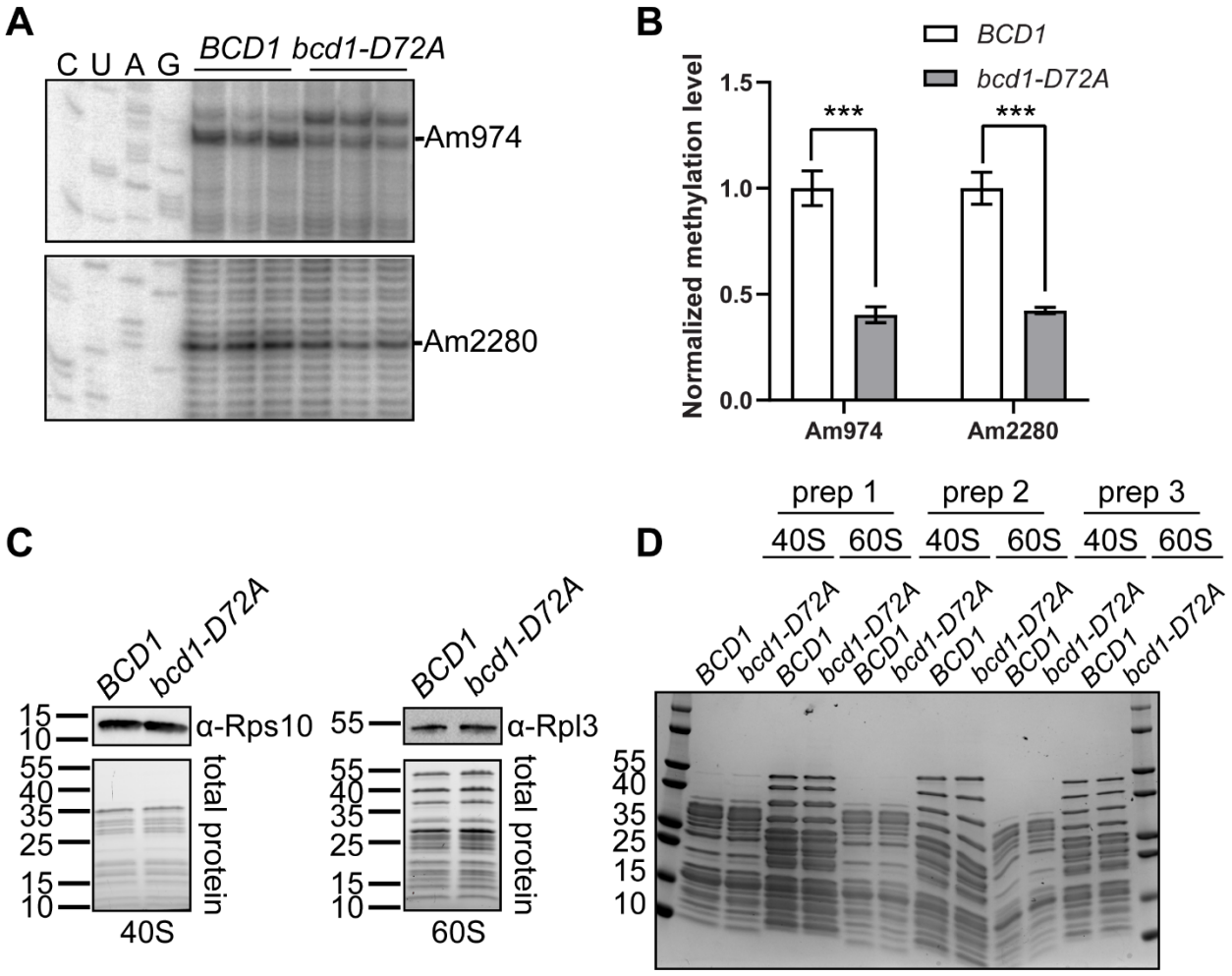

Figure S2. Comparing the modification and composition of mature ribosomes from *BCD1* and *bcd1-D72A* cells. (**A**) Reverse transcription at low concentration of dNTP combined with sequencing gel analysis was used to determine the methylation levels at a methylation site in 18S rRNA (Am947, upper panel) and 25S rRNA (Am2280, lower panel) of isolated mature ribosomes. Ribosomes isolated from three biological replicates were analyzed. (**B**) Quantification of the data shown in A. The intensity of bands at the reverse transcription stops were normalized to all band intensities below the stop signal. Both SSU A974 and LSU A2280 are less than 50% modified relative to the wild-type control, similar to their relative methylation levels as quantified by RiboMethSeq. Graph bars represent the mean and standard deviations from three biological replicates. Significance was analyzed using a t-test. ***$p \leq 0.001$. (**C**) 40S and 60S ribosomes

purified from *BCD1* and *bcd1-D72A* cells have the same composition as judged by Western blots against two ribosomal proteins. Top panels: Western blot against Rps10 (40S) or Rpl3 (60S); bottom panels: total ribosomal proteins. Rps10 antibody was a gift from K. Karbstein and Rpl3 antibody was obtained from the Developmental Studies Hybridoma Bank. (**D**) 40S and 60S ribosomes purified from *BCD1* and *bcd1-D72A* cells have the same composition as judged by SDS-PAGE. Three independent ribosome preps are shown.

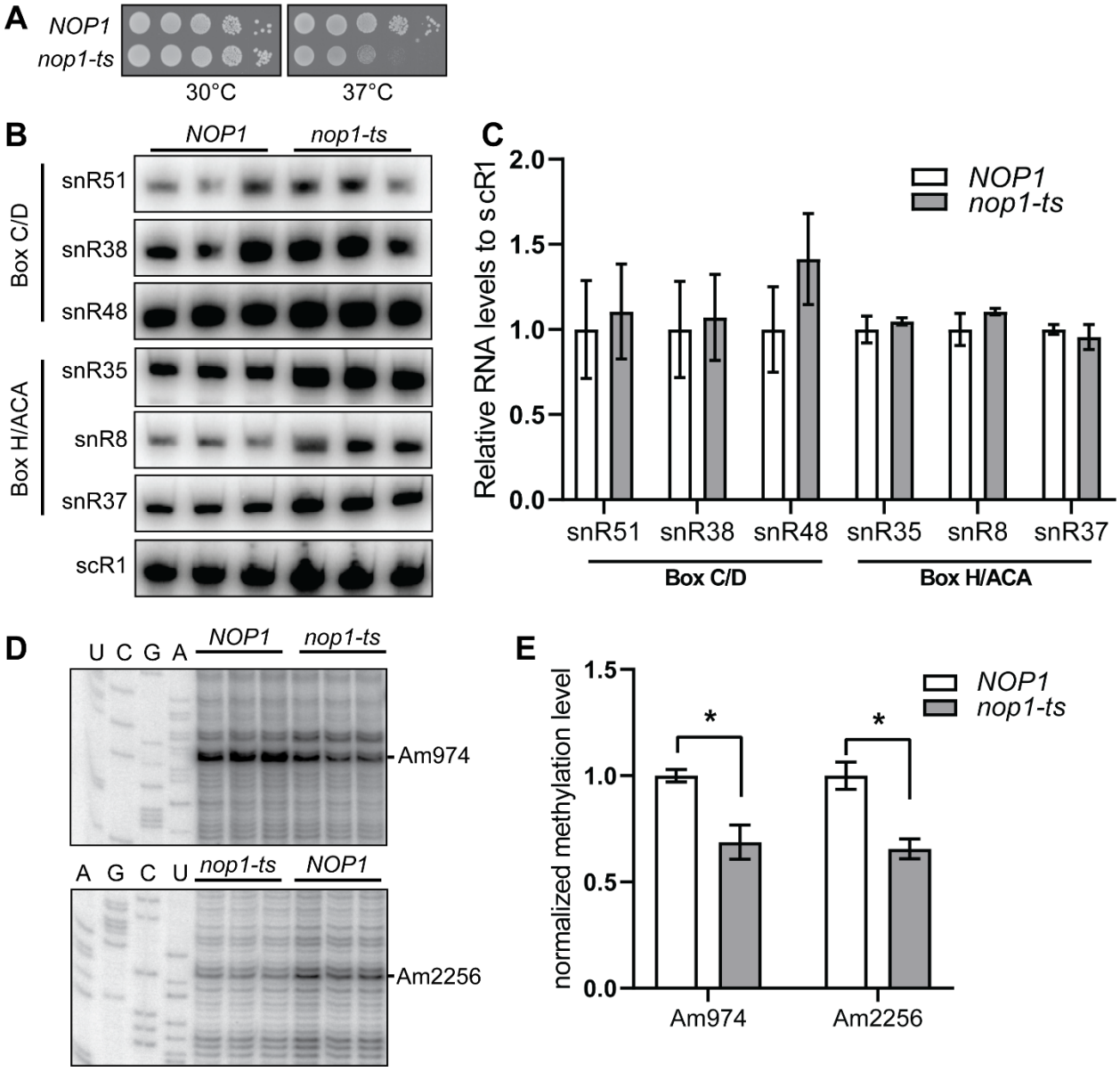

Figure S3. *nop1-ts* affects the rRNA 2'-O methylation but not the snoRNA levels. (A) *NOP1* and *nop1-ts* cells were serially diluted and spotted on YPD plates and incubated at 30°C or 37°C for two days. **(B)** Northern blotting analyses of steady-state expression levels of box C/D and box H/ACA snoRNAs in *NOP1* and *nop1-ts* cells. **(C)** Quantification of data shown in B as normalized to scR1. Graph bars represent the mean and S.D. from three biological replicates. There was no significant difference in the snoRNA levels between *NOP1* and *nop1-ts* cells as determined using

a t test. **(D)** Reverse transcription at low concentration of dNTP combined with sequencing gel analysis was used to determine the methylation levels at a methylation site in 18S rRNA (Am947) and 25S rRNA (Am2256). **(E)** Quantification of the data in D. Graph bars represent the mean and standard deviations from three biological replicates. Significance was analyzed using a t-test. *p $\leq$ 0.05.

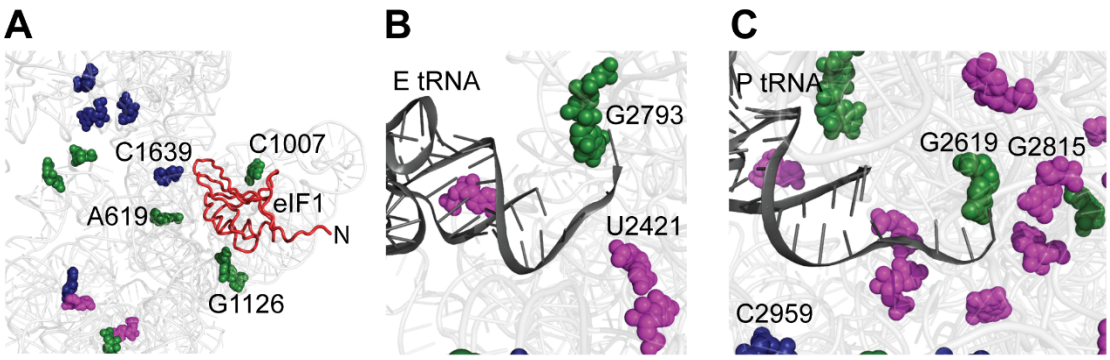

Figure S4. Position of rRNA 2'-O-methylations relative to eIf1 and the E- and P-site tRNAs. (**A**) eIF1 binding site (PDB: 6gsm). (**B**) The E-site tRNA (**C**) the P-site tRNA (PDB: 3j78). Methylation sites follow the same color coding as in Figure 1. The rRNA is in light gray, the eIF1 in red and the tRNA in dark gray.

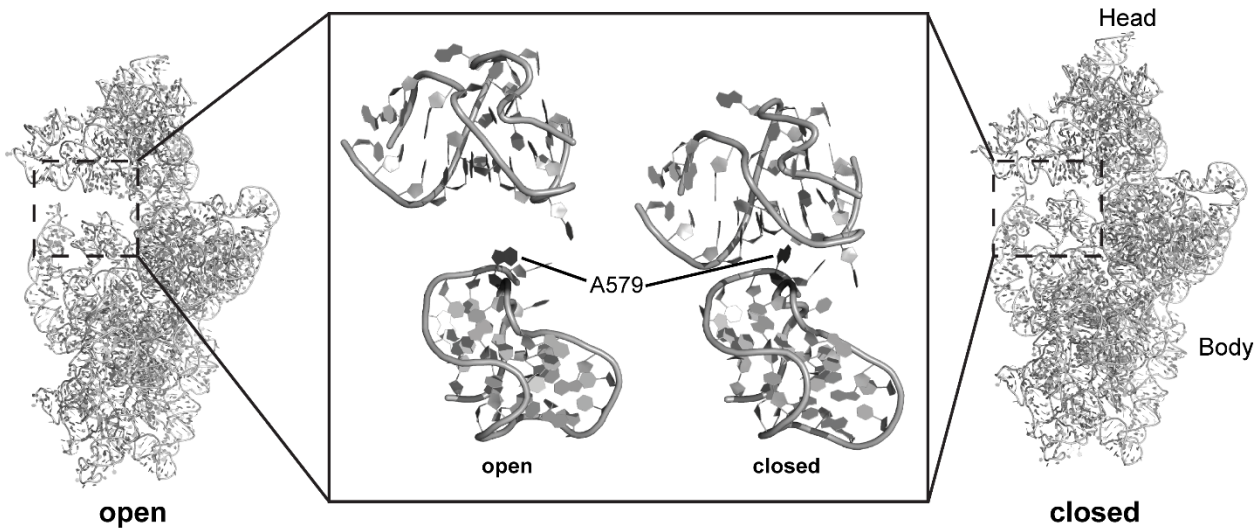

Figure S5. Comparing the position of SSU-A579 in the open and closed conformations. The left and right structures are the 18S rRNA in the open (PDB: 3jaq) and closed (PDB: 3jap) conformations, respectively. The position of the mRNA latch is boxed in both structures and zoomed in in the middle panel.

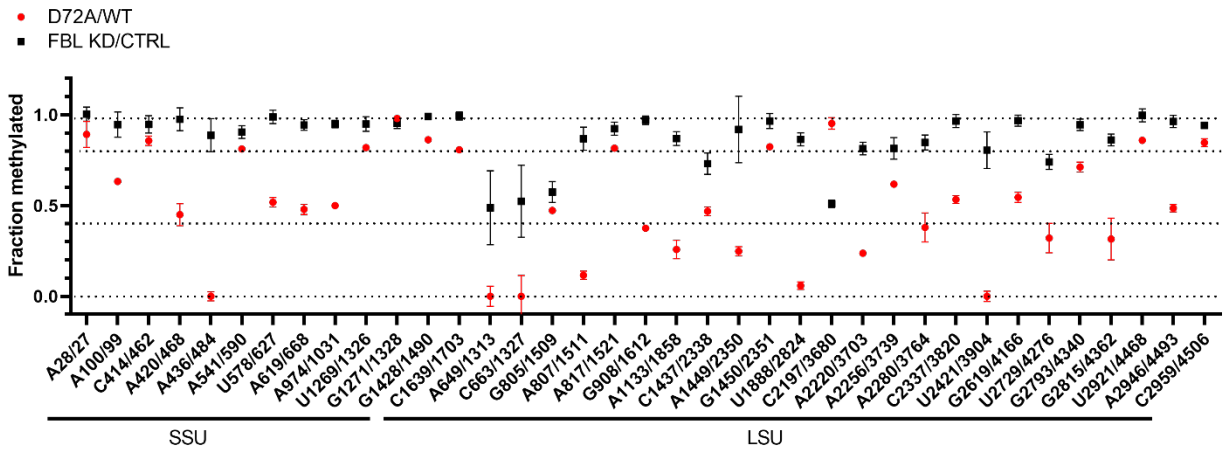

Figure S6. Comparison of the changes in rRNA 2'-O-methylation levels of the sites conserved between yeast and human. The red squares show mean methylation scores at each indicated site in *bcd1-D72A* cells relative to control wild-type yeast. The black squares show mean methylation scores from HEK cells after fibrillarin knockdown relative to control (1). Error bars represent standard deviations.

Chapter 5: Discussion

Summary

In this dissertation, I discuss three complementary studies, all of which use budding yeast as a model system to uncover novel snoRNA-mediated fundamental aspects of translational regulation. In the first study (1), we investigated the role of the essential box C/D snoRNP assembly factor Bcd1. Through a series of yeast genetic and biochemical assays, we revealed that a conserved N-terminal motif of Bcd1 is necessary for interactions of the protein with the core box C/D snoRNP protein, Snu13 and snoRNAs. Using a targeted mutational screen, we identified a variant of Bcd1 (Bcd1-D72A) which has impaired binding to Snu13 and snoRNAs. Functional characterization of the Bcd1-D72A variant revealed that the conserved N-terminal motif of Bcd1 is critical for the function of the protein in maintaining the steady-state levels of box C/D snoRNAs, proper rRNA processing, and ribosome biogenesis.

More recently, in a related study (2), we used *bcd1-D72A* cells as a tool and asked how the global downregulation of box C/D snoRNAs impacts rRNA 2'-O-methylation and cellular translation. Quantification of rRNA 2'-O-methylation levels by RiboMethSeq revealed a global yet site-specific change in the pattern of cellular rRNA 2'-O-methylations upon a global box C/D snoRNA downregulation. Furthermore, we showed that a change in the pattern of rRNA 2'-O-methylations impairs translation fidelity and affects ribosome binding to IRES elements, translation inhibitors, and initiation factor, eIF1. Finally, using RNA structure probing, we uncovered that hypo 2'-O-methylation impacts the ribosome dynamics by affecting the closed and open conformations and the rotational status of ribosomes.

The majority of my dissertation work was focused on the characterization of two disease-related variants of the critical box C/D snoRNP assembly factor, Hit1 (Dreggors-Walker RE et al.,

accepted at JBC). In humans, these two amino acid variations cause the genetic disease PEHO syndrome. I therefore generated budding yeast models of these variants using CRISPR-Cas9 mediated genome editing. My studies revealed that the PEHO-linked mutants in yeast result in reduced levels of box C/D snoRNAs, impaired rRNA processing, decreased levels of rRNA 2'-O-methylations, impaired translation fidelity, and impaired ribosomal ligand binding. These data provide the first insights into the molecular basis of PEHO syndrome in a yeast model and strongly suggest that PEHO syndrome is a ribosomopathy that is likely caused by impaired translation.

Taken together, the studies presented in this dissertation reveal several novel aspects of quality control steps required for box C/D snoRNP biogenesis that are essential for maintaining the efficiency and fidelity translation and suggest that their dysregulation can result in human disease.

Implications for understanding the fundamental aspects of snoRNP assembly and translation regulation

In the model organism budding yeast, there are currently five assembly factors identified that play a role in the formation of box C/D snoRNP complexes (3). These factors include the AAA+ ATPases Rvb1 and Rvb2, the Zf-HIT protein family members Bcd1 and Hit1, and the nuclear protein Rsa1 (3). Biogenesis of snoRNPs is thought to occur hierarchically, though the precise order and importance of the interactions that occur during the assembly process are not fully characterized (3,4).

Bcd1 is an early box C/D snoRNP assembly factor, which binds pre-snoRNPs co-transcriptionally (5). Proteomics studies in human cell cultures have revealed that the Bcd1 interactome consists of the core snoRNP proteins Snu13 and Nop58 along with other snoRNP assembly factors Rvb1/2, Hit1, and Rsa1 (6). How Bcd1 interacts with its binding partners to maintain the steady-state levels of box C/D snoRNAs is largely unknown. In one of the studies

presented in this dissertation (1), an N-terminal motif was identified and shown to be critical for the essential function of Bcd1. Uncovering this motif then allowed us to further characterize the Bcd1 function in interaction with the core snRNP protein Snu13 and the box C/D snoRNAs (1), and probe the impact of Bcd1-mediated events on cellular translation (2). Further, using disease-linked mutations in the box C/D snoRNP assembly factor Hit1, we revealed the downstream defects that result from impairment of snoRNP biogenesis. Together, these studies provide the proof of principle and evidence that snoRNP assembly factors play a key role in regulating the rRNA modification pattern. They also provide a platform for further investigation of the function of snoRNP assembly factor interactions and mechanisms of function.

Our results from analysis of rRNA modification patterns in cells with snoRNP assembly impairments, mutant for either Bcd1-D72A or Hit1-C11F, show that while many individual rRNA 2'-O-methylations are dispensable for cell growth in yeast, these modifications are cumulatively critical for maintaining ribosome structure and function. These data are in line with previous work on the functions of rRNA 2'-O-methylations which revealed that deletion of multiple rRNA modifications within the same functional domain of the rRNA can lead to impaired translational efficiency and fidelity, while individual deletion of rRNA modifications did not cause any defect (7-12). More specifically, our studies show that *bcd1-D72A*, *hit1-C11F*, and *hit1-S29L* cells have a global downregulation of translation, an increase in alternative start codon usage, and a decrease in stop codon readthrough. Further studies are required to uncover how impairment of snoRNP biogenesis results in these specific translational defects.

Implications for disease

Approximately 80% of yeast snoRNAs and their functions are conserved in humans (13). Furthermore, the core box C/D snoRNP proteins and the five critical box C/D snoRNP assembly

factors are conserved in both sequence and function between yeast and human (3). Because of this high level of evolutionary conservation, yeast provides a useful model system for studying box C/D snoRNP function and assembly (3). Attesting to the power of yeast for studying translation dysregulation in disease, previous studies of ribosomopathy-causing mutations in yeast have proved useful for informing what happens in human diseases. For example, a yeast model system was used to determine that mutations in *RPS19*, modelling those which cause Diamond Blackfan anemia in humans, indicated that the molecular basis of the disease is impaired ribosome biogenesis (14). This observation has held true in humans, and detection of the pre-rRNA processing defects that were established for this disease in the model organism yeast are now used to diagnose Diamond Blackfan anemia (15,16). Similarly, yeast model systems have been used to uncover the ribosomal defects underlying Acute Necrotizing Encephalopathy (ANE) syndrome and Shwachman–Diamond syndrome (17,18). Given the relevance of yeast model systems for studying ribosomopathies and the functional conservation between yeast Hit1 and human ZNHIT3 (19,20), we propose the results of my dissertation work, which suggest PEHO syndrome is a ribosomopathy, will be informative for future studies of this disease.

Our work in a yeast model uncovers the translational defects that may underly PEHO syndrome and could also have implications for other ribosomopathies. A number of ribosomopathies are caused by dysregulation of rRNA modification. Specifically, loss of rRNA 2'-O-methylation is implicated in the pathogenesis of the ribosomopathies dyskeratosis congenita and Treacher Collins syndrome (21,22). Furthermore, our fundamental discoveries on the functions of Bcd1 and rRNA modifications could have implications for cancer. Our studies uncovered the ribosomal defects in *bcd1-D72A* mutant yeast cells. The human homolog of Bcd1 is ZNHIT6, and the homologous residue to yeast D72 in humans is D277. A number of adenocarcinoma patient samples harbor

ZNHIT6 mutations around this conserved Asp-277 residue (23,24). The most common *ZNHIT6* mutation found in cancer cells is a nonsense mutation which truncates Bcd1 approximately twenty residues short of D277, before the critical Snu13-binding motif. Thus, Bcd1 variations and the resulting impairment of the cellular translatome could contribute to cancer pathology. Furthermore, snoRNAs and rRNA modifications are dysregulated in a multitude of cancers (25-35).

Together, our work provides insights into translational defects upon loss of rRNA 2'-O-methylations and snoRNAs and can therefore lay a groundwork for understanding the molecular mechanisms of cancers and ribosomopathies that are caused by dysregulated snoRNP biogenesis, beyond PEHO syndrome.

Future directions to uncover the role of assembly factors for snoRNP assembly

Our work reveals the importance of residues within the Zf-HIT domain of Hit1 for the stability of the protein. Interestingly, both Bcd1 and Hit1 contain N-terminal Zf-HIT domains, where a zinc ion is coordinated by four cysteine residues (36). Zinc-binding domains are important for mediating protein-protein and protein-nucleic acid interactions (37), though the Zf-HIT domains of Bcd1 and Hit1 are not critical for RNA binding *in vitro* (36). The human homologs of Hit1 and Bcd1, ZNHIT3 and ZNHIT6, also have Zf-HIT domains. These proteins are two of the six in humans with known Zf-HIT domains (38). All six Zf-HIT domain-containing proteins share the common functional partners Rvb1/2, and the Zf-HIT domains of all six proteins mediate interaction with Rvb1/2 *in vitro* (39). Zf-HIT domains are proposed to serve as adapters for Rvb1/2 binding, allowing distribution or recruitment of Rvb1/2 for different cellular purposes (39). NUFIP1, the human homolog of the Hit1 binding partner Rsa1, also has a putative Zf-HIT domain. Why three different Zf-HIT domains in three distinct proteins are necessary for box C/D snoRNP

is unclear. While neither the Bcd1 nor the Hit1 Zf-HIT domains are essential for their functions (36,40), the Zf-HIT domain of Bcd1 becomes essential at high temperatures (36). Hit1 itself is only essential at high temperatures, though it is not known whether its Zf-HIT domain specifically is essential for its function under heat stress. Whether all Zf-HIT containing proteins are recruited to Rvb1/2 simultaneously or each Zf-HIT domain is recruited at a specific step during snoRNP assembly is currently unknown. Possibly, multiple Zf-HIT domains become essential for recruiting Rvb1/2 to the pre-snoRNP complex when kinetics are disturbed by increased temperature. It is also possible that Zf-HIT domains in snoRNP assembly factors bind snoRNAs or contribute to snoRNA binding *in vivo*. Future work is required to determine the role of snoRNP assembly factor Zf-HIT domains *in vivo*.

Previous research shows that Hit1 interacts with and stabilizes another box C/D snoRNP assembly factor, Rsa1, in both yeast and human cells. The Hit1/Rsa1 complex interacts with a core box C/D snoRNP protein, Snu13. Beyond its critical role in stabilizing Rsa1, whether Hit1 is an active player in snoRNP assembly is unknown. Proteomic data reveal that ZNHIT3, the human homolog of Hit1, is involved in a complex with other snoRNP assembly components, including the assembly factors Bcd1, Rvb1, and Rvb2 and the core snoRNP protein Nop58 (6), though the functional relevance of these contacts is still undetermined. How these interactions contribute to the hierarchical formation of pre-snoRNP complexes is still poorly understood. Further studies are required to explore how loss of Hit1 disrupts the pre-snoRNP interactome in cells expressing PEHO-linked variants. Furthermore, while Bcd1 acts co-transcriptionally in snoRNP assembly (5), the timing of Hit1 binding and release remains unknown and requires future investigation.

Future directions to reveal the role of rRNA modifications in translation

Our studies show that *bcd1* and *hit1* mutant cells have a site-specific loss of rRNA 2'-O-

methylations. The *bcd1-D27A* mutant cells have overall lower levels of rRNA 2'-O-methylation than *hit1-C11F* cells, which coincides with the more severe phenotype and a more severe loss of box C/D snoRNAs in *bcd1-D72A* cells. Though *bcd1* mutant cells have lower levels of rRNA modification than *hit1* mutant cells, the site specificity of rRNA modification loss follows the same trend in the *bcd1* and *hit1* mutant cells. All rRNA 2'-O-methylation sites which are stable in *bcd1* mutant cells are also stable in *hit1* mutant cells. Most of the sites which are highly hypo 2'-O-methylated in *bcd1-D27A* cells are either also hypomethylated or variably methylated in *hit1-C11F* cells. There are two exceptions which are severely hypo 2'-O-methylated in *bcd1-D72A* cells and stably methylated in *hit-C11F* cells: 25S-A1449 and 25S-G2815, guided by U24 and snR38, respectively. Intriguingly, both snR38 and U24 are encoded within introns. Future work should determine whether Bcd1 plays a more important role in the processing of intronic snoRNAs than Hit1. Future experiments will also be required to determine why the loss of rRNA 2'-O-methylations in snoRNP assembly factor mutants is site-specific. We proposed a threshold model, where a threshold level of each snoRNA is sufficient to guide full rRNA modification. In our model, this threshold varies between different snoRNAs. Several factors could influence this threshold, including snoRNA stability, protein binding capabilities, or level of snoRNA transcription, though this remains to be determined. Testing this model requires further studies.

The *bcd1-D72A*, *hit1-C11F*, and *hit1-S29L* mutant cells show a global downregulation of translation, decreased rRNA 2'-O-methylation levels, an increase in alternative start codon usage, and a decrease in stop codon readthrough. Our work in *bcd1-D72A* mutant cells suggests that these translational defects are due to combinatorial local and long-range alterations in rRNA structure which alter ligand binding during translation. Previous work has revealed that even globally downregulating translation impacts the translational efficiency of specific mRNAs more than

others based on their coding sequence length, 5' UTR length, abundance, and half-life (41). Together, these findings suggest that impairment of snoRNP assembly causes mRNA-specific defects in translation. Future work using ribosome profiling, a method to determine which mRNAs in a cell are actively translated (42), will be necessary to determine how the translatome of cells lacking rRNA 2'-O-methylations is altered.

Future directions for the study of PEHO syndrome

The majority of my work in this dissertation focused on characterizing the cellular defects that arise from PEHO syndrome-causing missense mutations modeled in Hit1. Broadly, PEHO syndrome is characterized by progressive cerebellar atrophy, infantile spasms, and arrest of psychomotor development, though the specific phenotypes of PEHO syndrome vary between cases (43). Twenty-two of the twenty-three studied Finnish PEHO syndrome patients have the missense variation Ser31Leu (S31L) (44). An additional patient has compound heterozygous ZNHIT3 variants S31L and Cys14Phe (C14F) (45). Furthermore, in a class of diseases with similar phenotypes to PEHO syndrome, called PEHO-like syndrome, two of the forty studied patients were found to have the *ZNHIT3* missense variant S31L (44). While *ZNHIT3* mutations are the primary cause of Finnish PEHO syndrome, mutations in seventeen other genes have also been linked to PEHO and PEHO-like syndromes in many other countries (46). These genes include *CDKL5*, *CCDC88A*, *PRUNE1*, *TBCD*, *KIF1A*, *PCLO*, *PLAA*, *UBA5*, *CASK*, *CCDC88A*, *SCN1A*, *HESX1*, *SCN2A*, *UFM1*, *SPTAN1*, *SEPSECS* and *GNAO1* (46). Several of these genes are implicated in brain and neuron development/ function and thus the mechanisms by which they cause PEHO syndrome are more easily explained (47-51). However, the molecular mechanisms by which mutations in many of these genes contribute to PEHO syndrome pathogenicity remains unknown. Future work to uncover the molecular mechanisms of PEHO syndrome should

characterize the role of these genes in neurodevelopment or the link between the pathways they participate in and neurodevelopment.

Our work reveals that PEHO-linked *ZNHIT3* mutations modeled in yeast cause both global and specific dysregulation of translation. Because we observe translational defects that are both mRNA-specific (defect in recognition of IRES elements) and also a global decrease in translation, we suggest that the tissue-specific phenotypes seen in PEHO syndrome patients may arise from dysregulated translation of specific mRNAs that impact pathways essential for cerebellar granule cell formation and neurodevelopment. Future work using human cell line models or patient samples is required to confirm that PEHO syndrome is a ribosomopathy resulting from mRNA-specific defects. For example, cell lines such as SH-SY5Y and BE2-M17 that can be differentiated into a more neuron-like state can be used for further modelling PEHO syndrome (52,53). As PEHO syndrome results from a loss of ZNHIT3, future studies of ZNHIT3 knockdown in these cells could reveal whether ZNHIT3 is important for neuronal differentiation and how ZNHIT3 influences the translatome during neuronal differentiation.

While there is currently no evidence that the proteins produced by the 17 additional PEHO-linked genes play a role in regulating the ribosome or translation, variations in these proteins may impact similar cellular pathways to those impacted by mRNA-specific defects in translation observed upon *hit1* mutation. Proper maintenance of the neuronal proteome depends on highly localized translation (54). Because *hit1* mutant ribosomes have impaired ligand-binding capabilities, it is possible that PEHO syndrome arises from mis-localization of translation within cells. Given that another gene implicated in PEHO syndrome, *KIF1A*, encodes a neuron-specific motor protein which plays an important role in axon transport (51), it will be interesting to explore this possibility.

PEHO syndrome is currently diagnosed using a set of criteria developed in the 1990's, before recent advances in genetic testing and genome sequencing (43,46,55). Necessary criteria for the diagnosis of PEHO syndrome include infantile hypotonia, seizures, infantile spasms, and early loss of vision. There are additional criteria which support a diagnosis of PEHO syndrome, yet are not necessary for diagnosis and may vary between patients, such as dysmorphic features and oedema of the face and limbs (43). As we move towards genetic-based disease diagnosis and personalized medicine, the question of whether the diagnosis of cases caused by mutations in genes other than ZNHIT3 should be reclassified will need to be addressed.

In summary, the studies presented in this dissertation advance our fundamental understanding of box C/D snoRNP assembly, uncover the importance of rRNA 2'-O-methylations in translation, and outline how mutations in box C/D snoRNP assembly factors may cause disease. This fundamental knowledge may propel our understanding and treatment of the suggested ribosomopathy PEHO syndrome and other ribosomopathies caused by dysregulation of snoRNAs or rRNA modifications.

References

1. Khoshnevis, S., Dreggors, R.E., Hoffmann, T.F.R. and Ghalei, H. (2019) A conserved Bcd1 interaction essential for box C/D snoRNP biogenesis. *J Biol Chem*.

2. Khoshnevis, S., Dreggors-Walker, R.E., Marchand, V., Motorin, Y. and Ghalei, H. (2022) Ribosomal RNA 2'-. *Proc Natl Acad Sci U S A*, **119**, e2117334119.

3. Massenet, S., Bertrand, E. and Verheggen, C. (2017) Assembly and trafficking of box C/D and H/ACA snoRNPs. *RNA Biol*, **14**, 680-692.

4. Watkins, N.J., Dickmanns, A. and Lührmann, R. (2002) Conserved stem II of the box C/D motif is essential for nucleolar localization and is required, along with the 15.5K protein, for the hierarchical assembly of the box C/D snoRNP. *Mol Cell Biol*, **22**, 8342-8352.

5. Paul, A., Tiotiu, D., Bragantini, B., Marty, H., Charpentier, B., Massenet, S. and Labialle, S. (2019) Bcd1p controls RNA loading of the core protein Nop58 during C/D box snoRNP biogenesis. *RNA*, **25**, 496-506.

6. Bizarro, J., Charron, C., Boulon, S., Westman, B., Pradet-Balade, B., Vandermoere, F., Chagot, M.E., Hallais, M., Ahmad, Y., Leonhardt, H. *et al.* (2014) Proteomic and 3D structure analyses highlight the C/D box snoRNP assembly mechanism and its control. *J Cell Biol*, **207**, 463-480.

7. Baudin-Baillieu, A., Fabret, C., Liang, X.H., Piekna-Przybylska, D., Fournier, M.J. and Rousset, J.P. (2009) Nucleotide modifications in three functionally important regions of

the Saccharomyces cerevisiae ribosome affect translation accuracy. *Nucleic Acids Res*, **37**, 7665-7677.

8. Liang, X.H., Liu, Q. and Fournier, M.J. (2007) rRNA modifications in an intersubunit bridge of the ribosome strongly affect both ribosome biogenesis and activity. *Mol Cell*, **28**, 965-977.

9. Liang, X.H., Liu, Q. and Fournier, M.J. (2009) Loss of rRNA modifications in the decoding center of the ribosome impairs translation and strongly delays pre-rRNA processing. *RNA*, **15**, 1716-1728.

10. Baxter-Roshek, J.L., Petrov, A.N. and Dinman, J.D. (2007) Optimization of ribosome structure and function by rRNA base modification. *PLoS One*, **2**, e174.

11. Piekna-Przybylska, D., Przybylski, P., Baudin-Baillieu, A., Rousset, J.P. and Fournier, M.J. (2008) Ribosome performance is enhanced by a rich cluster of pseudouridines in the A-site finger region of the large subunit. *J Biol Chem*, **283**, 26026-26036.

12. King, T.H., Liu, B., McCully, R.R. and Fournier, M.J. (2003) Ribosome structure and activity are altered in cells lacking snoRNPs that form pseudouridines in the peptidyl transferase center. *Mol Cell*, **11**, 425-435.

13. Lestrade, L. and Weber, M.J. (2006) snoRNA-LBME-db, a comprehensive database of human H/ACA and C/D box snoRNAs. *Nucleic Acids Res*, **34**, D158-162.

14. Léger-Silvestre, I., Caffrey, J.M., Dawaliby, R., Alvarez-Arias, D.A., Gas, N., Bertolone, S.J., Gleizes, P.E. and Ellis, S.R. (2005) Specific Role for Yeast Homologs of the

Diamond Blackfan Anemia-associated Rps19 Protein in Ribosome Synthesis. *J Biol Chem*, **280**, 38177-38185.

15. Flygare, J., Aspesi, A., Bailey, J.C., Miyake, K., Caffrey, J.M., Karlsson, S. and Ellis, S.R. (2007) Human RPS19, the gene mutated in Diamond-Blackfan anemia, encodes a ribosomal protein required for the maturation of 40S ribosomal subunits. *Blood*, **109**, 980-986.

16. Quarello, P., Garelli, E., Carando, A., Mancini, C., Foglia, L., Botto, C., Farruggia, P., De Keersmaecker, K., Aspesi, A., Ellis, S.R. *et al.* (2016) Ribosomal RNA analysis in the diagnosis of Diamond-Blackfan Anaemia. *Br J Haematol*, **172**, 782-785.

17. Menne, T.F., Goyenechea, B., Sánchez-Puig, N., Wong, C.C., Tonkin, L.M., Ancliff, P.J., Brost, R.L., Costanzo, M., Boone, C. and Warren, A.J. (2007) The Shwachman-Bodian-Diamond syndrome protein mediates translational activation of ribosomes in yeast. *Nat Genet*, **39**, 486-495.

18. McCann, K.L., Teramoto, T., Zhang, J., Tanaka Hall, T.M. and Baserga, S.J. (2016) The molecular basis for ANE syndrome revealed by the large ribosomal subunit processome interactome. *Elife*, **5**.

19. Chagot, M.E., Boutilliat, A., Kriznik, A. and Quinternet, M. (2022) Structural Analysis of the Plasmodial Proteins ZNHIT3 and NUFIP1 Provides Insights into the Selectivity of a Conserved Interaction. *Biochemistry*, **61**, 479-493.

20. Quinternet, M., Chagot, M.E., Rothé, B., Tiotiu, D., Charpentier, B. and Manival, X. (2016) Structural Features of the Box C/D snoRNP Pre-assembly Process Are Conserved through Species. *Structure*, **24**, 1693-1706.

21. Nachmani, D., Bothmer, A.H., Grisendi, S., Mele, A., Bothmer, D., Lee, J.D., Monteleone, E., Cheng, K., Zhang, Y., Bester, A.C. *et al.* (2019) Germline NPM1 mutations lead to altered rRNA 2'-O-methylation and cause dyskeratosis congenita. *Nat Genet*.

22. Gonzales, B., Henning, D., So, R.B., Dixon, J., Dixon, M.J. and Valdez, B.C. (2005) The Treacher Collins syndrome (TCOF1) gene product is involved in pre-rRNA methylation. *Hum Mol Genet*, **14**, 2035-2043.

23. Cerami, E., Gao, J., Dogrusoz, U., Gross, B.E., Sumer, S.O., Aksoy, B.A., Jacobsen, A., Byrne, C.J., Heuer, M.L., Larsson, E. *et al.* (2012) The cBio cancer genomics portal: an open platform for exploring multidimensional cancer genomics data. *Cancer Discov*, **2**, 401-404.

24. Gao, J., Aksoy, B.A., Dogrusoz, U., Dresdner, G., Gross, B., Sumer, S.O., Sun, Y., Jacobsen, A., Sinha, R., Larsson, E. *et al.* (2013) Integrative analysis of complex cancer genomics and clinical profiles using the cBioPortal. *Sci Signal*, **6**, pl1.

25. Marcel, V., Ghayad, S.E., Belin, S., Therizols, G., Morel, A.P., Solano-Gonzàlez, E., Vendrell, J.A., Hacot, S., Mertani, H.C., Albaret, M.A. *et al.* (2013) p53 acts as a safeguard of translational control by regulating fibrillarin and rRNA methylation in cancer. *Cancer Cell*, **24**, 318-330.

26. Marcel, V., Kielbassa, J., Marchand, V., Natchiar, K.S., Paraqindes, H., Nguyen Van Long, F., Ayadi, L., Bourguignon-Igel, V., Lo Monaco, P., Monchiet, D. *et al.* (2020) Ribosomal RNA 2'O-methylation as a novel layer of inter-tumour heterogeneity in breast cancer. *NAR Cancer*, **2**, zcaa036.

27. Zhou, F., Liu, Y., Rohde, C., Pauli, C., Gerloff, D., Köhn, M., Misiak, D., Bäumer, N., Cui, C., Göllner, S. *et al.* (2017) AML1-ETO requires enhanced C/D box snoRNA/RNP formation to induce self-renewal and leukaemia. *Nat Cell Biol*, **19**, 844-855.

28. Mei, Y.P., Liao, J.P., Shen, J., Yu, L., Liu, B.L., Liu, L., Li, R.Y., Ji, L., Dorsey, S.G., Jiang, Z.R. *et al.* (2012) Small nucleolar RNA 42 acts as an oncogene in lung tumorigenesis. *Oncogene*, **31**, 2794-2804.

29. Romano, G., Veneziano, D., Acunzo, M. and Croce, C.M. (2017) Small non-coding RNA and cancer. *Carcinogenesis*, **38**, 485-491.

30. Yi, Y., Li, Y., Meng, Q., Li, Q., Li, F., Lu, B., Shen, J., Fazli, L., Zhao, D., Li, C. *et al.* (2021) A PRC2-independent function for EZH2 in regulating rRNA 2'-O methylation and IRES-dependent translation. *Nat Cell Biol*, **23**, 341-354.

31. Monaco, P.L., Marcel, V., Diaz, J.J. and Catez, F. (2018) 2'-O-Methylation of Ribosomal RNA: Towards an Epitranscriptomic Control of Translation? *Biomolecules*, **8**.

32. Gong, J., Li, Y., Liu, C.J., Xiang, Y., Li, C., Ye, Y., Zhang, Z., Hawke, D.H., Park, P.K., Diao, L. *et al.* (2017) A Pan-cancer Analysis of the Expression and Clinical Relevance of Small Nucleolar RNAs in Human Cancer. *Cell Rep*, **21**, 1968-1981.

33. Bellodi, C., McMahon, M., Contreras, A., Juliano, D., Kopmar, N., Nakamura, T., Maltby, D., Burlingame, A., Savage, S.A., Shimamura, A. *et al.* (2013) H/ACA small RNA dysfunctions in disease reveal key roles for noncoding RNA modifications in hematopoietic stem cell differentiation. *Cell Rep*, **3**, 1493-1502.

34. McMahon, M., Contreras, A. and Ruggero, D. (2015) Small RNAs with big implications: new insights into H/ACA snoRNA function and their role in human disease. *Wiley interdisciplinary reviews. RNA*, **6**, 173-189.

35. Stumpf, C.R. and Ruggero, D. (2011) The cancerous translation apparatus. *Curr Opin Genet Dev*, **21**, 474-483.

36. Bragantini, B., Tiotiu, D., Rothé, B., Saliou, J.-M., Marty, H., Cianférani, S., Charpentier, B., Quinternet, M. and Manival, X. (2016) Functional and Structural Insights of the Zinc-Finger HIT protein family members Involved in Box C/D snoRNP Biogenesis. *Journal of Molecular Biology*, **428**, 2488-2506.

37. Andreini, C., Banci, L., Bertini, I. and Rosato, A. (2006) Zinc through the three domains of life. *J Proteome Res*, **5**, 3173-3178.

38. Verheggen, C., Pradet-Balade, B. and Bertrand, E. (2015) SnoRNPs, ZNHIT proteins and the R2TP pathway. *Oncotarget*, **6**, 41399-41400.

39. Cloutier, P., Poitras, C., Durand, M., Hekmat, O., Fiola-Masson, É., Bouchard, A., Faubert, D., Chabot, B. and Coulombe, B. (2017) R2TP/Prefoldin-like component RUVBL1/RUVBL2 directly interacts with ZNHIT2 to regulate assembly of U5 small nuclear ribonucleoprotein. *Nat Commun*, **8**, 15615.

40. Rothe, B., Saliou, J.M., Quinternet, M., Back, R., Tiotiu, D., Jacquemin, C., Loegler, C., Schlotter, F., Pena, V., Eckert, K. *et al.* (2014) Protein Hit1, a novel box C/D snoRNP assembly factor, controls cellular concentration of the scaffolding protein Rsa1 by direct interaction. *Nucleic Acids Res*, **42**, 10731-10747.

41. Gaikwad, S., Ghobakhlou, F., Young, D.J., Visweswaraiah, J., Zhang, H. and Hinnebusch, A.G. (2021) Reprogramming of translation in yeast cells impaired for ribosome recycling favors short, efficiently translated mRNAs. *Elife*, **10**.

42. Ingolia, N.T., Ghaemmaghami, S., Newman, J.R. and Weissman, J.S. (2009) Genome-wide analysis in vivo of translation with nucleotide resolution using ribosome profiling. *Science*, **324**, 218-223.

43. Somer, M. (1993) Diagnostic criteria and genetics of the PEHO syndrome. *J Med Genet*, **30**, 932-936.

44. Anttonen, A.K., Laari, A., Kousi, M., Yang, Y.J., Jaaskelainen, T., Somer, M., Siintola, E., Jakkula, E., Muona, M., Tegelberg, S. *et al.* (2017) ZNHIT3 is defective in PEHO syndrome, a severe encephalopathy with cerebellar granule neuron loss. *Brain*, **140**, 1267-1279.

45. Õunap, K., Muru, K., Õiglane-Shlik, E., Ilves, P., Pajusalu, S., Kuus, I., Wojcik, M.H. and Reimand, T. (2019) PEHO syndrome caused by compound heterozygote variants in ZNHIT3 gene. *Eur J Med Genet*.

46. Sabaie, H., Ahangar, N.K., Ghafouri-Fard, S., Taheri, M. and Rezazadeh, M. (2020) Clinical and genetic features of PEHO and PEHO-Like syndromes: A scoping review. *Biomed Pharmacother*, **131**, 110793.

47. Hall, E.A., Nahorski, M.S., Murray, L.M., Shaheen, R., Perkins, E., Dissanayake, K.N., Kristaryanto, Y., Jones, R.A., Vogt, J., Rivagorda, M. *et al.* (2017) PLAA Mutations Cause a Lethal Infantile Epileptic Encephalopathy by Disrupting Ubiquitin-Mediated Endolysosomal Degradation of Synaptic Proteins. *Am J Hum Genet*, **100**, 706-724.

48. Ahmed, M.Y., Chioza, B.A., Rajab, A., Schmitz-Abe, K., Al-Khayat, A., Al-Turki, S., Baple, E.L., Patton, M.A., Al-Memar, A.Y., Hurles, M.E. *et al.* (2015) Loss of PCLO function underlies pontocerebellar hypoplasia type III. *Neurology*, **84**, 1745-1750.

49. Ohara, K., Enomoto, A., Kato, T., Hashimoto, T., Isotani-Sakakibara, M., Asai, N., Ishida-Takagishi, M., Weng, L., Nakayama, M., Watanabe, T. *et al.* (2012) Involvement of Girdin in the determination of cell polarity during cell migration. *PLoS One*, **7**, e36681.

50. Quirk, J. and Brown, P. (2002) Hesx1 homeodomain protein represses transcription as a monomer and antagonises transactivation of specific sites as a homodimer. *J Mol Endocrinol*, **28**, 193-205.

51. Shin, H., Wyszynski, M., Huh, K.H., Valtschanoff, J.G., Lee, J.R., Ko, J., Streuli, M., Weinberg, R.J., Sheng, M. and Kim, E. (2003) Association of the kinesin motor KIF1A with the multimodular protein liprin-alpha. *J Biol Chem*, **278**, 11393-11401.

52. Andres, D., Keyser, B.M., Petrali, J., Benton, B., Hubbard, K.S., McNutt, P.M. and Ray, R. (2013) Morphological and functional differentiation in BE(2)-M17 human neuroblastoma cells by treatment with Trans-retinoic acid. *BMC Neurosci*, **14**, 49.

53. Shipley, M.M., Mangold, C.A. and Szpara, M.L. (2016) Differentiation of the SH-SY5Y Human Neuroblastoma Cell Line. *J Vis Exp*, 53193.

54. Holt, C.E., Martin, K.C. and Schuman, E.M. (2019) Local translation in neurons: visualization and function. *Nat Struct Mol Biol*, **26**, 557-566.

55. Salonen, R., Somer, M., Haltia, M., Lorentz, M. and Norio, R. (1991) Progressive encephalopathy with edema, hypsarrhythmia, and optic atrophy (PEHO syndrome). *Clin Genet*, **39**, 287-293.